의학박사 학위논문

The roles of reactive astrocytes in cognitive function via the morphological and molecular changes in Alzheimer’s disease animal model

알츠하이머병 동물 모델에서 활성화 성상교세포의 형태학적 및 분자적 변화와 인지기능에서의 역할에 관한 연구

2020년 8월

서울대학교 대학원
의과학과 의과학 전공 (약리학)
최 문 석

A thesis of the Degree of Doctor of Philosophy

알츠하이머병 동물 모델에서 활성화 성상교세포의 형태학적 및 분자적 변화와 인지기능에서의 역할에 관한 연구

The roles of reactive astrocytes in cognitive function via the morphological and molecular changes in Alzheimer's disease animal model

August 2020

Seoul National University
College of Medicine
The Department of Biomedical Sciences and Pharmacology
Moonseok Choi

알츠하이머병 동물 모델에서 활성화 성상교세포의 형태학적 및 분자적 변화와 인지기능에서의 역할에 관한 연구

지도 교수 김 혜 선

이 논문을 의학박사 학위논문으로 제출함
2020년 8월

서울대학교 대학원
의과학과 의과학 전공 (약리학)
최 문 석

최문석의 의학박사 학위논문을 인준함
2020년 8월

위 원 장 육인희 (인)
부위원장 김혜선 (인)
위 원 이승재 (인)
위 원 서영호 (인)
위 원 [illegible] (인)

The roles of reactive astrocytes in cognitive function via the morphological and molecular changes in Alzheimer's disease animal model

by

Moonseok Choi

A thesis submitted to the Department of Biomedical Sciences in partial fulfillment of the requirements for the Degree of Doctor of Philosophy in Medical sciences at Seoul National University College of Medicine

August 2020

Approved by Thesis Committee:

Professor Mook, Inhee Chairman

Professor Kim, Hye-Sun Vice Chairman

Professor Lee, Seung-Jae

Professor Suh, Young Ho

Professor Rah, Joug-Cheol

ABSTRACT

Numerous roles of astrocytes have been reported in the central nervous system. Astrocytes have the potential to exist in two states, the reactive and the resting states. Reactive astrocytes have morphological features such as the increase in thickness, number of processes and volume of cell body. Molecular changes also occur, such as an increase in the expression of glial fibrillary acidic protein (GFAP). However, the morphological and molecular dynamics during the memory formation in astrocytes remain largely unknown. Moreover, the pathophysiological roles of the reactive state of astrocytes are thought to be of importance in the pathogenesis of neurodegenerative diseases, including Alzheimer's disease (AD). However, the detailed mechanisms underlying the transition of astrocytes from the resting state to the reactive state during neurodegenerative disease largely remain unclear. Here, I investigated the changes in astrocytes in the hippocampus of Fvb/n mice trained with contextual fear conditioning to memory induction, and the morphological and molecular dynamics were analyzed in astrocytes. One hour after fear conditioning, type II and type III astrocytes

displayed a unique status, not reactive nor resting state, with an increased the number of processes and decreased GFAP expression. In addition, the protein level of excitatory amino acid transporter 2 (EAAT 2) was increased at 1 hour to 24 hours after fear conditioning while EAAT1 did not show any changes. Connexin 43 protein expression was found to be increased at 24 hours after fear conditioning test. After L-α-aminoadipate treatment, an astrocyte-specific toxic molecule, mice showed the impairment of cognitive function. In addition, I investigated which pathways are involved in activating astrocytes from the resting state to the reactive state in an AD context such as JAK/STAT3, MAPK, NF-kB, and NFAT in primary cultured astrocytes treated with oligomeric amyloidβ peptide (oAβ) and in the hippocampus of 5XFAD mice. Treatment with oAβ induced an increase in reactive astrocytes, as assessed by the protein expression of GFAP and this increase was caused by signal transducer and activator of transcription 3 (STAT3) phosphorylation in primary cultured astrocytes. The treatment with Stattic, an inhibitor of STAT3 phosphorylation, rescued the activation of astrocytes in primary cultured astrocytes. Additionally, the systemic administration of Stattic rescued the activation of astrocytes

in the hippocampus of 6-month-old 5XFAD mice as well as impairments of cognitive function. Collectively, these results demonstrated that the status of astrocytes transit into a novel state, memory induction state, by hippocampus-based contextual memory process. These astrocytes in the memory induction state are thought to be not induced in 5XFAD mice brains, because astrocytes exist in the reactive state in the hippocampus of 5XFAD mice. Reactive astrocytes in the brains of 5XFAD mice were found to be induced via STAT3 phosphorylation and the impairments in learning and memory observed in the 5XFAD mice are rescued by the inhibition of STAT3 phosphorylation, suggesting that the inhibition of STAT3 phosphorylation in astrocytes may be a novel therapeutic target for cognitive impairment in AD.

Keywords: Alzheimer ' s disease, astrocytes, memory induction, contextual fear conditioning test, cognitive function, STAT3, 5XFAD mice

Student number: 2013-21792

CONTENTS

LIST OF FIGURES

Chapter 1 : Dynamics of astrocytes during memory induction

Chapter 2 : Pathophysiological roles of reactive astrocytes in Alzheimer’ s disease

LIST OF ABBREVIATIONS

5XFAD: Five mutations of familial Alzheimer's disease

Aβ: amyloidβ peptide

AD: Alzheimer's disease

AMPAR: α-Amino-3-hydroxy-5-methyl-4 isoxazolepropionic acid type glutamate receptors

APP: amyloid precursor protein

BACE1: β-site APP cleaving enzyme1

BDNF: brain-derived neurotrophic factor

CCL5: C-C motif ligand 5

CD80: cluster of differentiation 80

CNS: central nervous system

CX43: connexin 43

CXCL 10: C-X-C motif chemokine ligand 10

DMEM: Dulbecco's modified Eagle's medium

DMSO: dimethyl sulfoxide

EAAT: excitatory amino acid transporter

GABA: γ-aminobutyric acid

GFAP: glial fibrillary acidic protein

GLAST-1: glutamate aspartate transporter1

GLT-1: glutamate transpoter1

GPCR: G-protein coupled receptors

HFIP: hexafluoroisopropanol

IL-6: interleukin 6

IL-8: interleukin 8

IP3R2: inositol 1,4,5-triphosphate receptor type 2

JAKs: Janus tyrosine kinases

JAK/STAT3: Janus kinase/signal transducers and activators of transcription

LTP: long-term potentiation

MAO-B: monoamine oxidase-B

MAPK: the mitogen-activated protein kinase

MMP2: metalloproteinase 2

NeuN: neuronal nuclei

NF-κB: the nuclear factor κ light chain enhancer of activated B cells

NFAT: nuclear factor of activated T-cells

NL1B: neuroligin-1B

NMDAR: N-methyl-D-aspartate-type glutamate receptor

NRX-1 α: neurexin-1 α

oAβ: oligomeric Aβ

P1: postnatal day 1

PD: Parkinson's disease

p-ERK: phospho-ERK

p-p65: phospho-p65

p-STAT3: phospho-STAT3

p-tau: phosphorylated tau

PS1: presenilin-1

PSD-95: postsynaptic density protein 95

SH2: Src homology 2

SPARC: secreted protein acidic, enriched in cysteine

STAT3: Signal transducer and activator of transcription 3

TNF-α: tumor necrosis factor-α

TSP: thrombospondin

VGLUT: vesicular glutamate transporter

VNUT: vesicular nucleotide transporter

VSERT: vesicular $_{D}$-serine transporter

WB: western blotting

WT: wild type

INTRODUCTION

Morphology of astrocytes

Astrocytes were named from its star-shaped morphology and represent the most abundant cell type in mammalian brains [1]. Astrocytes have complex spongiform with many processes [2]. These processes are classified based on the size and location, branches and branchlets are the first and second processes, respectively. Leaflets are peripheral fine processes of which processes cannot be imaged in light microscopy. End feet of astrocytes contact with blood vessels and synapses [3]. Single astrocyte contacts with over 2 million synapses [4]. In humans, astrocytic complexity is higher than rodents. Intelligence might be involved the astrocytic complexity [5].

Astrocytes are classified by the morphology such as fusiform, elongated and spherical cell [6]. Type I astrocytes display a higher morphological complexity as short and numerous processes. Type II astrocytes display an elongated and bipolar shape. Type III astrocytes display the star shape with GFAP staining [7].

Function of astrocytes

Astrocytes are well known for their various functions what they serve within the CNS such as metabolic energy support [8-10], maintenance of extracellular ionic homeostasis [11-13], modulation of neurotransmitter actions [14-16] and protection of the CNS from peripheral system via the blood-brain barrier [9, 17, 18]. In addition to these well-known roles of astrocytes, bidirectional communication between astrocytes and neurons has been shown to regulate neuronal excitability and synaptic transmission and plasticity [19-21]. Recent studies are extensively focusing on the roles of astrocytes in synaptic formation and neurogenesis [10, 22, 23], and in supporting learning and memory formation [24, 25].

Gliotransmitter of astrocytes

Astrocytes release gliotransmitters such as glutamate, $_{D}$-serine, GABA and ATP, which bind to the receptors on synapses to modulate neuronal firing frequency and synaptic transmission [26, 27]. Alterations of gliotransmitter release-related proteins such as vesicular transporters, vesicle-associated membrane proteins and release channels cause brain disorders and abnormal behaviors [28, 29]. The molecular mechanisms governing gliotransmitter release have

not been fully elucidated. The unknown extracellular signals induce the intracellular calcium level via the inositol 1,4,5 triphosphate-mediated calcium release from the endoplasmic reticulum [26, 30, 31]. These increased intracellular calcium levels spread out other astrocytes through gap-junction proteins, called 'calcium waves' [32, 33]. The increased intracellular calcium levels activate gliotransmitter release such as glutamate, $_{D}$-serine and ATP from astrocytes, which is called calcium-dependent gliotransmitter release [34-36]. The uptake and release of each gliotransmitter through exocytotic vesicles are mediated by vesicular glutamate transporter (VGLUT) [37], vesicular $_{D}$-serine transporter (VSERT) [38] and vesicular nucleotide transporter (VNUT) [30]. These gliotransmitters are released via P2X receptor [39], the cell swelling-induced anion transporter and such hemichannels as connexin 43 (Cx43) [40].

Glutamate uptake transporters of astrocytes

Astrocytes regulate synaptic transmission to modulate excitotoxicity by glutamate uptake via excitatory amino acid transporters (EAATs) [41]. EAAT1 is known as glutamate aspartate transporter 1 (GLAST-1) [42] and EAAT2 is known

as glutamate transporter 1 (GLT-1) [43]. Both EAAT1 and EAAT2 are predominantly expressed on astrocytes to uptake glutamate from synapses [44]. Specifically, EAAT2 is responsible for approximately 90% of total glutamate uptake [45, 46]. EAAT3, 4 and 5 are expressed on the axon terminal, postsynaptic membrane and dendrite [47].

Modulate synaptic plasticity by astrocytes

$_{D}$-Serine, a gliotransmitter, moderates synaptic plasticity as a physiological coagonist of the N-methyl-D-aspartate-type glutamate receptor (NMDAR), a key neurotransmitter receptor [48]. $_{D}$-Serine released from astrocytes activates NMDAR in neurons. NMDAR synaptic potentials and long-term potentiation (LTP) are reported to be regulated by $_{D}$-serine in the hippocampus [49, 50].

Synaptogenesis by astrocytes

Thrombospondins (TSPs), a family of 5 extracellular matrix proteins, secreted from astrocytes serve as synaptogenic factors [51]. Treatment with TSP promotes the formation of synapses, but these synapses are not fully functional. Because these synapses that are newly formed by TSP do not express

α-amino-3-hydroxy-5-methyl-4-isoxazolepropionic acid type glutamate receptors (AMPARs), these receptors are nonfunctional [52]. In addition, other astrocyte-derived factors, such as secreted protein acidic, enriched in cysteine (SPARC) and hevin are reported to control synapse formation. SPARC and hevin are highly expressed during the early stage of mouse development [53]. Hevin regulates the formation of glutamatergic synapses by serving as a bridge between presynaptic neurexin-1 α (NRX1 α) and postsynaptic neuroligin-1B (NL1B) [54]. Furthermore, astrocytes promote neuronal differentiation and proliferation by IL-1β, IL-6, WNT3 and neurogenesis by IL-6 but suppress neuronal differentiation and proliferation by decorin, IGFBP6 and enkephalin [55].

JAK / STAT pathway

STAT3 protein belongs to the seven-membered STAT family (1-7). STAT is the transcription factors to respond to transmitting signals form surface receptors. Cytokines, growth factors and hormones binding to respective receptors activate STAT pathway. STAT family serves important roles such as angiogenesis, immune response, cell proliferation and

survival [56, 57].

Structure of STAT3

STAT3 is the most studied among the seven STAT family members. STAT3 is expressed in many organs as lung, liver, pancreas, heart, skeletal muscle, kidney, placenta and brain [58]. STAT3 consists of the N-terminal domain, coiled-coil domain, DNA-binding domain, linker region, Src homology 2 (SH2) domain and C-terminal transactive domain [59, 60]. The coiled-coil domain attends to the initiation of gene expression. The SH2 domain attend to stabilize STAT3-STAT3 dimerization and STAT3-receptor interaction. These dimerized STAT3 bind to DNA motif and initiate gene transcription [61].

Phosphorylation of STAT3

Janus tyrosine kinases (JAKs) attend to phosphorylation of cell surface receptors as JAK-STAT pathway. STAT3 is recruited to phospho-tyrosine residues of the activated receptor through SH2 domain [62]. STAT3 is phosphorylated at tyrosine 705 [63]. Phosphorylated STAT3 promotes dimer formation and translocation into the nucleus [64].

Hyperactivation of STAT3 has been reported in tumors such as brain cancer, breast cancer, liver cancer, lung cancer, kidney cancer, prostate cancer, ovary cancer and multiple myeloma [65-70]. Additionally, STAT3 phosphorylation promotes cancer metastasis as migration and invasion via Twist, vimentin, Snail and matrix metalloproteinase 2 (MMP2)[71].

Immune responses are reported to be altered by STAT3 activation. STAT3 affects the gene expression to upregulate interukin-6 (IL-6) and 10 (IL-10), and to downregulate interferons, IL-12, cluster of differentiation 80 (CD80), CD86, C-C motif ligand 5 (CCL5) and C-X-C motif chemokine ligand 10 (CXCL10) [72].

Classification of reactive astrocytes

Recently, it has been reported that reactive astrocytes are classified by genetic expression patterns as A1-type and A2-type [73, 74]. A1-type reactive astrocytes show neurotoxic effects such as decreasing synaptic functions and astrocytic phagocytic capacity [75]. A1-type reactive astrocytes are activated by LPS or microglia-derived IL-1 α, TNF α and C1q [73]. A1- type reactive astrocytes have specific genetic

expression, such as H2T23, Serping1, H2D1, Ggta1, Iigp1, Gbp2, Fbln5, Ugt1a, Fkbp5, Psmb8, Srgn and Amigo20. A2-type reactive astrocytes display neuroprotective effects, such as neuronal survival and tissue repair. A2-type reactive astrocytes have specific genetic expression profiles, such as the increases in Clcf1, Tgm1, Ptx3, S100a10, Sphk1, Cd109, Ptgs2, Emp1, Sic10a6, Tm4sf1, B3gnt5 and Cd14 [73].

Alzheimer's disease

The first discovery of Alzheimer's disease (AD) is attributed to Alois Alzheimer, a German neurologist at the beginning of the 20th century (1906). Auguste Deter who was the first patient diagnosed as AD was suffering with continuous memory and language problems at 55-year-old. The patient's autopsy revealed neuritic plaques and neurofibrillary tangles [76, 77]. In further research, neuritic plaques are identified as the aggregation of amyloid β peptide (A β) [78, 79]. Additionally, glial cells such as astrocytes and microglia are activated and found around neuritic plaques [80, 81]. AD is caused by the aberrant processing of amyloid precursor protein (APP) and accumulation of A β [82]. APP is processed by β-site APP cleaving enzyme1 (BACE1) and γ-secretase to produce

Aβ[83]. Additionally, the genetic mutations on APP and / or presenilin 1 (PS1) promote the early onset of AD [84, 85]. However, AD is a complex disease with a multifactorial etiological view. AD cases present less than 1% in familial form and the heritability is estimated up to 60 – 80% in monozygotic twins [86].

Oligomeric form of Aβdiffuses into synapses and affect the abnormal synaptic signaling and the activity of kinases [87]. In addition, aggregated Aβleads to hyperphosphorylation of the microtubule-associated tau protein in neurons [88]. The polymerization of phosphorylated tau (p-tau) aggregates into neurofibrillary tangles inside neurons [89].

AD is an extremely complex and progressive neurodegenerative disease. Age is a major risk factor for AD [90]. However, it is not enough to fully account for AD [91]. Other risk factors of AD such as cardiovascular risk factor, brain trauma, hypertension, insulin resistance, obesity, metabolic syndrome, inflammation and apolipoprotein gene E4 alleles have been suggested [92, 93]. Furthermore, the whole etiology of the AD is still not elucidated. Several hypotheses suggested various causative factors such as Aβ accumulation, tau hypophosphorylation, acetylcholine deficiency, brain-

derived neurotrophic factor (BDNF) deficit, mitochondrial dysfunction and other factors [94]. Many compounds are tested to AD clinical trials to target anti-Aβ, anti-tau, anti-neuroinflammation and neuroprotection [95].

AD drugs

However, unfortunately, most of AD drug candidates have been failed in clinical trials. Donepezil, galantamine, rivastigmine, tacrine and memantine are the only used FDA-approved drugs for AD, to date [96]. Various candidate drugs targeting AD by various methods have been tested in clinical trials or have failed [97]. Triptolide extract, punicalagin, WIN, 2-AG and methanandamide are natural phytochemical cannabinoid agonists [98-100]. Pelargonidine, Bambusea Concretio Salicea and monascin are endogenous antioxidant factors [101, 102]. Resveratrol (in Phase 1 of clinical trial), tocoteienol, anthocyanins (in Phase 2), epicatechin and 3H-1,2-ditheiole-3-thione are exogenous antioxidant compounds [103, 104]. Penicillin, sephalosporin, ampicillin, estrogen (in Phase 2), riluzole (in Phase 2) and insulin (in Phase 1) are stimulators of GLT1 expression [105]. Pyridazone and LDN/OSU-0212320 are activators of GLT1 translation [106].

INTRODUCTION SUMMARY

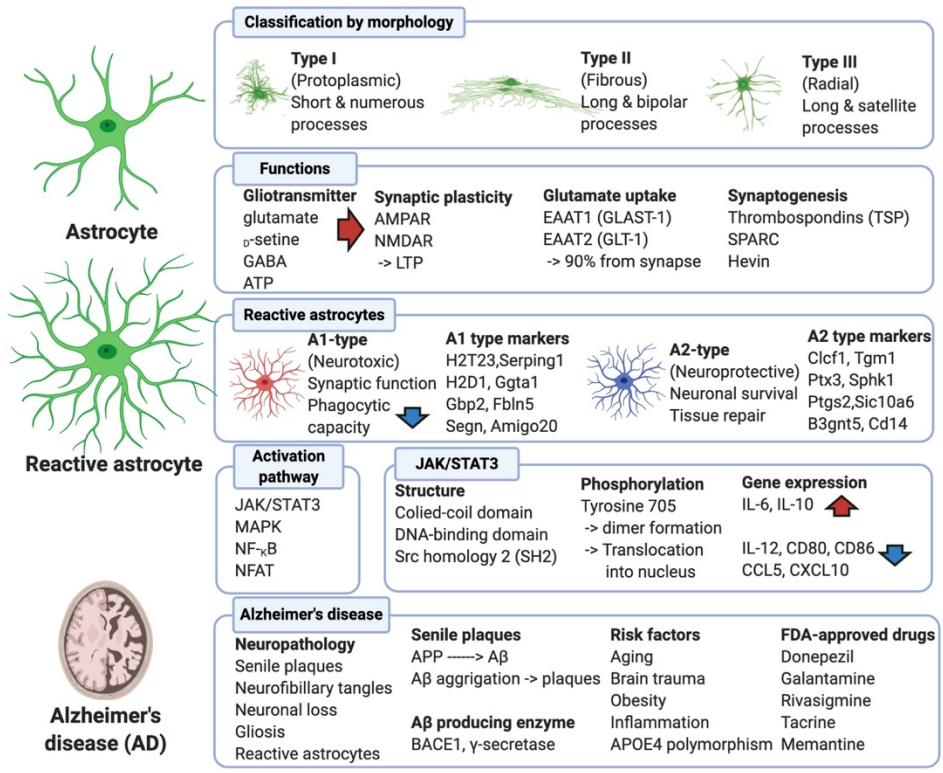

CHAPTER 1

Dynamics of astrocytes during memory induction

INTRODUCTION

Morphological changes and synaptic invasion of astrocytes are known to be required for controlling synaptic strength [20]. However, morphological or molecular changes of astrocytes during learning and memory processes still remain to be elucidated.

According to previous reports, astrocytes are classified based on their morphology such as cell body size, the number of processes, thickness of processes, direction of processes or length of processes into type I, II and III. Type I astrocytes have a small cell body size and numerous short processes, type II astrocytes have a bipolar shape and long processes. Type III astrocytes are characterized by a star shape and long processes [107-109]. The morphological characteristics of astrocytes are thought to be important for their functions [107, 109]. However, each type of astrocyte is classified by its morphological characteristics, but the different functions, genetic expression and protein markers of each type of astrocytes have not been determined [110, 111].

Contextual fear conditioning test has been exploited to test hippocampus-dependent memory in rodents [112-114]. Fvb/n

mice were subjected to contextual fear conditioning test, and checked for morphological and molecular changes in astrocytes at 1 hour and 24 hours after contextual fear conditioning. After fear conditioning test, type II and type III astrocytes exhibited a unique status with an increased number of processes and decreased protein level of GFAP and increased level of EAAT2 and Cx43 protein which differs from the typical resting or reactive state.

These results showed that hippocampus-based contextual memory processes results in changes in the status of astrocytes towards a novel status different from typical resting or reactive states. These morphological and molecular changes may be in line with functional changes of astrocytes.

In this study, I aimed to examine time-dependent morphological and/or molecular changes in astrocytes based on the hypothesis that astrocytes play critical roles in memory formation accompanied by morphological, molecular and functional changes.

MATERIALS AND METHODS

1. Reagents and antibodies

RNA and protein isolation kit were purchased from NucleoSpin (#740933.50, Macherey-Nagel, Dűren, Germany) and Pierce™ BCA Protein Assay Kit were purchased from Thermo (#23227, MA, USA). Anti-GFAP, rabbit polyclonal antibody was purchased from DAKO (#Z0334, CA, USA). Anti-Iba1, rabbit polyclonal antibody was purchased from WAKO (#016-20001, Osaka, Japan). Anti-mouse, sheep polyclonal horseradish peroxidase (HRP) tagged antibody was purchased from Abcam (#ab26116, #ab26113 and #ab6808, EA, UK). Anti-EAAT2 rabbit monoclonal antibody was purchased from Cell signaling (#3838, MA, USA). Anti-Cx43 mouse monoclonal and anti-EAAT1 antibodies were purchased from Santacruz (#sc-59949 and #sc-15316, Taxas, USA). Anti-NeuN rabbit monoclonal antibody was purchased from Millipore (#3838, MA, USA). Anti-GAPDH, rabbit polyclonal antibody was purchased from AbFrontier (#LF-PA0018, Seoul, Korea). Anti-PSD-95, mouse monoclonal antibody and anti-rabbit, goat polyclonal tagged Alexa fluor 488 and 4’, 6-diamidino-2-phenylinodole (DAPI) were purchased from

ThermoFisher (#MA1-046, #A11034, #A11012 and #D3571, MA, USA).

2. Experimental animals

FVB/N mice were obtained from Central Laboratory Animal Incorporation (Seoul, Korea) and the 6 to 8-week-old male mice were used for the experiments. The mice were housed in group of five per cage with a 12 h light/dark cycle and ad libitum access to food and water as under standard laboratory housing condition.

3. Contextual fear conditioning

Contextual fear conditioning was performed as described previously [115, 116]. Each scrambler was connected to an electronic constant-current shock source that was controlled via an interface connected to a Windows 7 computer running EthoVision XT 8 software (Noldus Information Technology, VA, USA). A digital camera was mounted on the steel ceiling of each chamber, and video signals were sent to the same computer for analysis. Prior to training, mice were placed into the chamber for 60 min for habituation. During training, mice were placed in the conditioning chamber (13 × 13 × 25 cm)

for 3 min (for pre-shock) and received three repetitions of a foot-shock (0.7 mA, 2 sec) at 1 min inter-trial intervals. On the next day, conditioned mice were placed in the same chamber, and the “freezing” time was measured over periods of 3 min. Conditioned freezing was defined as immobility except for respiratory movements. The total freezing time in the test period was represented as a percentage. Animals were divided into 2 groups. The sham control group (control group) did not receive electric foot shocks even though all other the fear conditioning procedures were the same as the test group. The test group was exposed to contextual fear conditioning with electric foot shock on day 2.

4. Western Blotting

For brain tissue preparation, mice were deeply anesthetized with Zoletil (12.5 mg/kg) and Rompun mix (17.5 mg/kg) administered intraperitoneally. Mice were perfused transcardially with heparin dissolved in PBS (pH 7.2). The dissected brain tissues were frozen at -80° C for Western blotting. Tissues were homogenized with total RNA and protein isolation with NucleoSpin RNA/Protein kit. The

protein samples were quantified with Pierce™ BCA Protein Assay Kit and 50 μg protein sample were used for each Western blot. The primary antibodies were applied in the following concentrations: anti-GFAP (rabbit, 1: 1,000), anti-Iba1 (rabbit, 1:300), anti-EAAT1 (rabbit, 1:1,000, anti-EAAT2 (rabbit, 1:1,000), anti-Cx43 (mouse, 1:1,000), anti-PSD95 (mouse, 1:2,000), anti-NeuN (mouse, 1:1,000), anti-GAPDH (rabbit, 1:10,000). Secondary antibodies were conjugated with horse-radish peroxidase (HRP) (1: 2,000). The HRP signals were visualized using an enhanced chemiluminescent (ECL, Abfrontier) substrate.

5. Immunohistochemistry

Brains were perfused transcardially with heparin dissolved in PBS (pH 7.2) for 5 min. Brains were fixed in a 4 % paraformaldehyde in PBS for 24 h at 4° C and incubated in 30 % sucrose solution for 48 h at 4° C. For immunohistochemical experiments, brain tissues were coronal sectioned 30 μm with a Crystat (Cryotome, Thermo Elctron Corporation, MA, USA) and stored in cryoprotection solution at 4° C. For antigen retrieval, brain sections were incubated with 10mM sodium citrate (pH 8.5) in an 80° C water bath for 30 min. Brain

sections were then blocked with 0.3 % triton X-100, 2 % horse serum and 2 % BSA in PBS for 1 hour. The anti-GFAP (rabbit) antibody was applied at a concentration of 1: 1,000. Secondary antibodies were applied in the following concentrations; anti-rabbit-488 (goat, 1:200) and 1 μM DAPI. Sections were mounted in microscope slides in a mounting solution. Confocal microscopic observation was performed using LSM 510.

6. Analysis of Astrocytes morphology

Sholl analysis was performed to investigate the changes in astrocytes morphology as previously described [117]. Astrocytes were stained with anti-GFAP antibody in the hippocampal dentate gyrus and the images were obtained every 1 μm interval between 0 to 30 μm depth with Z-Stack system using LSM 510 confocal microscope. Confocal Z-stacks were reconstructed in 3-D using LSM software and sholl analysis was performed with the 3-D reconstructed confocal image. Concentric circles with 10 um diameters were drawn from the center of the cell body of an astrocyte. Processes intersecting the concentric circles were manually counted at each distance from the cell body by adobe Photoshop CC 2014. This manual counting method allowed analysis of the finest

astrocyte processes.

7. Stereotaxic surgery for LAA injection

Stereotaxic surgery was performed as described previously [118]. All the mice were deeply anesthetized with isoflurane. LAA (20 μg) was bilaterally injected via a Hamilton syringe into the dentate gyrus of the hippocampus. (AP - 1.5, ML ± 1.4, DV - 3.1 at a rate of 0.15 μ m/min up to 1 μl)

8. Statistical analysis

Data are expressed as the mean ± SEM (means ± standard error of the mean). One-way ANOVA followed by Fisher's LSD post-hoc analysis or Students' t-test (SPSS, IL, USA) was performed to determine statistical significance. The results were considered to be statistically significant at $p<0.05$.

EXPERIMENTAL SCHEME

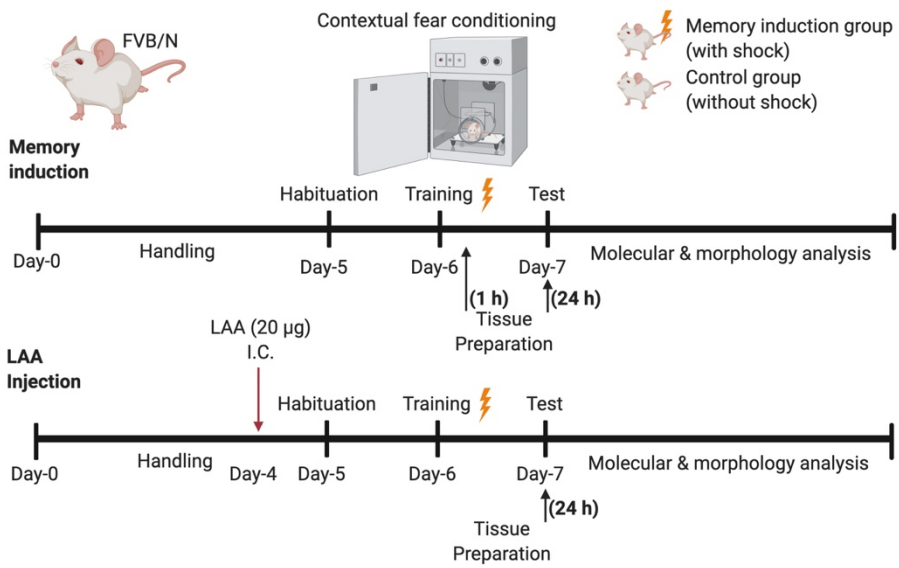

RESULTS

1. Fvb/n mice were exposed to contextual fear conditioning

I performed contextual fear conditioning for expressing hippocampus-dependent long-term spatial memory. Generally, a conditioned stimulus and an unconditioned stimulus are used for this behavior test. However, I employed a contextual fear conditioning test without a sound cue, because I aimed to focus only on the hippocampus-dependent memory. A schematic time-schedule of the fear conditioning test we used in this study is shown in Fig. 1-1a.

It was confirmed that at intervals between the 1^{st} and 2^{nd} electric shocks (1/2), the 2^{nd} and 3^{rd} (2/3) and after the 3^{rd} electric shocks (3/E), the mice displayed increased freezing behavior. These results indicate that the mice were well-trained by the fear conditioning (Fig. 1-1b). At day 3, the freezing time of the control and the test group mice were analyzed. The test group exhibited a significantly increased freezing time, compared to the control group (Fig. 1-1b). These data indicated that contextual fear memory was induced by contextual fear conditioning protocol.

2. Alterations in astrocytic morphological characteristics were observed in the hippocampal dentate gyrus after contextual fear conditioning in Fvb/n mice

Confocal images of hippocampal slices from the 2 group mice were taken with Z-stack at 0 ~ 30 μm by 1 μm interval and reconstructed into 3-D images. The number of intersections between astrocyte processes and concentric circles were manually counted.

In humans, patients with amnestic mild cognitive impairment show shape and volume changes in the CA3 and dentate gyrus of the hippocampus [119]. Therefore, the dentate gyrus is one of the important regions for long-term memory and was chosen as the focus of this study. Type I astrocytes were found to constitute only a small percentage of astrocytes in the dentate gyrus (data not shown). The intersections of type II astrocytes and thus the processes of these cells, were significantly increased at 15 μm from the cell body at 1 hour but not at 24 hours after fear conditioning was performed. At 20 μm, the number of intersections were significantly increased at both 1 hour and 24 hours. At 25 μm, the number of intersections was significantly increased at 1 hour (Fig. 1-2b).

The intersections of type III astrocytes were significantly increased at 10㎛ from the cell body at 1 hour but not at 24 hour. At 15 ㎛, the number of intersections was significantly increased at 1 hour but not at 24 hour. At 20 ㎛, the number of intersections was also significantly increased at 1 hour but not at 24 hour. At 25㎛, the number of intersections was significantly increased at 1 hour but not at 24 hour. At 30㎛, the number of intersections was significantly increased at 1 hour but not at 24 hour (Fig. 1-2b). These data indicate that hippocampues-dependent memory induction causes the changes in the number of processes of type II and type III astrocytes in the dentate gyrus at 1 hour after a test of fear conditioning. Meanwhile, the intersections of type III astrocytes were not changed in the auditory cortex (Fig.1-3b). In this area, the numbers of type I and II astrocytes were much smaller than type III astrocytes, unlike in the dentate gyrus.

3. Protein levels of GFAP, PSD-95, EAAT2 and Cx43 were altered in the hippocampus by contextual fear conditioning

Next, I analyzed the protein levels of GFAP, postsynaptic density protein 95 (PSD-95), EAAT1, EAAT2 and Cx43 to investigate the molecular changes accompanied by

morphological changes in astrocytes induced by hippocampal contextual memory formation. I found that the protein levels of GFAP, a reactive astrocyte marker, were significantly decreased in the hippocampus of the test group at 1 hour after the conditioning test compared with the control group (Fig. 1-4b).

Long-term memory induction strengthened synaptic connectivity of hippocampal neurons. The protein levels of PSD-95, a major post-synaptic scaffolding protein, was evaluated in the hippocampus after fear conditioning was performed [120]. PSD-95 protein level was significantly increased at 1 hour and at 24 hours (Fig 1-4b).

The protein level of EAAT2, glutamate transporter which is specifically expressed in astrocytes [121, 122], was increased at 1 hour and 24 hour (Fig. 1-5b), while EAAT1 did not show any changes (data not shown). Cx43 is a major gap junction protein that connects astrocytes. Recently, it has been reported that Cx43 not only serves as a gap junction protein but also exerts functions as a hemichannel to affect neuron functions during inflammation [123]. The protein level of Cx43 was not significantly increased at 1 hour in the test group. But it was increased at 24 hour (Fig. 1-5b). Taken

together, these data suggest that during the formation of contextual fear memory formation, astrocytes change dynamically with reduced protein levels of GFAP and increased levels of EAAT2 and Cx43 proteins. This appears to be a different status of astrocytes from the typical resting or reactive states.

4. LAA injection into the dentate gyrus inhibited the contextual fear memory expression after the fear conditioning

L-α-aminoadipate (LAA), a glutamate analogue, has been generally accepted to exert astrocyte-specific toxicity, although the exact mechanism is not fully elucidated [124-126]. 20 μg of LAA was injected into the dentate gyrus via stereotaxic surgery. Forty-eight hours after the injection, I evaluated the protein levels of GFAP and NeuN via Western blotting and immunohistochemistry (Fig. 1-6a, b). The protein level of GFAP was significantly decreased by LAA injection by approximately 70 %, while that of NeuN was not significantly altered. This result was also confirmed with immunohistochemistry (Fig. 1-6c). These data indicate that LAA injection into the dentate gyrus specifically reduced the numbers of astrocytes but not of neurons.

I performed contextual fear conditioning test with the control and LAA-injected mice groups. The timetable for LAA injection and contextual conditioning is shown in Fig. 1-7a. Motor function did not show a significant difference between the control and LAA-injected mice group during fear conditioning (Fig. 1-7b). There was no significant difference in the freezing time between the control and LAA-injected group during fear conditioning (Fig. 1-8a). However, in the test, 24 hours after fear conditioning, the LAA group showed significantly decreased time freezing compared to the vehicle-treated control group (Fig. 1-8a)

(a)

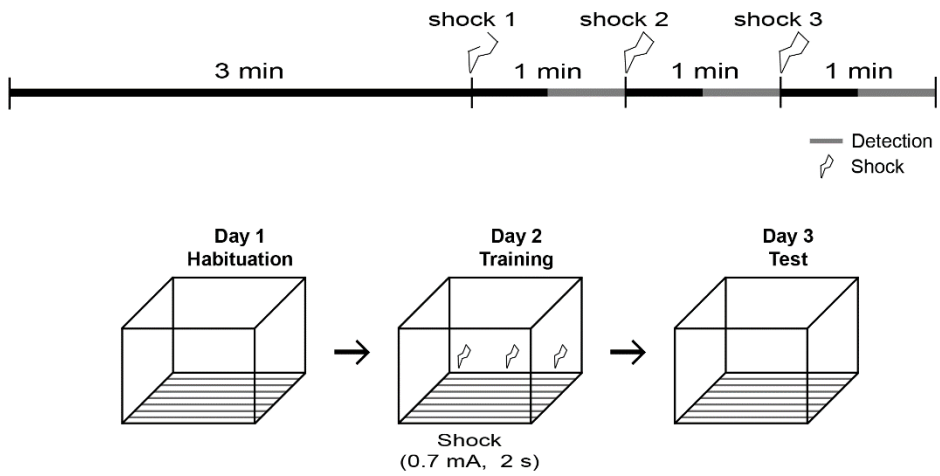
shock 1
shock 2
shock 3
3 min
1 min
1 min
1 min
Detection
Shock
Day 1
Habituation
Day 2
Training
Day 3
Test
Shock
(0.7 mA, 2 s)

(b)

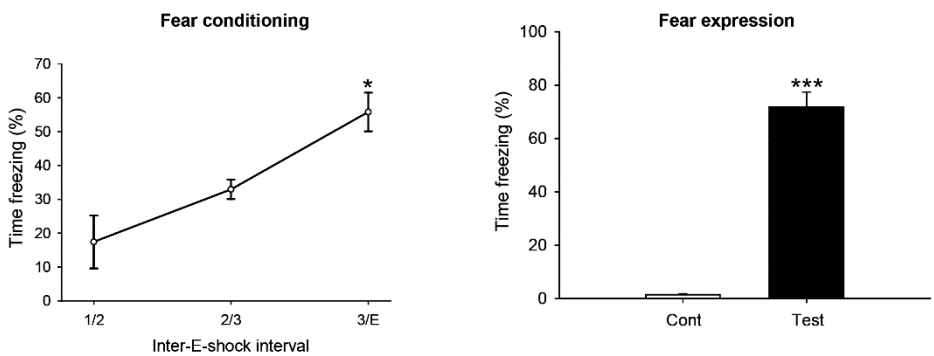
Fear conditioning
Time freezing (%)
70
60
50
40
30
20
10
0
*
1/2
2/3
3/E
Inter-E-shock interval
Fear expression
Time freezing (%)
100
80
60
40
20
0
***
Cont
Test

Figure 1-1. Fvb/n mice were trained to contextual fear conditioning

(a) Illustration of the scheme for contextual fear conditioning test (b) At training day, mice displayed the increased freezing time at 1^{st} and 2^{nd} electric shocks (1/2), the 2^{nd} and 3^{rd} (2/3) and after the 3^{rd} electric shocks (3/E) 1/2, 2/3 and 3/E, (17.43 ± 7.86 %, 32,95 ± 2.88 % and 55.83 ± 5.72 %, N=10), At teat day, the test group exhibited the increased freezing (71.786 ± 3.84 %, N=10, ***p<0.001), compared to the control group (4.817 ± 0.447 %). The data are displayed as the mean ± SEM.

(a)

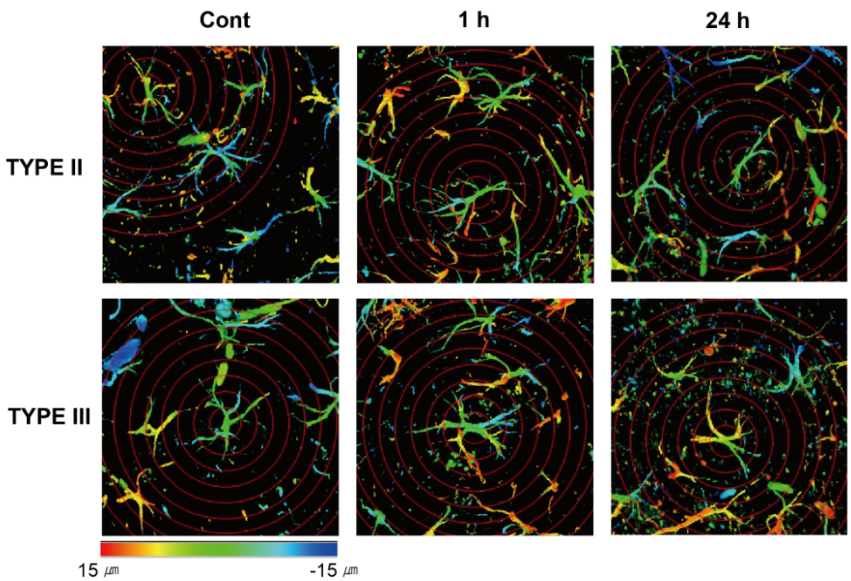
Cont
1 h
24 h
TYPE II
TYPE III
15 μm
-15 μm

(b)

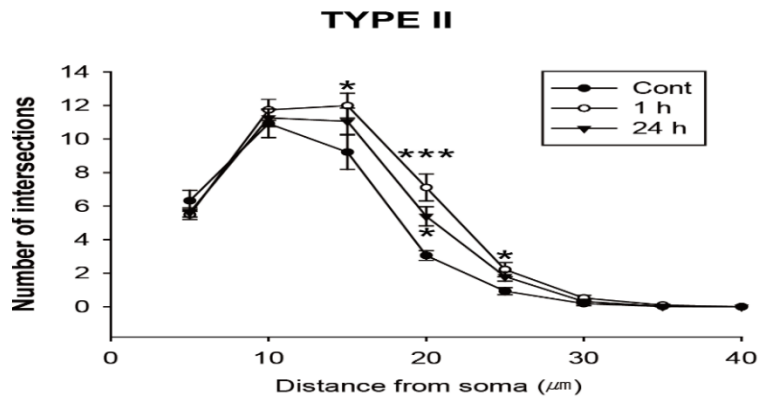
TYPE II
Number of intersections
Distance from soma (μm)
Cont
1 h
24 h
0
2
4
6
8
10
12
14
0
10
20
30
40
*
***

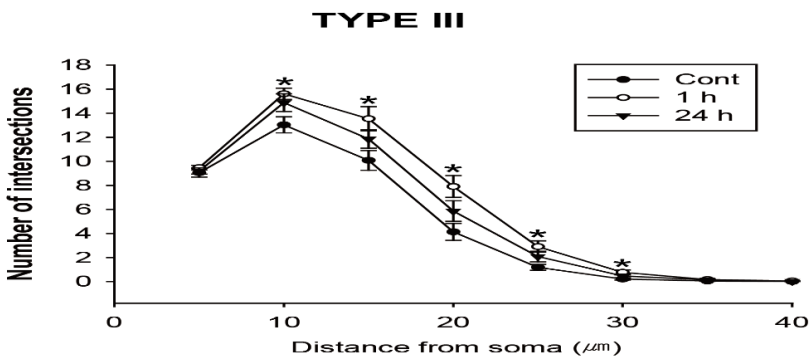
TYPE III
Number of intersections
Distance from soma (μm)
Cont
1 h
24 h
0
2
4
6
8
10
12
14
16
18
0
10
20
30
40
*

Figure 1-2. Morphological changes in astrocytes were detected in the hippocampal dentate gyrus

(a) Morphological analysis of type II and type III astrocytes by sholl analysis., Concentric circles are spaced at 10 μm). (b) The number of intersections between each circle and processes of type II astrocytes in dentate gyrus from control, 1 hour and 24 hour groups at 15 μm (control: 9.216 ± 1.023, 1 hour: 11.988 ± 0.737 $*p<0.05$). At 20 μm (control; 3.056 ± 0.285, 1 hour; 7.106 ± 0,798 $***p<0.001$), 24 hour; 5.391 ± 0.569, $*p<0.05$). At 25 μm (control: 0.929 ± 0.0213, 1h; 2.217 ± 0.420, $**p<0.01$)) (control, N=9, 1 hour, N=10, 24 hour, N=8). (C) the number of intersections between each circle and processes of type III astrocyte in the dentate gyrus from control, 1 hour and 24 hour group, at 15 μm (control; 13.036 ± 0.669, 1 hour; 15.618 ± 0.473, $**p<0.01$). At 15 μm (control; 10.083 ± 0.821, 1 hour 13.543 ± 0.998, $*p<0.05$). At 20 μm (control, 4.132 ± 0.704, 1 hour; 7.906 ± 0.908, $*p<0.05$). At 25 μm (control; 1.184 ± 0.248, 1 hour; 2.905 ± 0.476, $*p<0.05$). At 30 μm (control; 0.207 ± 0.081, 1 hour; 0.767 ± 0.199, $*p<0.05$) (control, N=10, 1 hour, N=12, 24 hour, N=10). The data are displayed as the mean ± SEM.

(a)

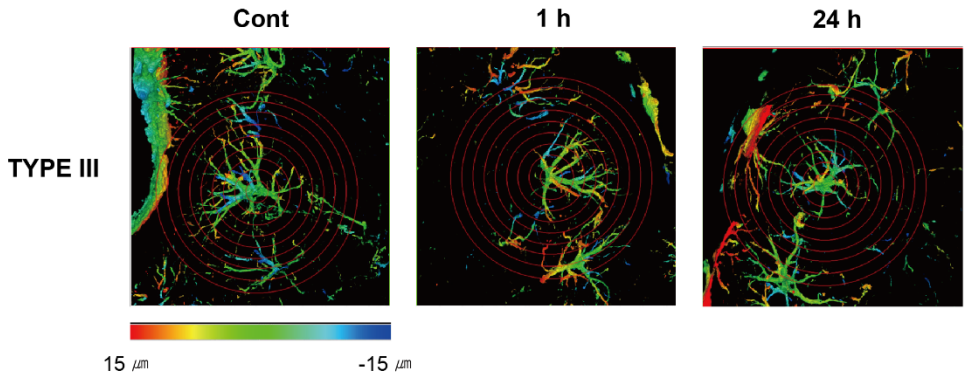
Cont
1 h
24 h
TYPE III
15 μm
-15 μm

(b)

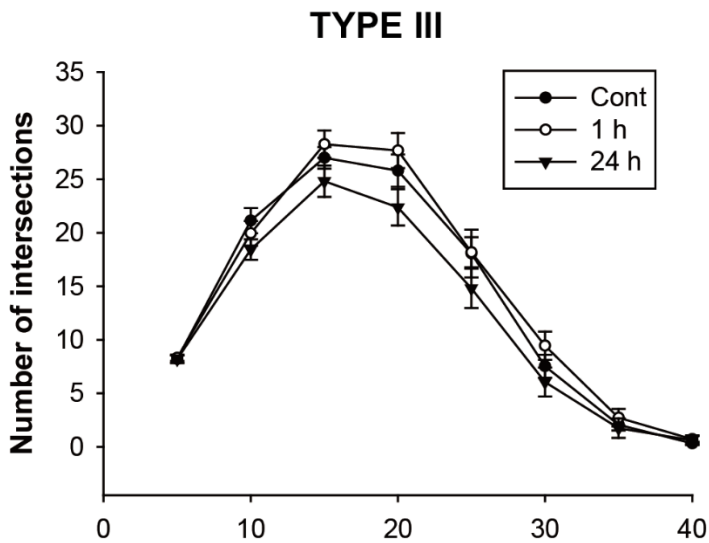
TYPE III
Number of intersections
35
30
25
20
15
10
5
0
0
10
20
30
40
Cont
1 h
24 h

Figure 1-3. Morphological changes in astrocytes were examined in the auditory cortex

(A) Morphological analysis of type III astrocytes by a Sholl analysis. (Immunofluorescence for GFAP, gradation from red to blue; depth of Z-projection is 0-30 μm, Concentric circles are spaced at 10 μm). (B) Number of intersections between each circle and processes of type III astrocytes in auditory cortex from control, 1 hour and 24 hour groups at 10μm (control; 21.133 ± 1.171, 1 hour; 19.955 ± 1.150, 24 hour; 18.438 ± 0.953). At 15μm (control; 27.000 ± 1.009, 1 hour; 28.273 ± 1.269, 24 hour; 24.813 ± 1.461). At 20μm (control; 25.800 ± 1.509, 1 hour; 27.682 ± 1.641, 24 hour; 22.375 ± 1.695). At 25μm (control; 18.067 ± 2.233, 1 hour; 18.182 ± 1.411, 24 hour; 14.813 ± 1.844). At 30μm (control; 7.533 ± 1.077, 1 hour; 9.455 ± 1.314, 24 hour; 6.063 ± 1.349) (control, N=7, 1 hour, N=8, 24 hour, N=7). The data are displayed as the mean ± SEM.

(a)

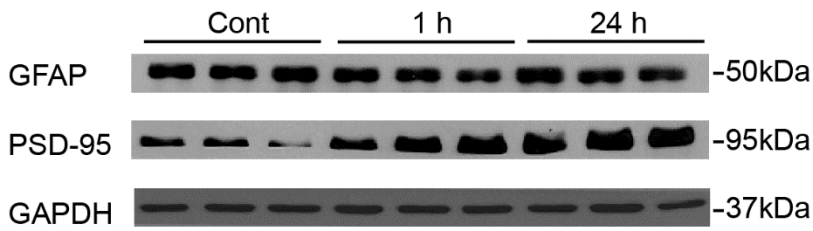
Cont
1 h
24 h
GFAP
-50kDa
PSD-95
-95kDa
GAPDH
-37kDa

(b)

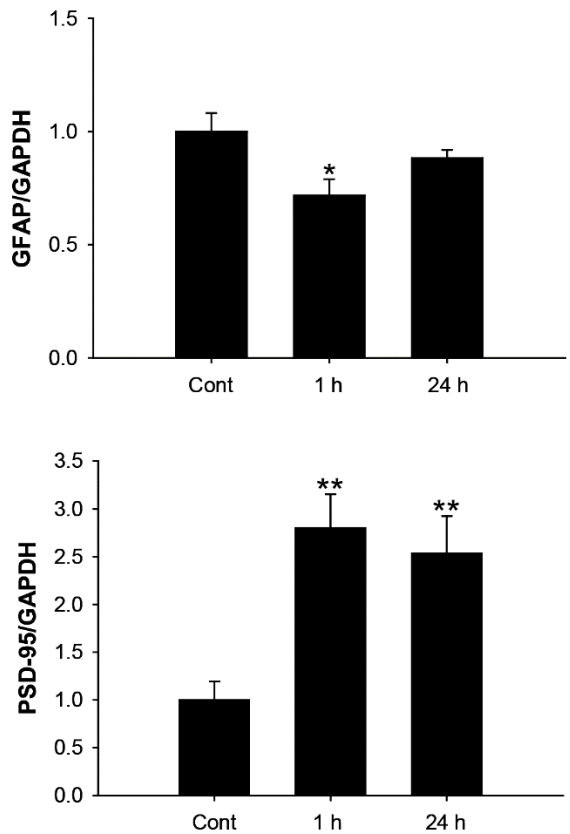
GFAP/GAPDH
1.5
1.0
0.5
0.0
*
Cont
1 h
24 h
PSD-95/GAPDH
3.5
3.0
2.5
2.0
1.5
1.0
0.5
0.0
**
**
Cont
1 h
24 h

Figure 1-4. Protein expression of GFAP and PSD-95 were altered in the hippocampus by contextual fear conditioning

(A) Representative immunoblots for GFAP, PSD-95 and GAPDH for control, 1 hour and 24 hour groups. (B) Densitometric analysis of immunoblots for GFAP (control, 1.000 ± 0.8198, 1 hour, 0.7173 ± 0.07201, $*p<0.05$, N=9) and PSD95 (control; 1.000 ± 0.193, 1 hour; 2.800 ± 0.352, $**p<0.01$, 24 hour; 2.535 ± 0.388, $*p<0.05$, N=9). The data are displayed as the mean ± SEM.

(a)

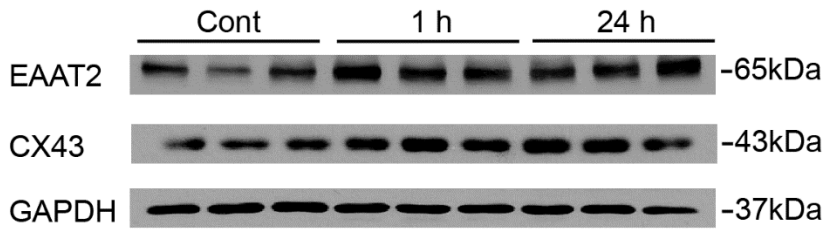
Cont
1 h
24 h
EAAT2
-65kDa
CX43
-43kDa
GAPDH
-37kDa

(b)

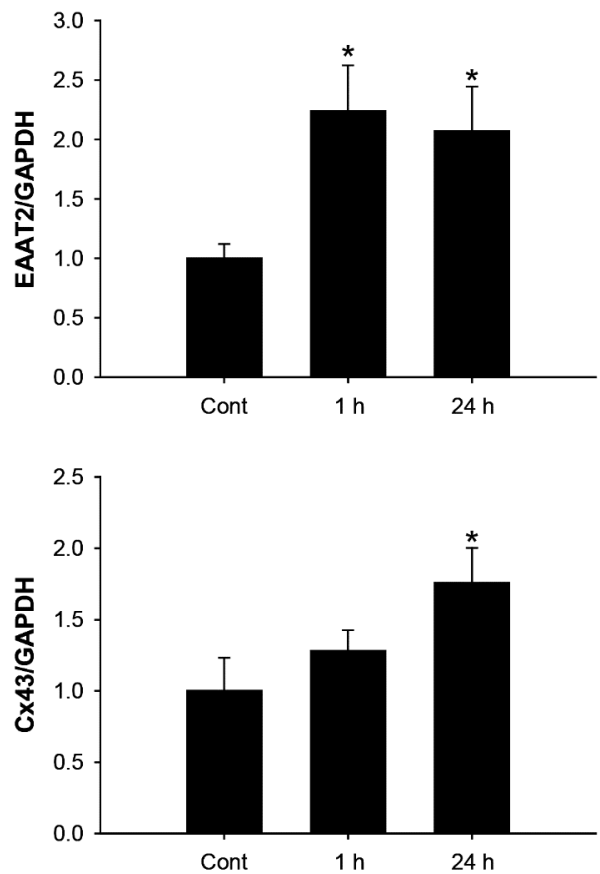
EAAT2/GAPDH
3.0
2.5
2.0
1.5
1.0
0.5
0.0
*
*
Cont
1 h
24 h
Cx43/GAPDH
2.5
2.0
1.5
1.0
0.5
0.0
*
Cont
1 h
24 h

Figure 1-5. Protein expression of EAAT2 and CX43 were altered in the hippocampus by contextual fear conditioning

(a) Immunoblots for EAAT2, Cx43 and GAPDH for control, 1 hour and 24 hour groups. (b) Densitometric analysis of immunoblots for EAAT2 (control; 1.000 ± 0.121, 1 hour; 2.238 ± 0.386, $*p<0.05$, 24 h; 2.070 ± 0.377, $*p<0.05$, N=6) and Cx43 (control; 1.000 ± 0.233, 1 hour; 1.280 ± 0.146, 24 hour; 1.759 ± 0.245, $*p<0.05$). The data are displayed as the mean ± SEM.

(a)

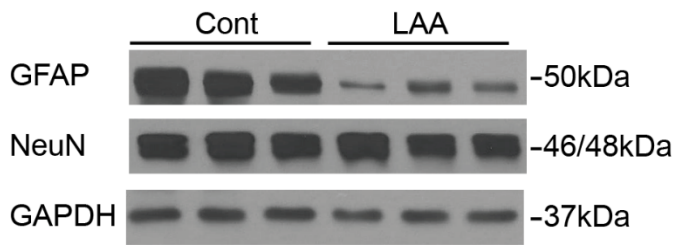
Cont
LAA
GFAP
-50kDa
NeuN
-46/48kDa
GAPDH
-37kDa

(b)

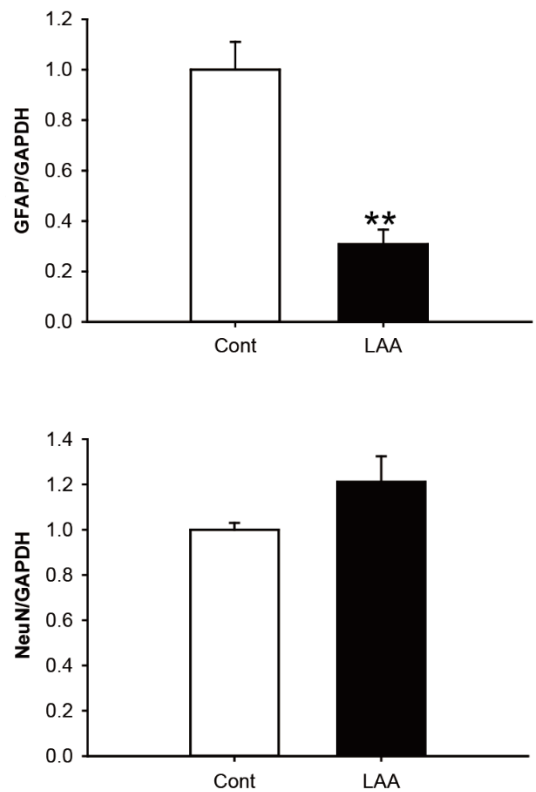
GFAP/GAPDH
1.2
1.0
0.8
0.6
0.4
0.2
0.0
**
Cont
LAA
NeuN/GAPDH
1.4
1.2
1.0
0.8
0.6
0.4
0.2
0.0
Cont
LAA

(c)

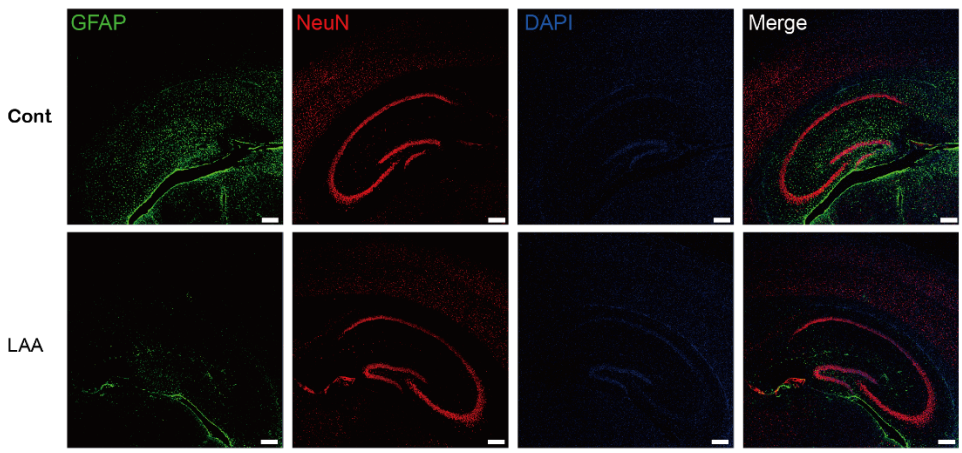

Figure 1-6. LAA injection in the dentate gyrus reduced the population of astrocytes but not that of neurons

(a) Representative immunoblots for GFAP, NeuN and GAPDH in hippocampus for the control and LAA groups. (b) Densitometric analysis of immunoblots for GFAP (control; 1.000 ± 0.11, LAA; 0.307 ± 0.058, $**p<0.01$, N=5) and NeuN (control; 1.000 ± 0.011, LAA; 1.285 ± 0.021, N=5). (c) Immunofluorescence for GFAP, NeuN and DAPI in hippocampus for the control and LAA groups. The data are displayed as the mean ± SEM.

(a)

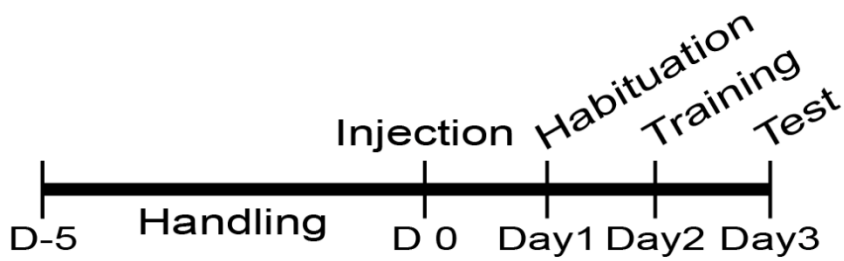
Injection
Habituation
Training
Test
D-5
Handling
D 0
Day1
Day2
Day3

(b)

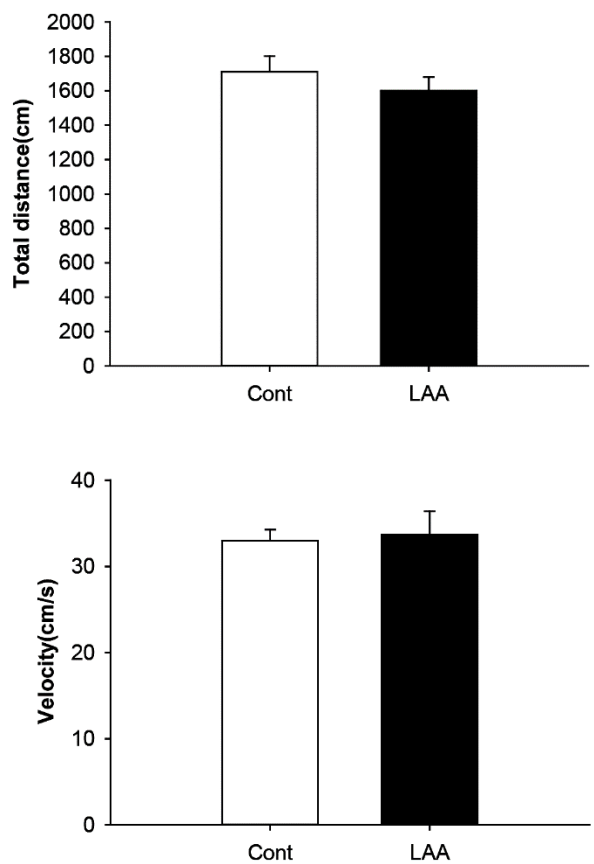
Total distance(cm)
2000
1800
1600
1400
1200
1000
800
600
400
200
0
Cont
LAA
Velocity(cm/s)
40
30
20
10
0
Cont
LAA

Figure 1-7. LAA injection did not affect the motor function

(a) Schedule for contextual fear conditioning with control and LAA- injected mice. (b) The total distance was examined for both control and LAA group with auto-tracking system in Ethovision. (control; 1711.334 ± 90.161, LAA; 1600.309 ± 80.135, N=10). The velocity was calculated for the control and LAA groups with the auto-tracking system in Ethovision (control; 32.997 ± 1.281, LAA; 33.680 ± 2.735, N=10). The data are displayed as the mean ± SEM.

(a)

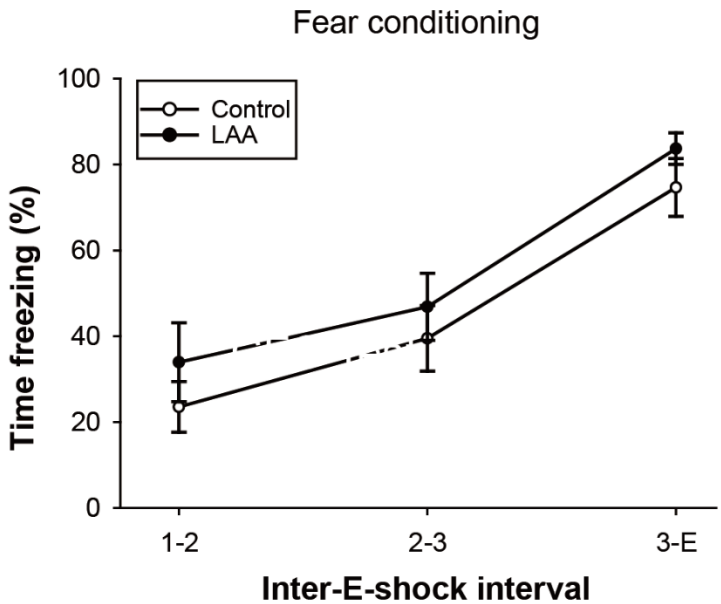
Fear conditioning
Control
LAA
Time freezing (%)
100
80
60
40
20
0
1-2
2-3
3-E
Inter-E-shock interval

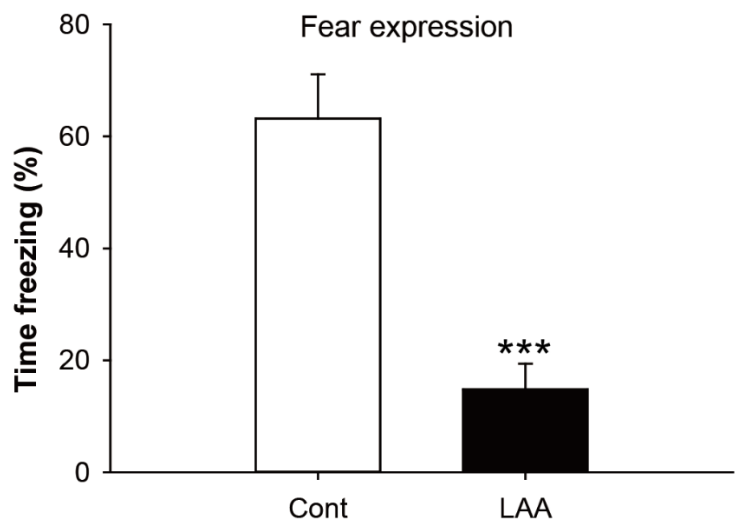
Fear expression
Time freezing (%)
80
60
40
20
0
***
Cont
LAA

Figure 1-8. LAA injection in the dentate gyrus reduced the expression of fear memory after contextual fear conditioning

(a) During fear conditioning, the control and LAA groups displayed increased time freezing at 1^{st} and 2^{nd} electric shocks (1/2), the 2^{nd} and 3^{rd} (2/3) and after the 3^{rd} electric shocks (3/E) (control; (1/2) 25.54 ± 5.888%, (2/3) 29.51 ± 7.649%, (3/E) 74.66 ± 6.732%, LAA; (1/2) 34.00 ± 9.110%, (2/3) 47.00 ± 7.824%, (3/E) 83.63 ± 3.698%, N=10). During fear expression, after 24 hours the electric shock, the control and LAA groups showed increased time freezing (control; 63.169 % ± 7.911%, LAA; 14.784 % ± 4.610 %, ***p<0.001, N=10). The data are displayed as the mean ± SEM.

DISCUSSION

In the present study, I investigated the morphological and molecular changes in astrocytes based on the hypothesis that these changes are accompanied by long-term memory induction in the dentate gyrus of the hippocampus. Fvb/n mice were exposed to contextual fear conditioning test, and checked for morphological and molecular changes in astrocytes. I found that 1 hour after fear conditioning, type II and type III astrocytes exhibit a unique status with an increased number of processes and decreased protein level of GFAP which differ from the typical resting or reactive states. The reactive state of astrocyte is known to show increased GFAP expression level [127]. However, my results showed that hippocampus-dependent contextual memory induced increased intersections of type II and type III astrocytes but decreased GFAP protein levels were observed. In addition, I also found that the protein levels of EAAT2 and Cx43 were increased. Previously, it has been reported that physical exercise improved learning and memory capability and induced an increase in the number of astrocyte processes [128]. Taken together, these results suggest that an altered astrocytic state

is necessary to induce the learning and memory process. In a recent MRI study in humans and rodents, Sagi et al showed that the complexity of the hippocampal dentate gyrus was increased after acquisition of spatial memory [129]. In addition, the intensity of GFAP protein was increased in the hippocampus in an immunofluorescence study.

In my study, I used confocal laser scanning microscopy. A live imaging system such as two-photon confocal laser scanning microscopy is needed to observe dynamic morphological changes of hippocampal astrocytes during contextual memory formation.

The increased number of astrocyte processes suggest an increase in the interaction with neurons, i.e. number of tripartite synapses. In addition, other studies have demonstrated that improved learning and memory capability is accompanied by the increased number of astrocyte processes. Further study with high resolution, such as at the electron microscope level is needed to image invasion into tripartite synapse structure. Additionally, the mechanism between the increased number of astrocyte processes and decreased expression of GFAP observed in the current study remains unclear.

These morphological and molecular changes during memory induction in astrocytes might involve increased action potentials on neurons. Neurons with action potentials increase the secretion of neurotransmitters, especially glutamate from presynaptic terminals [130]. Glutamate released from presynaptic terminals binds to glutamate receptors and is uptaken via EAATs in astrocytes [131]. These receptors bind glutamate to promote the intracellular calcium level in astrocytes [132]. The increased calcium levels promote functional changes in astrocytes as changes in gene expression and gliotransmitter release. This phenomenon is one of the mechanisms for the molecular changes in the expression of EAAT2 and Cx43 on astrocytes. The increased EAAT2 protein expression on astrocytes might reduce excitotoxicity at synapses. The increased Cx43 protein expression on astrocytes might be responsible for the spread of signals around astrocytes to harmonize such function as glutamate uptake or gliotransmitter release. LAA is well known to exert astrocyte-specific toxicity. A previous report showed that 20 μg of LAA was injected into the dentate gyrus to reduce the number of astrocytes in this area [133]. I confirmed that LAA-injected mice group showed a significant decreased freezing

time in the test day of contextual fear conditioning test. The reason of cognitive impairment of LAA injected mice are supposed the absence of gliotransmitter as $_{D}$-serine from astrocytes. The $_{D}$-serine has the important function to modulate LTP in hippocampal neurons. The one of main reason of cognitive impairment are suggested the neuronal dysfunction as the alteration of LTP [134-136]. These data suggest that the presence of astrocyte is critically required for the formation of long-term memory. The results shown in Chapter 1 and the hypothesis for the study of Chapter 2 are summarized in Graphical Summary as below.

Collectively, the increased numbers of astrocyte processes and the decreased GFAP expression level in the dentate gyrus are correlated with hippocampal dependent long-term memory induction. These morphological and biological changes, i.e., the altered protein level of GFAP was returned to the control level at 24 hour. The characteristics of astrocytes observed in the current study are different from the resting or reactive states of astrocytes. Thus, a dynamic change from the memory induction state astrocyte is correlated with the induction of long-term memory.

These results show that hippocampus-dependent contextual

fear memory process results in the changes in the status of astrocytes towards a novel status different from typical resting or reactive states. These morphological and molecular changes may be in line with functional changes. In Chapter 2, I investigated the relationship between reactive astrocytes and cognitive impairments using an AD animal model, 5XFAD mice. Morphological and molecular changes were investigated in astrocytes after memory induction by a hippocampus-dependent contextual fear conditioning test. In addition, the interaction between neurons and astrocytes at synapses was also evaluated.

CHAPTER 1 GRAPHICAL SUMMARY

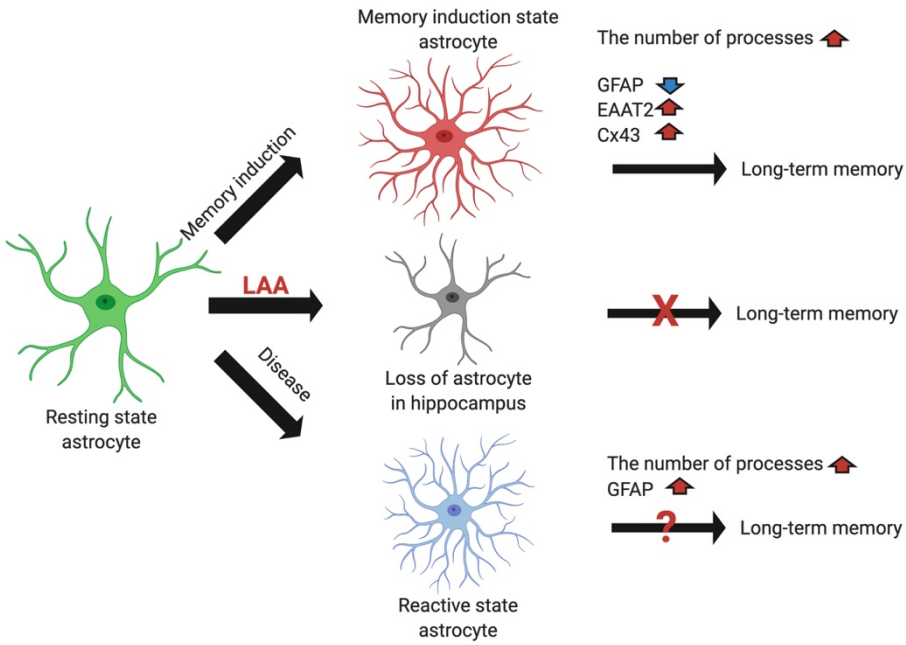

Graphical Summary: Chapter 1

The dynamics of molecular and morphological change in astrocytes after memory induction

CHAPTER 2

Pathophysiological role of reactive astrocyte in Alzheimer's disease model

INTRODUCTION

Reactive astrocytes often observed in AD brains are thought to lose neuroprotective functions of astrocytes in resting state including uptake and degradation of Aβ[137]. Resulting accumulated Aβ in turn stimulates to induce pro-inflammatory factors in glial cells [138]. Astrocytes are reported to be activated into the reactive state via JAK/STAT3, NF-κB, MAPK and NFAT pathways [139].

Reactive astrocytes show functional and morphological changes as a result of diversity of brain insults. The characteristics of reactive astrocytes is represented by increased gene expression of a number of structural proteins, such as GFAP and vimentin. Also, reactive astrocytes show the morphological changes, such as hypertrophy of the cell soma and increased the number of processes. Proliferation of astrocytes is especially important in the formation of scar formation around tissue lesions [7, 140-142].

However, complicated mechanisms underlying the transition from the resting state to the reactive state of astrocyte in neurodegenerative diseases largely remain unclear. Additionally, how reactive astrocytes affect cognitive function

apart from their neurotoxic effects remains still unclear.

I investigated which pathways are involved in the activation of astrocytes into reactive astrocytes in the context of AD. Oligomeric Aβ (oAβ) was treated to primary cultured astrocytes. oAβ-treated astrocytes was activated into reactive state via phosphorylated signal transducer and activator of transcription 3 (p-STAT3). The inhibition of STAT3 to oAβ-treated astrocytes attenuated the activation of astrocytes into reactive astrocytes. In addition, systemic administration of Sttatic, an inhibitor of STAT 3, for 14 days attenuated the impairment of cognitive function in 6-month-old 5XFAD mice as assessed by contextual fear conditioning test.

MATERIALS AND METHODS

1. Reagents and antibodies

Protein isolation with RIPA lysis buffer was purchased from Elpis biotech (#EBA-1149, Daejeon, Korea) and Pierce™ BCA Protein Assay Kit was purchased from Thermo (#23227, MA, USA). Anti-GFAP, rabbit polyclonal antibody was purchased from DAKO (#Z0334, CA, USA). Anti-NeuN rabbit monoclonal antibody, synaptophysin mouse monoclonal antibody were purchased from Millipore (#3838 and #MAB329, MA, USA). Anti-PSD-95, mouse monoclonal antibody, anti-rabbit, goat polyclonal tagged Alexa Fluor 488, anti-mouse, goat polyclonal tagged Alexa Fluor 555 and 4’. 6-diamidino-2-phenylinodole (DAPI) were purchased from ThermoFisher (#MA1-046, #A11034, #A11012, #A21426 and #D3571, MA, USA). Anti-GAPDH, rabbit polyclonal antibody was purchased from AbFrontier (#LF-PA0018, Seoul, Korea). Rabbit polyclonal antibody was purchased from WAKO (#016-20001, Osaka, Japan). Anti-mouse, sheep polyclonal horseradish peroxidase (HRP) tagged antibody was purchased from Abcam (#ab26116, #ab26113 and #ab6808, EA, UK). Anti-p-STAT3 (Tyr 705), STAT3, p-p44/42, p44/42 rabbit polyclonal

antibody was purchased from Cell signaling (#9145, #12640, #4377 and #4695 MA, USA). Anti-NF-κB mouse monoclonal, Anti-BACE1 rabbit polyclonal antibodies were purchased from Santa Cruz (#sc-7151, Taxas, USA). Anti-β-amyloid, 1-16 mouse monoclonal antibody was purchased from Biolegend(#803001, San Diego, USA). Anti-Aβ neutralizing antibody was purchased from BPS Bioscience (#71223, San Diego, USA).

2. Experimental animals

All of the experimental procedures were approved by the Animal Care Committee of Seoul National University (Approval number: SNUIBC-171011-2). Transgenic mice with 5XFAD mutations were purchased from Jackson Laboratories (strain: B6SJL-Tg [APP Sw, Fl, Lon, PS1, M146L, L286V] 6799Vas/J) and maintained by crossing hemizygous transgenic mice with B6SJL F1 mice. Six-month-old male mice were used for the experiments. The mice were housed in four or five per cage with a 12-hour light/dark cycle and ad libitum access to food and water under standard laboratory housing conditions.

3. Primary astrocyte culture

The primary astrocyte culture was described previously [143]. Briefly, primary mixed glial cultures were prepared from postnatal day 1 (P1) C57B/L6 mice. The cortex was dissociated and it was incubated with 0.25% trypsin in 37° C water bath for 20 minutes. The incubated cortex filtered with a cell strainer. The mixed glia cells was grown in Dulbecco's modified Eagle's medium (DMEM), supplemented with 10% (vol/vol) heat-inactivated FBS and penicillin (10 units/ml) and streptomycin (10 mg/ml) in a humidified cell incubator (Binder, Germany) at 37° C under a 5% CO2 atmosphere. When the mixed glia filled 80% of the T75 plate at DIV-14, astrocyte and microglia were separated via a 250 rpm shaking incubator at 37° C for overnight. Microglia were detached from the plate after shaking isolation. The astrocytes were detached with incubation 0.25% trypsin-EDTA at 37° C under a 5% CO2 atmosphere for 5 minutes. Next the astrocytes seeded onto poly-L-lysine coated plates for the experiment.

4. Oral administration of Stattic

Sttatic (25 mg/kg per day) dissolved in drinking water was freely administrated to 6-month-old WT and 5XFAD mice.

Animals were divided into 4 groups consisting of 9–10 mice. WT-vehicle and 5XFAD vehicle, which drank only water, were used as control groups. WT-stattic and 5XFAD-stattic, which drank stattic included water, were used as administration groups. To examine toxicity of Sttatic, water, food intake and body weight was evaluated at 2 weeks. After all groups of mice were scarified the brain weight was measured. Behavior tests were performed after 15 days' treatment.

5. Oligomeric Aβ_{1-42} preparation

oAβ oligomerization was prepared previously described [144, 145]. Synthetic human Aβ1-42 peptide (American Peptide, Sunnyvale, CA, USA) was dissolved to 1 mM in 100% hexafluoro isopropanol (HFIP, Sigma Chemical Company, MO, USA). The solution was evaporated to filmization Aβ in a Speed Vac (SPD2010, Thermo Savant, NY, USA) for 2 hours. The resulting peptide film was stored at −20°C or immediately resuspended in dimethyl sulfoxide (DMSO, Sigma Chemical Company) to produce a 1 mM solution. Then, this solution was diluted to 100 μM in phenol red-free Ham's F-12 medium (Life Technology, NY, USA) and incubated for 12 hours at 4° C.

6. Contextual fear conditioning test

Contextual fear conditioning test was performed as previously described [7]. Briefly, all experimental animals had been handling for 5 days before preforming contextual fear conditioning test. Prior to training, all 4 groups mice were positioned into the chamber (13 × 13 × 25 cm) for 10 min to habituation. On the second day, each mouse was positioned in the conditioning chamber for 3 min and acquired three repetitions of a foot-shock (0.7 mA, 2 sec) at 1 min intertrial intervals during the training day. On the next day, the trained mice were positioned in the same chamber, and the freezing behavior was measured over periods of 3 min. The freezing behavior was defined as immobility except for respiratory movements. The latency of total freezing time was analyzed as a percentage in the test period. The all groups mice were sacrificed after the test day.

7. T-maze test

T-maze test was performed as previously described [146]. Briefly, prior to training, all four groups mice were placed the room with deem light to habituation for 1 hour. The testing

mice was positioned at the starting zone. After the mice choose one way, the way was blocked and the mice stay for 30 sec. During clean the T-maze with 30% EtOH, the mice stayed in the home cage for 1 min and return into the starting zone. If the mice chose the other way, it will get 1 point. If the mice chose the same way, it will get 0 point. This trial performed the next day.

8. Western blotting

Western blotting analysis was described previously [146]. Briefly, the mice were anesthetized with Zoletil (12.5 mg/kg) and Rompun mix (17.5 mg/kg) and the dissected brain tissues were stored at -80° C before protein lysis. Hippocampi were homogenized with RIPA mix including as protease inhibitor, Sodium fluoride, phenylmethylsulfonyl fluoride and sodium orthovanadate. The primary antibodies were applied in the following concentrations: anti-GFAP (rabbit, 1: 5,000), anti-NeuN (rabbit, 1: 1,000), anti-p-STAT3 (rabbit, 1:1,000), anti-STAT3 (rabbit, 1:1,000), anti-p-p44/42 (rabbit, 1:1,000), anti-p44/42 (rabbit, 1:1,000), anti-p-p65 (rabbit, 1:1,000), anti-p65 (rabbit, 1:1,000), anti-PSD95 (mouse, 1:2,000), anti-synaptophysin (mouse, 1:2,000), anti-Aβ

(mouse 1:1,000), anti-BACE1 (rabbit, 1:1,000), anti-GAPDH (rabbit, 1:10,000). Secondary antibodies were conjugated with HRP (1: 2,000). The HRP signals were visualized using an enhanced chemiluminescent substrate.

9. Immunofluorescence

The protocol was previously described in the paper by Choi et al [7]. The brains were perfused with heparin dissolved in PBS (pH 7.2) for 5 min were fixed with 4 % paraformaldehyde for 24 hours. The fixed brains were transferred into 30 % sucrose solution for 48 hours. The brain tissue was sectioned into 30 μm thick slices with a cryotome with the chamber at -20° C and the bar temperature at -25° C.

For GFAP and NeuN staining, the brain sections were heated in a 95° C water bath for 30 min with 10 mM citrate acid (pH 6.0) for antigen retrieval. The sections were blocked with 2 % BSA and 0.3 % Triton X-100 in PBS for 1 hour. Primary antibodies GFAP (1:1,000) and NeuN (1:500) were applied overnight at 4° C. Secondary antibodies, anti-rabbit-488 (1:200) and anti-mouse-555 (1:200) were applied for 2 hours at room temperature. For p-STAT3 and GFAP staining, the brain sections were permeabilized with MetOH in -20° C for

20 min. The permeabilized brain sections heated in 85° C water bath for 10 min with 10 mM sodium citrate (pH 8.5) for antigen retrieval. The sections were blocked with 2 % BSA and 0.3 % Triton X-100 in PBS for 1 hour. Primary antibodies p-STAT3 (1:200) and GFAP (1:1,000) were applied overnight at 4° C. Secondary antibodies, anti-rabbit-488 (1:200) and anti-goat-555 (1:200) The stained brain tissue samples were imaged with confocal microscopy using LSM 510 (Carl Zeiss, Germany) or A1 (Nikon, Japan).

10. Statistical analysis

Data are expressed as the mean ± SEM (means ± standard error of the mean). One-way ANOVA followed by Tuckey post hoc analysis or Student's t-test (SPSS, IL, USA) was performed to determine statistical significance. The results were considered to be statistically significant at $p<0.05$.

EXPERIMENTAL SCHEME

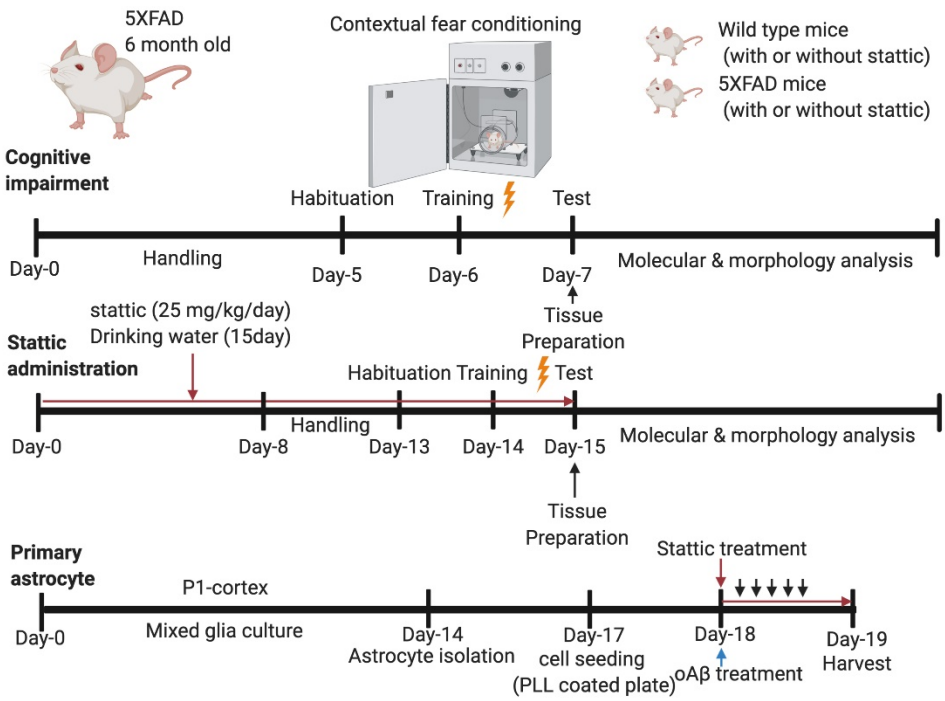

RESULTS

1. Six-month-old 5XFAD mice showed the increase in the reactive astrocytes and the impairments in hippocampal dependent long-term memory formation

First, in order to determine which cell type is altered in the hippocampi of 6-month-old WT and 5XFAD mice, I evaluated the protein expression of GFAP and NeuN. 5XFAD mice shown an increase in reactive astrocytes as compared to the WT group as assessed by the protein expression of GFAP. However, the protein level of NeuN was not different between WT and 5XFAD mice (Fig. 2-1a, b). Next, I stained the brain slices of 6-month-old 5XFAD mice and age matched WT mice with GFAP, NeuN and DAPI and assessed immunofluorescence. Consistently, GFAP immunoreactivity was higher in 5XFAD mice than in WT mice, whereas NeuN immunoreactivity was not different between the WT and 5XFAD groups (Fig. 2-1c). Even in the absence of neuronal loss in the hippocampus, neuronal function can be altered by the degradation of synaptic proteins. Thus, I evaluated the protein levels of synaptophysin, presynaptic maker and PSD-95, postsynaptic marker. respectively, to determine whether the pre- or

postsynaptic components are altered and damaged in the hippocampus of 6-month-old WT and 5XFAD mice. Altered protein expression was not observed for both synaptic marker proteins expression such as PSD-95 and synaptophysin in 6-month-old 5XFAD mice (Fig. 2-2a, b).

To test hippocampus-dependent long-term spatial memory, contextual fear conditioning test was performed with 6-month-old WT and 5XFAD mice. The time schedule of contextual fear conditioning test is shown (Fig. 2-3a). First, I analyzed the time of freezing behavior at intervals between every electric shock on the training day. WT group mice showed a significant increase the freezing time throughout the training session. The 5XFAD mice group also showed a significant increase the freezing time throughout the session (Fig. 3b). These results indicate that neither both groups showed not altered short-term memory formation. But both groups were well trained via the contextual fear conditioning test training procedure. The freezing behavior of the WT and 5XFAD mice were analyzed on the test day. 5XFAD mice displayed significantly decreased the freezing time than WT mice (Fig. 2-3c). These results showed that 6-month-old 5XFAD mice increased in reactive astrocytes as assessed by

the protein expression of GFAP, and impaired hippocampal-dependent long-term spatial memory. However, significant differences in neuronal and synaptic marker proteins were not observed.

2. Astrocytes were activated via STAT3 phosphorylation *in vitro* and *in vivo* AD model

Astrocytes are activated into reactive state by cytokines, chemokines and aggregated proteins via the JAK/STAT3, NF-κB, MAPK and NFAT pathways [139]. Primary cultured astrocytes treatment with 250 nM oAβ for 24 hours, I analyzed the protein expression of GFAP by western blot. The protein expression of GFAP was significantly increased in oAβ-treated group (Fig. 2-4a and b). Next, I performed western blot to determined which pathways are activated by oAβ treatment in primary cultured astrocytes (Fig. 2-5a). The protein expression of p-STAT3 and STAT3 were significantly increased in oAβ-treated primary cultured astrocytes. However, p-p65, p65, p-ERK and ERK protein expression were not altered (Fig. 2-5b). The protein expression of p-STAT3 and total STAT3 was significantly higher in the hippocampus of 6- month-old 5XFAD mice than in that of WT

mice, while the protein expression of p-p65, p65, p-ERK and ERK was not altered (Fig. 2-6a and b). These results indicated that the STAT3 pathway was activated in the hippocampus of 6-minth-old 5XFAD mice. Then, immunofluorescent experiment was performed to investigate which cell types display p-STAT3 in the brains. It was found that p-STAT3 fluorescent signals were colocalized over approximately 80% in the nucleus of astrocytes statined with GFAP in the hippocampus of 5XFAD mice (Fig. 2-7a and b). The p-STAT3 signal was rarely colocalized with Iba-1 and NeuN in the hippocampus of 6-month-old 5XFAD mice (Fig. 2-7c). These results indicate that astrocytes are activated into a reactive state via STAT3 phosphorylation in 6-month-old 5XFAD mice.

3. Oral administration of Stattic, an inhibitor of STAT3, attenuated the cognitive impairments in 5XFAD mice

STAT3 inhibitors such as Stattic, S31-201 and crypotanshinone have been developed and used for breast and prostate cancer therapy [147, 148]. Primary cultured astrocytes were treated time-dependently with 1μM Stattic from 1 hour to 12 hours (Fig. 2-8a). The p-STAT3 protein

expression was significantly decreased than in those treated with vehicle in Stattic-treated primary cultured astrocytes from 1 hour to 6 hours (Fig. 2-8b). The STAT3 protein expression was not altered from 1 hour to 12 hours. The p-STAT3 and STAT3 ratio was also significantly decreased in Stattic-treated primary cultured astrocytes form 1 hour to 6 hours (Fig. 2-8b). In addition, the GFAP protein expression was significantly decreased in Stattic-treated primary cultured astrocytes from 3 hours to 6 hours (Fig. 2-8b).

The time schedule of administration and behavior tests are shown (Fig. 2-9a). After sacrificed experiment mice, the hippocampi were removed and STAT3 pathway activated in astrocytes was analyzed. The hippocampi of vehicle-treated 5XFAD mice (5XFAD-V) showed significantly increased expression of p-STAT3 than those of vehicle-treated WT mice (WT-V). Stattic significantly reduced the phosphorylation of STAT3 in Stattic-treated 5XFAD mice (5XFAD-S), although the p-STAT3 levels were still increased than those in WT-V (Fig. 2-9b). The STAT expression was not changed in WT-S, 5XFAD-V and 5XFAD-S (Fig. 2-9b). The protein expression of GFAP was found to be significantly increased in the hippocampi of 5XFAD-V

mice than in those of WT-V mice. Stattic administration significantly reduced the protein expression of GFAP (Fig. 2-9b). These results suggest that the systemic administration of Stattic restored the activation of astrocyte in the hippocampus via the STAT3 pathway.

I confirmed whether Stattic administration exerts detrimental effects in experimental animals. Body weight and brain weight were not significantly different between the vehicle- and Stattic-treated groups over 15 days (Fig. 2-10a). Next, I performed the T-maze test to determine the working memory. The percentage of alternation was significantly decreased in 5XFAD-V than in the WT-V. However, Stattic treatment significantly increased the percentage of alternation in 5XFAD-S compared with 5XFAD-V (Fig. 2-11a). Additionally, I performed the contextual fear conditioning test to determine hippocampal-dependent long-term spatial memory. On the habituation day, all groups displayed similar the time of freezing behavior less than 5% (Fig. 2-11b). On the training day, all groups displayed a significant increase the time of freezing behavior after each electric shock, but this increase the freezing time did not differ significantly among the groups (Fig. 2-11b). On the test day, the time of freezing

behavior was significantly decreased in the 5XFAD-V group than in the WT-V group. However, 5XFAD-S mice displayed a significantly increased the time of freezing behavior than the 5XFAD-V mice (Fig. 2-11b).

These results suggest that administration of Stattic show the effect of Stattic on restoring the working and long-term spatial memory via inhibition of the STAT3 pathway in 5XFAD mice.

4. Oral administration of Stattic restored the activation of astrocytes in 5XFAD mice

Here, I analyzed the activation state of astrocytes and p-STAT3 expression after the systemic administration of Stattic in mice. I performed immunofluorescence analysis to indicate which cell types expression of p-STAT3 protein and the activation of astrocyte were changed by administration of Stattic in 5XFAD mice (Fig. 2-12a). In the hippocampus of both WT-V and WT-S group mice, the expression of p-STAT3 protein was too low to detect. The region of intensity (ROI) of p-STAT3 was significantly decreased in 5XFAD-S mice than in 5XFAD-V mice (Fig. 2-12b). Next, I analyzed the colocalization of p-STAT3 and GFAP after the administration

of Stattic in 5XFAD mice. The colocalization was significantly decreased in 5XFAD-S mice than in 5XFAD-V mice (Fig. 2-12b). GFAP immunoreactivity was significantly increased in the 5XFAD-V group than in the WT-V group. The ROI of GFAP was significantly decreased in 5XFAD-S mice than in 5XFAD-V mice (Fig. 2-12b). In addition, I quantified the characteristic features of reactive astrocytes, such as the number of processes and cell volume. The Z-stack image of GFAP immunofluorescence with brain slice were 3D reconstructed. The number of intersections were analyzed with sholl anlysis. The number of intersections was significantly increased in 5XFAD-V mice and significantly decreased in 5XFAD-S (Fig. 2-13a, b). The Z-stack image of GFAP immunofluorescence with brain slice were processed with IMARIS software. The volume of astrocyte was significantly increased in 5XFAD-V mice and significantly decreased in 5XFAD-S mice (Fig. 2-14a, b). These results suggest that the systemic administration of Stattic has the potential to restore the STAT3 phosphorylation in astrocytes, the increase in reactive astrocytes and cognitive function in 5XFAD.

5. Oral administration of Stattic reversed the decrease in the number of tripartite synapses in the hippocampus of 5XFAD mice

Next, the interaction between PSD-95-positive dendritic spines and GFAP-positive astrocytic processes was analyzed to identify tripartite synapses. Brain slices of contextual fear conditioning-trained WT-V, WT-S, 5XFAD-V and 5XFAD-S were stained with anti-PSD-95 and anti-GFAP antibodies to identify the number of tripartite synapses (Figure 2-15a). These stained brain slices were imaged via Z-stack confocal microscopy. The 3-D reconstructed images were sectioned by the X-Z axis and the interaction of the PSD-95 and GFAP signals in the cross-sections of the hippocampal dentate gyrus images was measured (Figure 2-15b). Intriguingly, the PSD-95 and GFAP interaction was significantly lower in the 5XFAD-V mice than in the WT-V and WT-S mice and recovered to WT-V levels with Stattic treatment (Figure 2-15b). These results indicated that the administration of Stattic has the potential to restore the number of tripartite synapses and cognitive function in AD.

6. Oral administration of Stattic reduced the protein level of

Aβ in 5XFAD mice

Protein level of Aβ and the number of senile plaques was evaluated after systemic administration of Stattic in 6-month-old 5XFAD mice. Thioflavin-S staining was performed to determine the number of senile plaques after Stattic administration in 5XFAD mice (Fig. 2-16a). The number of senile plaques was significantly higher in 5XFAD-V mice than in WT-V mice and found to be significantly decreased in 5XFAD-S (Fig. 2-16b). Next, the protein level of Aβ was analyzed after systemic administration of Stattic in 5XFAD mice by western blotting. The protein level of Aβ was significantly decreased in 5XFAD-S mice than in 5XFAD-V mice (Fig. 2-17a, b). The reduction in Aβ may be caused by deceased production or increased clearance. To determine which mechanisms are involved in the reduced protein level of Aβ, the protein expression of BACE1 was investigated after systemic administration of Stattic in 6-month-old 5XFAD mice. The protein level of BACE1 was significantly decreased in 5XFAD-S mice (Fig. 2-18a, b). These results suggest that the systemic administration of Stattic has a potential to reduce the Aβ production by reducing the expression of BACE1.

(a)

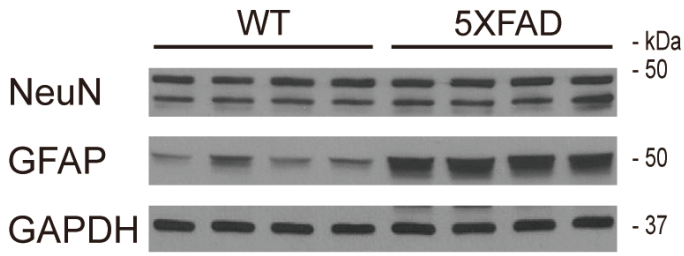
WT
5XFAD
- kDa
NeuN
- 50
GFAP
- 50
GAPDH
- 37

(b)

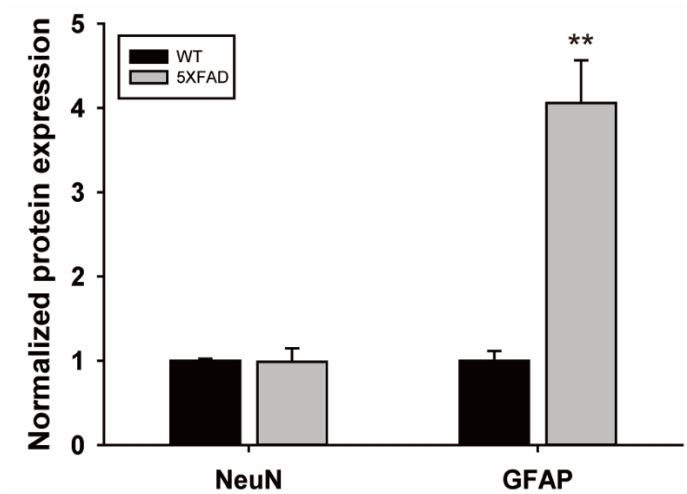
Normalized protein expression
5
4
3
2
1
0
WT
5XFAD
**
NeuN
GFAP

(c)

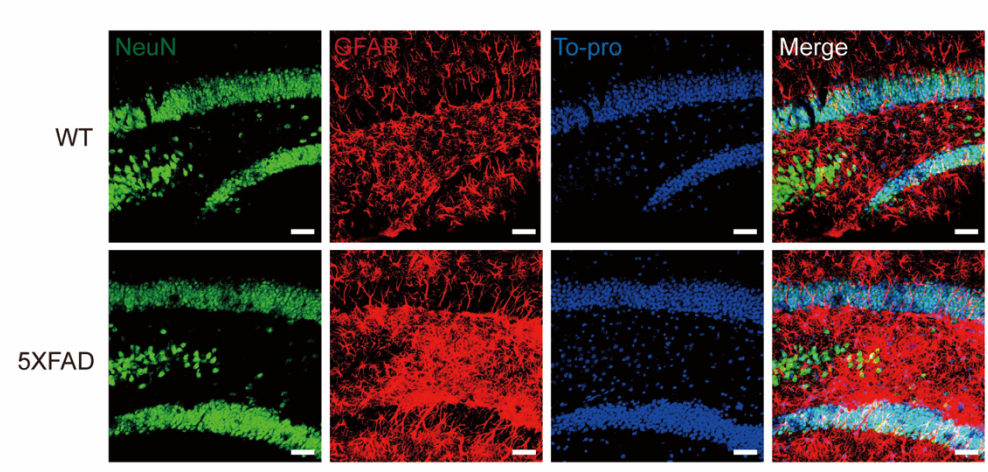

Figure 2-1. Astrocytes were activated without neuronal loss in the hippocampus of 6-month-old 5XFAD mice

(a) Representative immunoblots for neuronal marker NeuN and astrocyte marker GFAP from the WT (N = 7) and 5XFAD (N = 9) hippocampus. (b) Densitometric analysis of immunoblots for NeuN (WT: 1.00 ± 0.024, N=7, 5XFAD: 1.024 ± 0.149, N=9) and GFAP (WT: 1.00 ± 0.159, N=7, 5XFAD: 3.476 ± 0.424, N=9, $**p<0.01$). (c) Immunofluorescence for NeuN and GFAP in the hippocampal dentate gyrus of both WT and 5XFAD mice (scale bar = 50 μm). The data are displayed as the mean ± SEM.

(a)

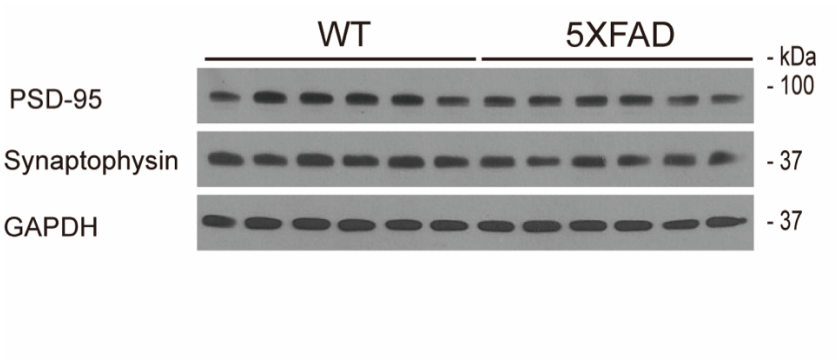
WT
5XFAD
- kDa
PSD-95
- 100
Synaptophysin
- 37
GAPDH
- 37

(b)

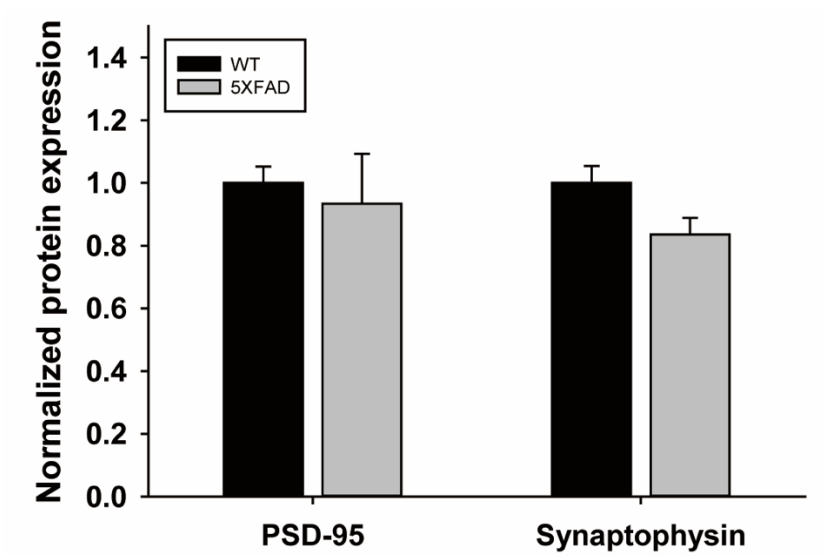
Normalized protein expression
1.4
1.2
1.0
0.8
0.6
0.4
0.2
0.0
WT
5XFAD
PSD-95
Synaptophysin

Figure 2-2. Synaptic proteins were not altered in the hippocampus of 6-month-old 5XFAD mice

(a) Representative immunoblots for postsynaptic marker. PSD-95 and presynaptic marker, synaptophysin from the WT and 5XFAD hippocampus. (N = 6) (b) Densitometric analysis of immunoblots for PSD-95 (WT: 1.00 ± 0.052, N=6, 5XFAD: 0.933 ± 0.159, N=6) and synaptophysin (WT: 1.00 ± 0.054, N=6, 5XFAD: 0.835 ± 0.053, N=6). The data are displayed as the mean ± SEM.

(a)

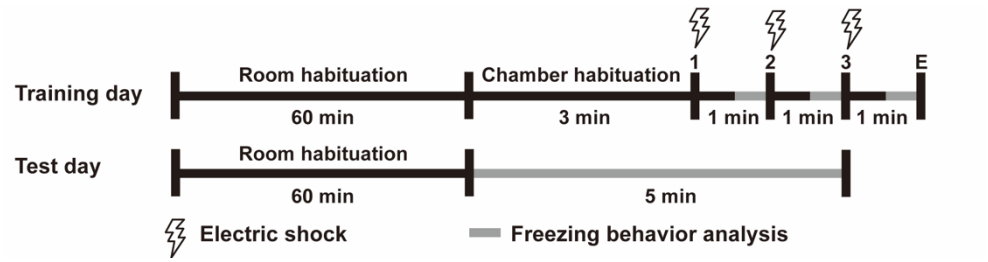
Training day
Room habituation
60 min
Chamber habituation
3 min
1
2
3
E
1 min
1 min
1 min
Test day
Room habituation
60 min
5 min
Electric shock
Freezing behavior analysis

(b)

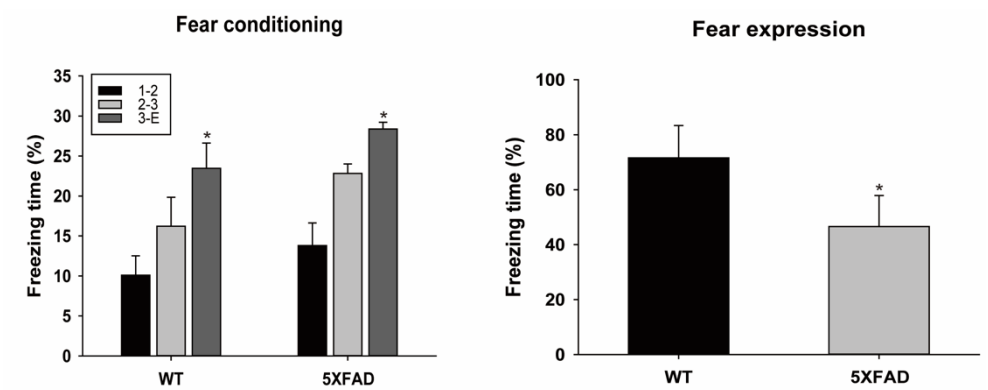
Fear conditioning
Freezing time (%)
1-2
2-3
3-E
WT
5XFAD
Fear expression
Freezing time (%)
WT
5XFAD

Figure 2-3. Cognitive function was impaired when tested with contextual fear conditioning test in 6-month-old 5XFAD mice

(a) A time schedule for the contextual fear conditioning test is shown. (b) Quantification of freezing behavior for fear conditioning (WT: 10.09 ± 2.42 %, 16.23 ± 3.61 % and 23.46 ± 3.16 %, N=10, $*p<0.05$, 5XFAD: 13.80 ± 2.83 %, 22.82 ± 1.18 % and 28.38 ± 0.84 %, N=10, $*p<0.05$) and expression (WT: 79.27 ± 10.29 %, n =10, 5XFAD: 39.28 ± 9.87 %, N=10, $*p<0.05$) in age-matched 6-month-old WT and 5XFAD mice. The data are displayed as the mean ± SEM.

(a)

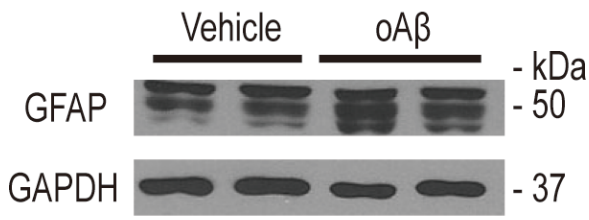
Vehicle
oAβ
- kDa
GFAP
- 50
GAPDH
- 37

(b)

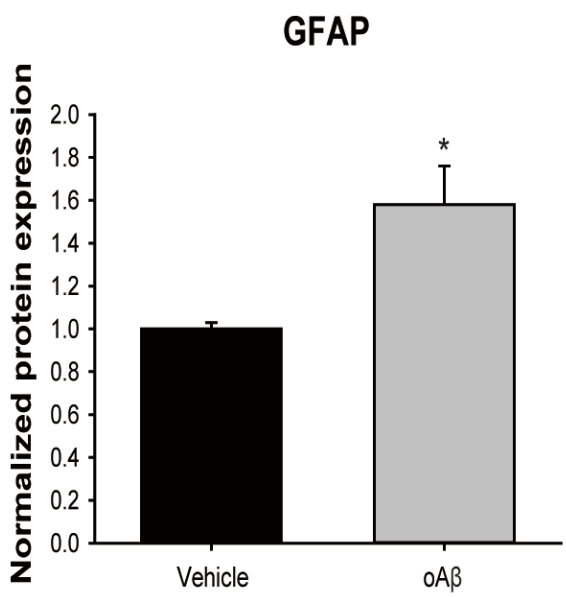
GFAP
Normalized protein expression
2.0
1.8
1.6
1.4
1.2
1.0
0.8
0.6
0.4
0.2
0.0
*
Vehicle
oAβ

Figure 2-4. Treatment with oligomeric Aβ_{1-42} activated primary cultured astrocytes *In vitro*

(a) Representative immunoblots for GFAP in vehicle- and oAβ-treated primary cultured astrocytes from C57B/L6 p1 mice. (b) Densitometric analysis of immunoblots for GFAP (Vehicle: 1.00 ± 0.181, N=4, oAβ: 1.586 ± 0.169, N=4, $*p<0.05$). The data are displayed as the mean ± SEM.

(a)

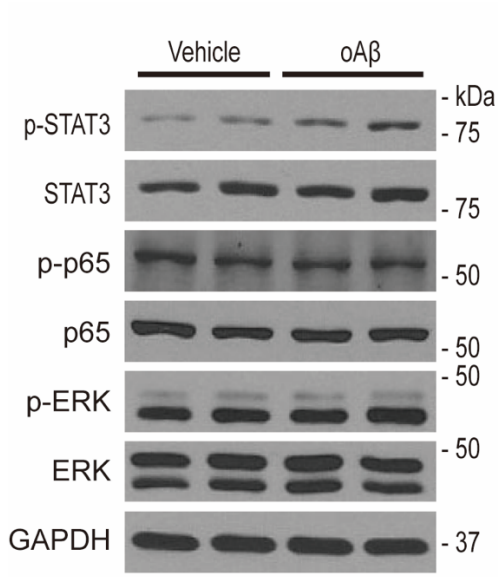
Vehicle
oAβ
kDa
p-STAT3
75
STAT3
75
p-p65
50
p65
50
p-ERK
50
ERK
50
GAPDH
37

(b)

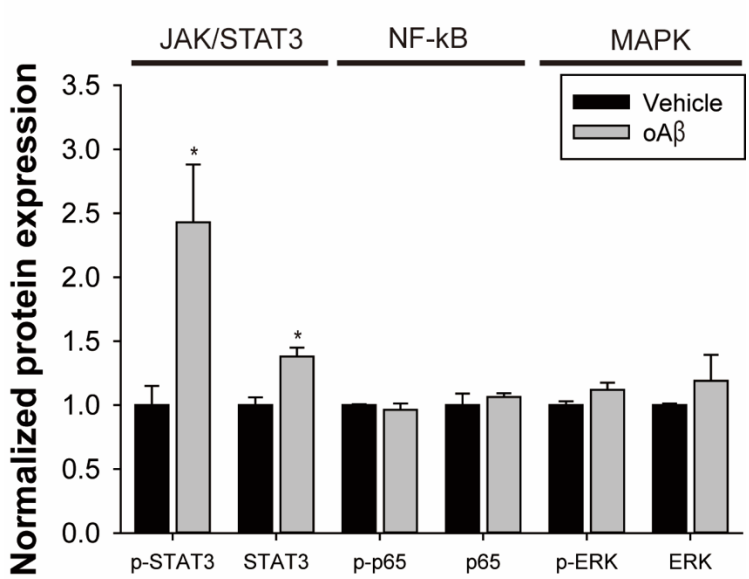
JAK/STAT3
NF-kB
MAPK
Vehicle
oAβ
Normalized protein expression
3.5
3.0
2.5
2.0
1.5
1.0
0.5
0.0
*
*
p-STAT3
STAT3
p-p65
p65
p-ERK
ERK

Figure 2-5. Astrocytes were activated via STAT3 phosphorylation *in vitro*

(a) Representative immunoblots for p-STAT3, STAT3, p-p65, p65, p-ERK and ERK for vehicle- and oAβ-treated primary cultured astrocytes from C57B/L6 p1 mice. (N = 4) (b) Densitometric analysis of immunoblots for p-STAT3 (Vehicle: 1.00 ± 0.157, N=4, oAβ: 2.440 ± 0.454, N=4, $*p<0.05$), STAT3 (Vehicle: 1.00 ± 0.066, N=4, oAβ: 1.385 ± 0.079, N=4, $*p<0.05$), p-p65 (Vehicle: 1.00 ± 0.007, N=4, oAβ: 0.963 ± 0.050, N=4), p65 (Vehicle: 1.00 ± 0.095, N=4, oAβ: 1.063 ± 0.032, N=4), p-ERK (Vehicle: 1.00 ± 0.147, N=4, oAβ: 1.020 ± 0.076, N=4) and ERK (Vehicle: 1.00 ± 0.130, N=4, oAβ: 1.045 ± 0.140, N=4). The data are displayed as the mean ± SEM.

(a)

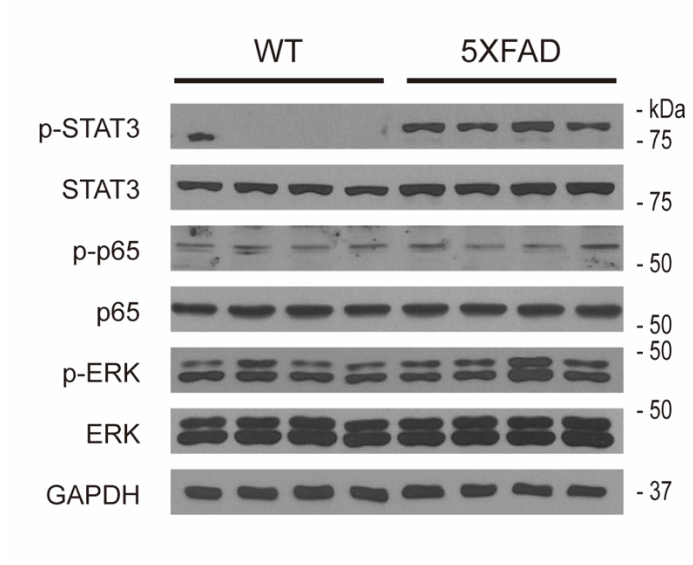
WT
5XFAD
p-STAT3
STAT3
p-p65
p65
p-ERK
ERK
GAPDH
- kDa
- 75
- 75
- 50
- 50
- 50
- 50
- 37

(b)

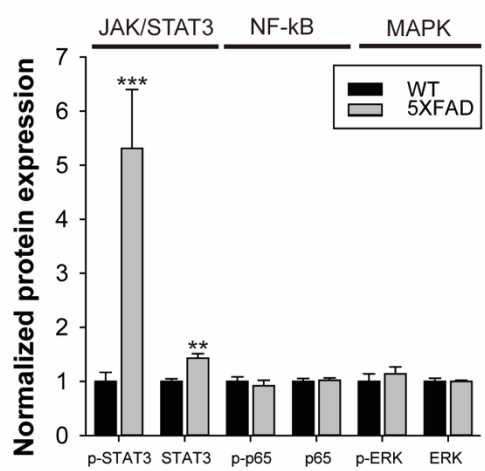
JAK/STAT3
NF-kB
MAPK
WT
5XFAD
Normalized protein expression
0
1
2
3
4
5
6
7
***
**
p-STAT3
STAT3
p-p65
p65
p-ERK
ERK

Figure 2-6. STAT3 phosphorylation was increased in the hippocampus of 6-month-old 5XFAD mice

(a) Representative immunoblots for p-STAT3, STAT3, p-ERK, ERK, p-p65 and p65 in the WT (N=7) and 5XFAD (N = 9) hippocampus. (b) Densitometric analysis of immunoblots for p-STAT3 (WT: 1.00 ± 0.166, N=7, 5XFAD: 5.312 ± 1.087, N=9, ***p<0.001), STAT3 (WT: 1.00 ± 0.049, N=7, 5XFAD: 1.433 ± 0.081, N=9, **p<0.01), p-p65 (WT: 1.00 ± 0.083, N=7, 5XFAD: 0.924 ± 0.101, N=9), p65 (WT: 1.00 ± 0.055, N=7, 5XFAD: 1.024 ± 0.044, N=9), p-ERK (WT: 1.00 ± 0.078, N=7, 5XFAD: 0.996 ± 0.057, N=9) and ERK (WT: 1.00 ± 0.072, N=7, 5XFAD: 1.054 ± 0.064, N=9). The data are displayed as the mean ± SEM.

(a)

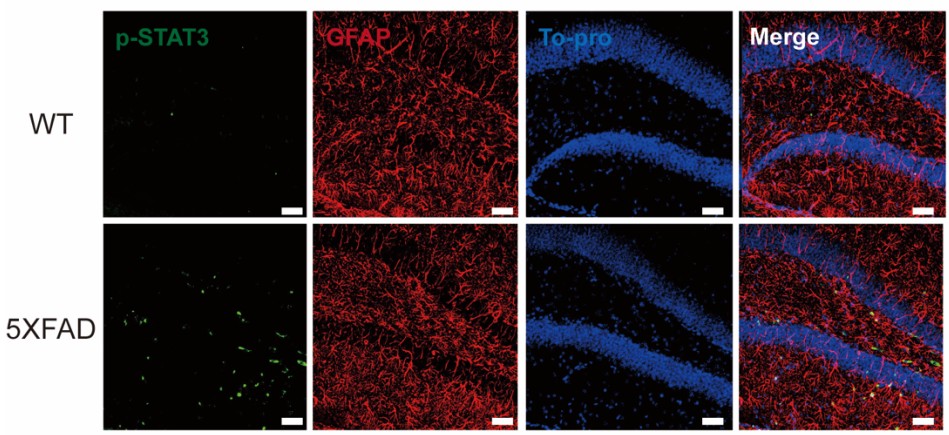
p-STAT3
GFAP
To-pro
Merge
WT
5XFAD

(b)

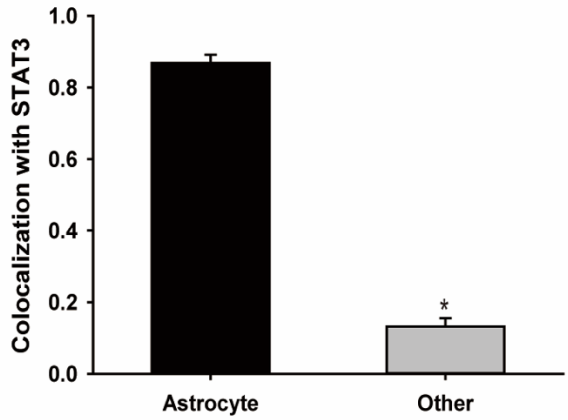
Colocalization with STAT3
1.0
0.8
0.6
0.4
0.2
0.0
*
Astrocyte
Other

(c)

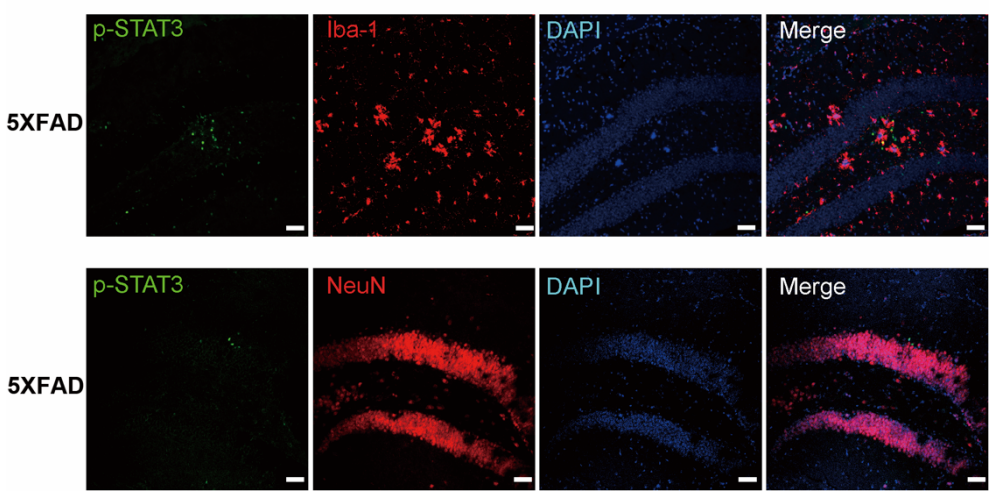

Figure 2-7. STAT3 phosphorylation was colocalized with astrocytes in the hippocampus of 6-month-old 5XFAD mice

(a) Immunofluorescence for p-STAT3 and GFAP in the hippocampal dentate gyrus of both WT and 5XFAD mice (scale bar = 50 μm). (b) Colocalization of p-STAT3 and GFAP in the hippocampal dentate gyrus (p-STAT3-GFAP colocalization: 86.02 ± 1.79%, N=5, p-STAT3 only: 13.97 ± 1.79%, N=5, $*p<0.05$). (c) Immunofluorescence for p-STAT3 and Iba-1, NeuN in the hippocampal dentate gyrus of 5XFAD mice (scale bar = 50 μm). The data are displayed as the mean ± SEM.

(a)

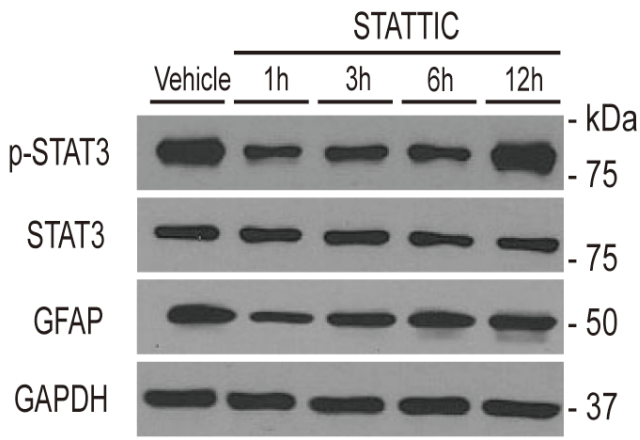
STATTIC
Vehicle
1h
3h
6h
12h
kDa
p-STAT3
75
STAT3
75
GFAP
50
GAPDH
37

(b)

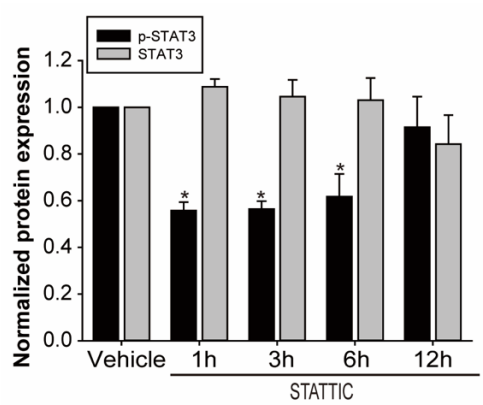
p-STAT3
STAT3
Normalized protein expression
1.2
1.0
0.8
0.6
0.4
0.2
0.0
*
*
*
Vehicle
1h
3h
6h
12h
STATTIC

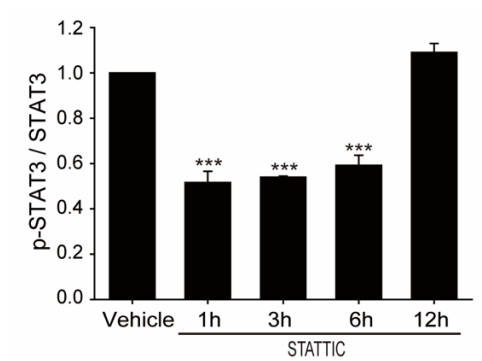
p-STAT3 / STAT3
1.2
1.0
0.8
0.6
0.4
0.2
0.0
***
***
***
Vehicle
1h
3h
6h
12h
STATTIC

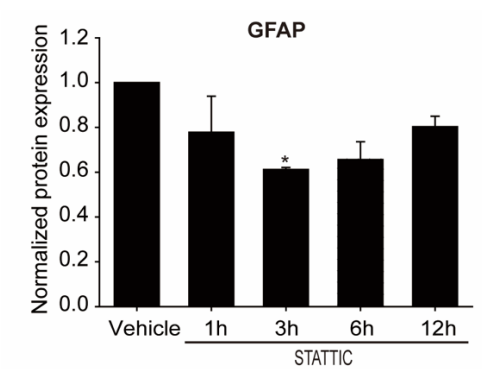
GFAP
Normalized protein expression
1.2
1.0
0.8
0.6
0.4
0.2
0.0
*
Vehicle
1h
3h
6h
12h
STATTIC

Figure 2-8. Stattic attenuated the activation of astrocyte by inhibition of STAT3 phosphorylation *In vitro*

(a)Representative immunoblots for p-STAT3, STAT3 and GFAP from vehicle and 1 μM Stattic-treated time dependently in primary cultured astrocyte. (b) Densitometric analysis of immunoblots for p-STAT3 (Vehicle: 1.00 ± 0.000, N=3, 1h: 0.557 ± 0.036, N=3, $*p<0.05$, 3h: 0.564 ± 0.033, N=3, $*p<0.05$, 6h: 0.617 ± 0.097, N=3, $*p<0.05$, 12h: 0.914 ± 0.130, N=3), STAT3 (Vehicle: 1.00 ± 0.000, N=3, 1h: 1.087 ± 0.033, N=3, 3h: 1.045 ± 0.071, N=3, 6h: 1.030 ± 0.094, N=3, 12h: 0.842 ± 0.124, N=3), ratio of p-STAT3 per total STAT3 (Vehicle: 1.00 ± 0.000, N=3, 1h: 0.515 ± 0.049, N=3, $***p<0.001$, 3h: 0.539 ± 0.004, N=3, $***p<0.001$, 6h: 0.592 ± 0.044, N=3, $***p<0.001$, 12h: 1.090 ± 0.039, N=3) and GFAP (Vehicle: 1.00 ± 0.000, N=3, 1h: 0.778 ± 0.160, N=3, 3h: 0.612 ± 0.009, N=3, $*p<0.05$, 6h: 0.657 ± 0.079, N=3, 12h: 0.803 ± 0.046, N=3) in the vehicle and Stattic treatment groups. The data are displayed as the mean ± SEM.

(a)


STATTIC adminiatration
25mg / kg / day
T-maze
C.F.C
15 day
2 day
3 day
6 month old
Harvest

(b)

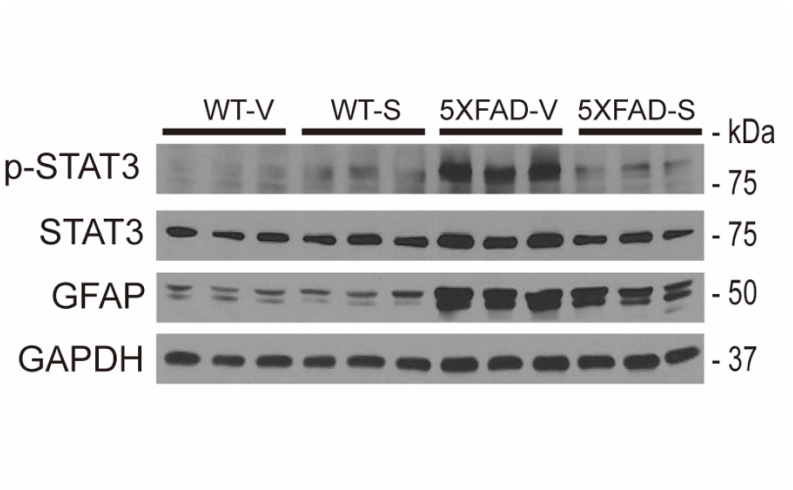
WT-V
WT-S
5XFAD-V
5XFAD-S
kDa
p-STAT3
75
STAT3
75
GFAP
50
GAPDH
37

(c)

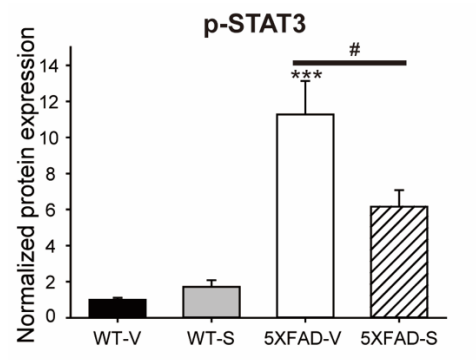
p-STAT3
Normalized protein expression
0
2
4
6
8
10
12
14
***
#
WT-V
WT-S
5XFAD-V
5XFAD-S

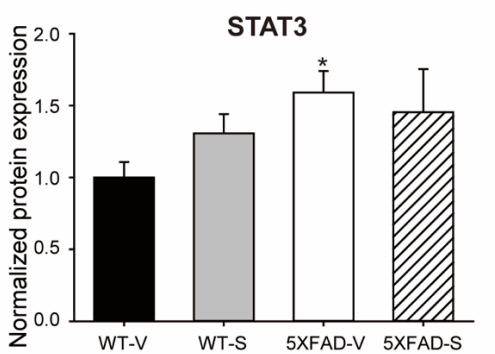
STAT3
Normalized protein expression
0.0
0.5
1.0
1.5
2.0
*
WT-V
WT-S
5XFAD-V
5XFAD-S

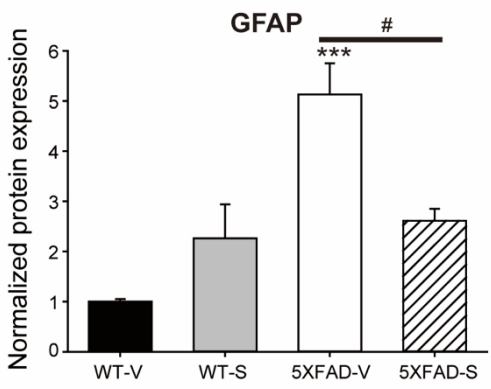
GFAP
Normalized protein expression
0
1
2
3
4
5
6
***
#
WT-V
WT-S
5XFAD-V
5XFAD-S

Figure 2-9. Oral administration of Stattic restored the activation of astrocytes in the hippocampus of 6-month-old 5XFAD mice

(a) A time schedule for the Stattic administration and behavior testes with WT and 5XFAD mice is shown. (b) Representative immunoblots for p-STAT3, STAT3 and GFAP from WT and 5XFAD mice that received vehicle or Stattic treatment. (N = 6) (c) Densitometric analysis of immunoblots for p-STAT3 (WT-V: 1.00 ± 0.110, N=6, WT-S: 1.716 ± 0.361, N=6, 5XFAD-V: 11.273 ± 1.862, N=6, ***p<0.001, 5XFAD-S: 6.155 ± 0.919, N=6, #p<0.05), STAT3 (WT-V: 1.00 ± 0.107, N=6, WT-S: 1.306 ± 0.134, N=6, 5XFAD-V: 1.590 ± 0.150, N=6, 5XFAD-S: 1.454 ± 0.299, N=6) and GFAP (WT-V: 1.00 ± 0.051, N=6, WT-S: 2.262 ± 0.679, N=6, 5XFAD-V: 5.131 ± 0.620, N=6, ***p<0.001, 5XFAD-S: 2.610 ± 0.242, N=6, #p<0.05). The data are displayed as the mean ± SEM.

(a)

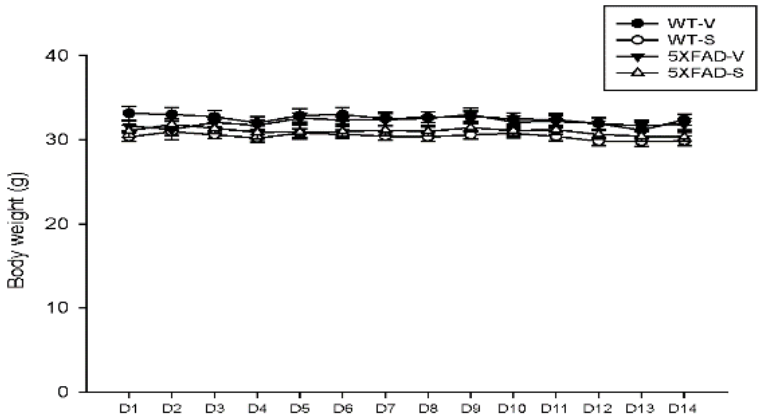
WT-V
WT-S
5XFAD-V
5XFAD-S
Body weight (g)
0
10
20
30
40
D1
D2
D3
D4
D5
D6
D7
D8
D9
D10
D11
D12
D13
D14

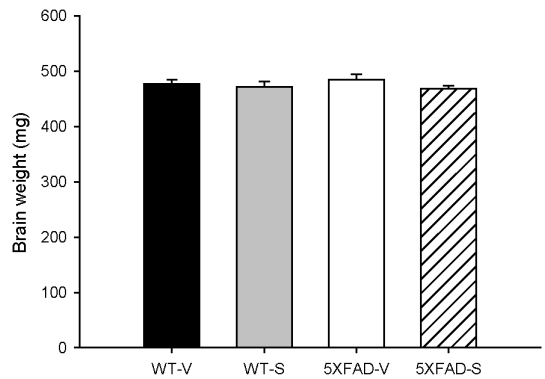
Brain weight (mg)
0
100
200
300
400
500
600
WT-V
WT-S
5XFAD-V
5XFAD-S

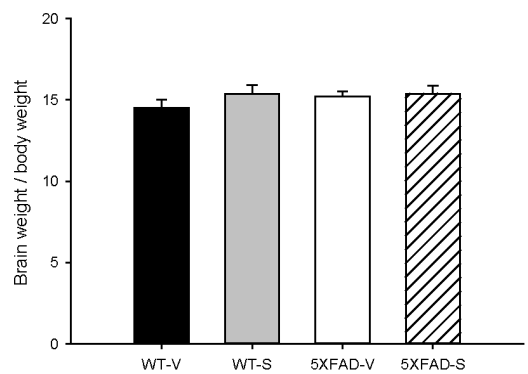
Brain weight / body weight
0
5
10
15
20
WT-V
WT-S
5XFAD-V
5XFAD-S

Figure 2-10. Physiological characteristics of Stattic administrated mice

(a) Line graph showing the body weights of WT and 5XFAD mice treated with vehicle or Stattic. (WT-V-day 1: 33.136 ± 0.832, N=11, WT-V-day 2: 33.009 ± 0.809, N=11, WT-V-day 3: 32.736 ± 0.736, N=11, WT-V-day 4: 32.000 ± 0.772, N=11, WT-V-day 5: 32.882 ± 0.814, N=11, WT-V-day 6: 33.000 ± 0.804, N=11, WT-V-day 7: 32.500 ± 0.754, N=11, WT-V-day 8: 32.645 ± 0.650, N=11, WT-V-day 9: 32.764 ± 0.614, N=11, WT-V-day 10: 32.473 ± 0.682, N=11, WT-V-day 11: 32.373 ± 0.731, N=11, WT-V-day 12: 31.918 ± 0.708, N=11, WT-V-day 13: 31.136 ± 0.962, N=11, WT-V-day 14: 32.373 ± 0.644, N=11, WT-S-day 1: 30.345 ± 0.550, N=11, WT-S-day 2: 30.954 ± 0.460, N=11, WT-S-day 3: 30.600 ± 0.434, N=11, WT-S-day 4: 30.181 ± 0.446, N=11, WT-S-day 5: 30.809 ± 0.527, N=11, WT-S-day 6: 30.645 ± 0.508, N=11, WT-S-day 7: 30.418 ± 0.507, N=11, WT-S-day 8: 30.327 ± 0.520, N=11, WT-S-day 9: 30.590 ± 0.525, N=11, WT-S-day 10: 30.763 ± 0.529, N=11, WT-S-day 11: 30.400 ± 0.560, N=11, WT-S-day 12: 29.818 ± 0.516, N=11, WT-S-day 13: 29.790 ± 0.544, N=11, WT-S-day 14: 29.845 ± 0.570, N=11, 5XFAD-V-day 1: 31.640 ± 0.596, N=10,

5XFAD-V-day 2: 31.220 ± 1.235, N=10, 5XFAD-V-day 3: 32.070 ± 0.512, N=10, 5XFAD-V-day 4: 31.700 ± 0.672, N=10, 5XFAD-V-day 5: 32.570 ± 0.635, N=10, 5XFAD-V-day 6: 32.350 ± 0.562, N=10, 5XFAD-V-day 7: 32.390 ± 0.723, N=10, 5XFAD-V-day 8: 32.540 ± 0.774, N=10, 5XFAD-V-day 9: 32.990 ± 0.808, N=10, 5XFAD-V-day 10: 32.100 ± 0.738, N=10, 5XFAD-V-day 11: 32.190 ± 0.708, N=10, 5XFAD-V-day 12: 31.920 ± 0.696, N=10, 5XFAD-V-day 13: 31.67 ± 0.654, N=10, 5XFAD-V-day 14: 31.850 ± 0.657, N=10, 5XFAD-S-day 1: 31.036 ± 0.740, N=11, 5XFAD-S-day 2: 31.836 ± 0.714, N=11, 5XFAD-S-day 3: 31.372 ± 0.628, N=11, 5XFAD-S-day 4: 30.900 ± 0.787, N=11, 5XFAD-S-day 5: 30.936 ± 0.821, N=11, 5XFAD-S-day 6: 30.981 ± 0.621, N=11, 5XFAD-S-day 7: 31.127 ± 0.613, N=11, 5XFAD-S-day 8: 30.981 ± 0.560, N=11, 5XFAD-S-day 9: 31.436 ± 0.507, N=11, 5XFAD-S-day 10: 31.072 ± 0.524, N=11, 5XFAD-S-day 11: 31.200 ± 0.516, N=11, 5XFAD-S-day 12: 30.618 ± 0.499, N=11, 5XFAD-S-day 13: 30.418 ± 0.531, N=11, 5XFAD-S-day 14: 30.336 ± 0.543, N=11). And bar graph showing brain weights (WT-V: 477.300 ± 7.671, N=11, WT-S: 472.214 ± 9.812, N=11, 5XFAD-V: 485.320 ± 8.960, N=10, 5XFAD-S: 468.200 ±

6.443, N=11). Bar graph showing the ratios of brain weight to body weight (WT-V: 14.491 ± 0.532, N=11, WT-S: 15.359 ± 0.567, N=11, 5XFAD-V: 15.203 ± 0.330, N=10, 5XFAD-S: 15.375 ± 0.479, N=11). The data are displayed as the mean ± SEM.

(a)

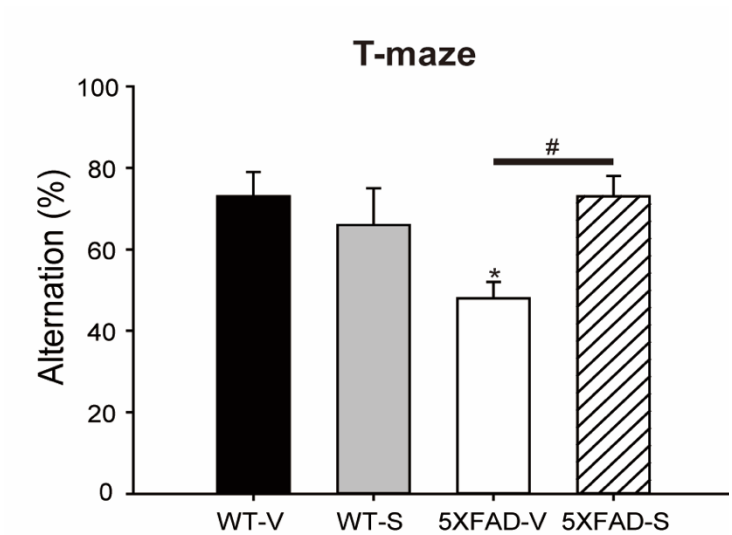

(b)

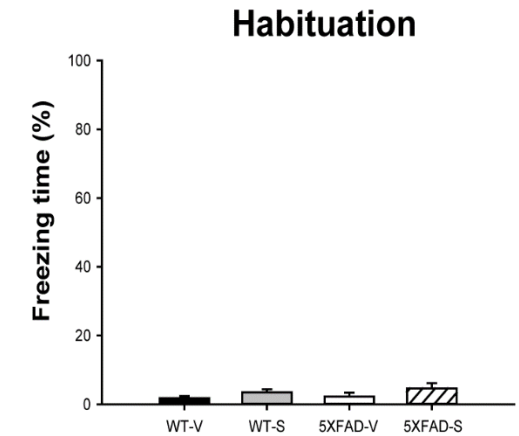
Habituation
Freezing time (%)
100
80
60
40
20
0
WT-V
WT-S
5XFAD-V
5XFAD-S

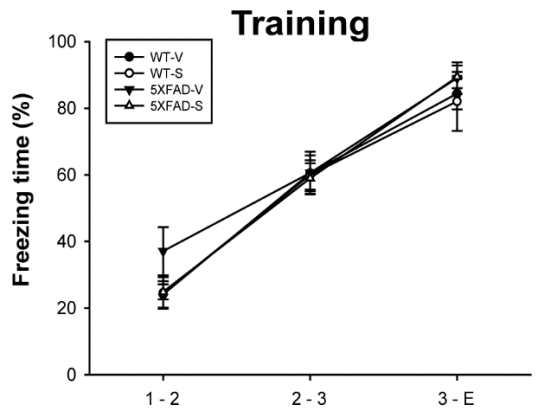
Training
Freezing time (%)
WT-V
WT-S
5XFAD-V
5XFAD-S
100
80
60
40
20
0
1 - 2
2 - 3
3 - E

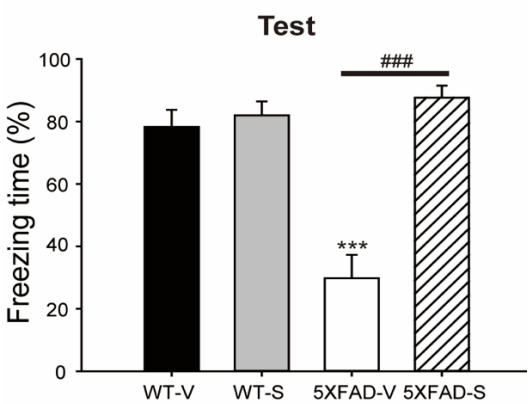
Test
###
Freezing time (%)
***
100
80
60
40
20
0
WT-V
WT-S
5XFAD-V
5XFAD-S

Figure 2-11. Oral administration of Stattic restored the impairment of cognitive function in 6-month-old 5XFAD mice

(a) A graph showing the alternation percentage in the T-maze test after vehicle or Stattic oral administration to 5XFAD mice (WT-V: 72.727 ± 6.265, N=11, WT-S: 65.909 ± 9.091, N=11, 5XFAD-V: 45.500 ± 4.488, N=10, 5XFAD-S: 72.727 ± 5.281, N=11). (b) A graph showing the freezing time percentage at habituation (WT-V: 1.791 ± 0.602, N=11, WT-S: 3.499 ± 0.836, N=11, 5XFAD-V: 2.237 ± 1.171, N=10, 5XFAD-S: 4.608 ± 1.556, N=11), training (WT-V-1^{st}: 24.121 ± 3.965, N=11, WT-V-2^{nd}: 60.515 ± 5.350, N=11, WT-V-3^{rd}: 84.439 ± 4.756, N=11, WT-S-1^{st}: 24.558 ± 4.725, N=11, WT-S-2^{nd}: 60.006 ± 4.426, N=11, WT-S-3^{rd}: 82.094 ± 8.864, N=11, 5XFAD-V-1^{st}: 37.100 ± 7.225, N=10, 5XFAD-V-2^{nd}: 60.600 ± 6.382, N=10, 5XFAD-V-3^{rd}: 89.060 ± 4.753, N=10, 5XFAD-S-1^{st}: 24.888 ± 2.272, N=11, 5XFAD-S-2^{nd}: 58.991 ± 4.540, N=11, 5XFAD-S-3^{rd}: 89.442 ± 3.410, N=11) and expression (WT-V: 78.288 ± 5.453, N=11, WT-S: 81.985 ± 4.460, N=11, 5XFAD-V: 29.814 ± 7.485, N=10, 5XFAD-S: 87.624 ± 3.825, N=11) in the contextual fear conditioning test after vehicle or Stattic oral administration to 5XFAD mice. The data are displayed as the mean ± SEM.

(a)

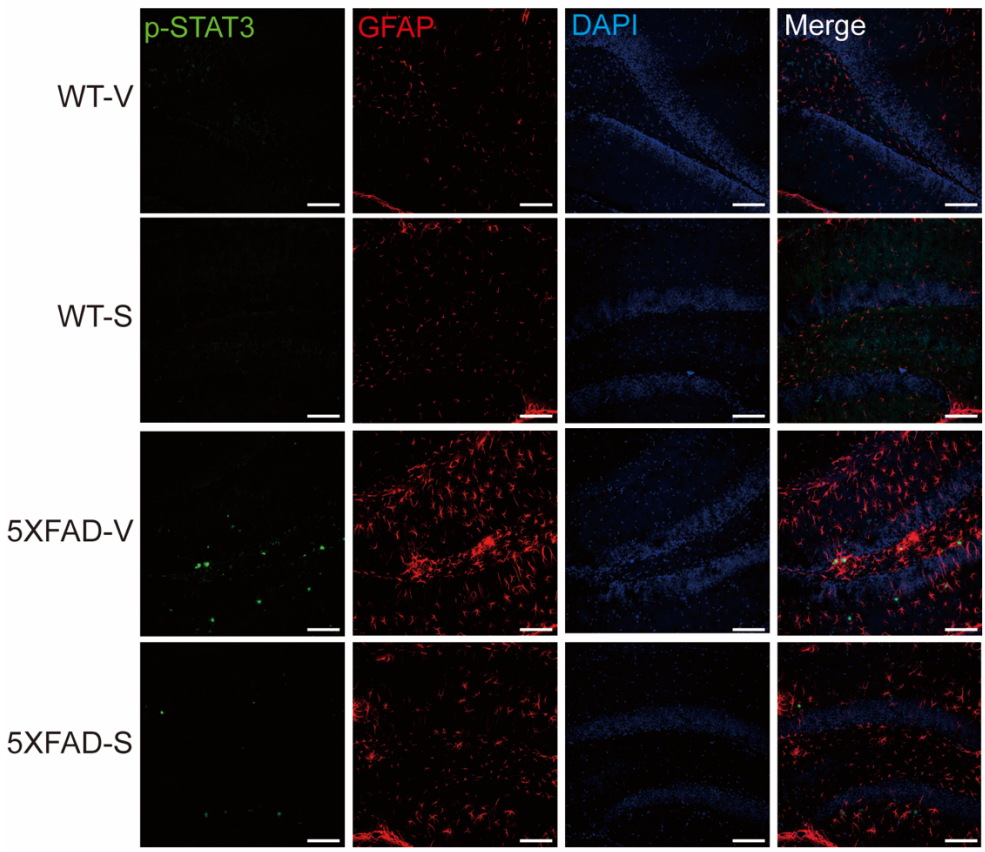

(b)

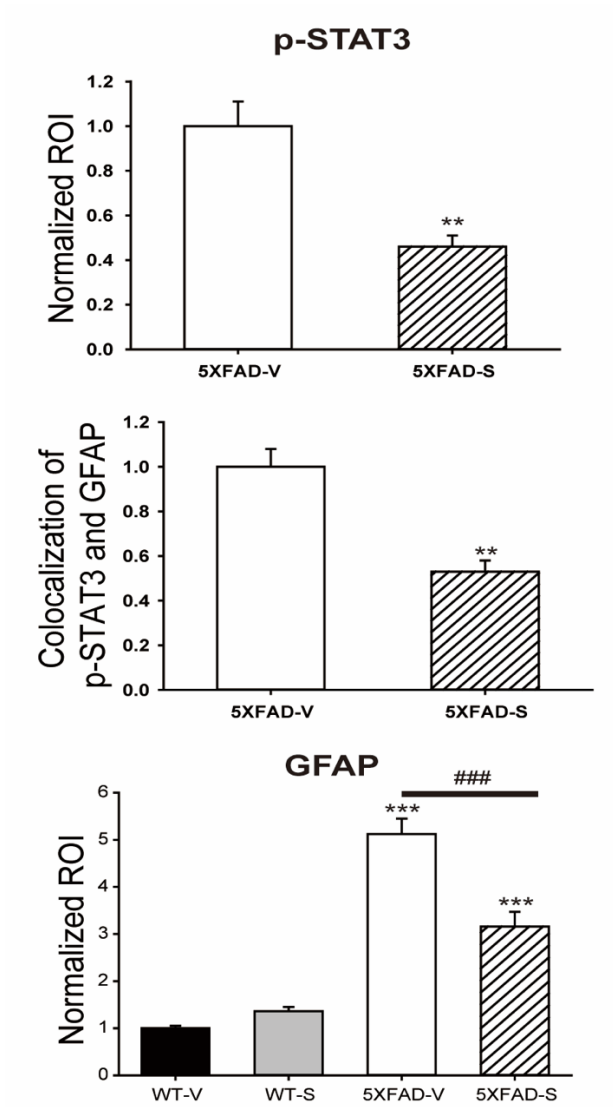
p-STAT3
Normalized ROI
1.2
1.0
0.8
0.6
0.4
0.2
0.0
**
5XFAD-V
5XFAD-S
Colocalization of p-STAT3 and GFAP
1.2
1.0
0.8
0.6
0.4
0.2
0.0
**
5XFAD-V
5XFAD-S
GFAP
###
***
***
Normalized ROI
6
5
4
3
2
1
0
WT-V
WT-S
5XFAD-V
5XFAD-S

Figure 2-12. Oral administration of Stattic restored the activation of astrocytes in the hippocampus of 6-month-old 5XFAD mice

(a) Immunofluorescence for p-STAT3 and GFAP in the hippocampal dentate gyrus of both WT and 5XFAD mice that received vehicle or Stattic treatment (scale bar = 100 μm). (N $\geq$ 9) (b) Quantification of immunoblots for p-STAT3 (WT-V: N.D. N=11, WT-S: N.D. N=11, 5XFAD-V: 1.000 $\pm$ 0.110, N=9, 5XFAD-S: 0.456 $\pm$ 0.049, N=10, $^{**}p<0.01$), p-STAT-GFAP colocalization (WT-V: N.D. N=10, WT-S: N.D. N=10, 5XFAD-V: 1.000 $\pm$ 0.079, N=9, 5XFAD-S: 0.530 $\pm$ 0.054, N=10, $^{**}p<0.01$) and GFAP (WT-V: 1.000 $\pm$ 0.051, N=10, WT-S: 1.362 $\pm$ 0.092, N=10, 5XFAD-V: 5.116 $\pm$ 0.333, N=9, $^{***}p<0.01$, 5XFAD-S: 3.158 $\pm$ 0.307, N=10, $^{***}p<0.01$, $^{\#\#\#}p<0.001$). The data are displayed as the mean $\pm$ SEM.

(a)

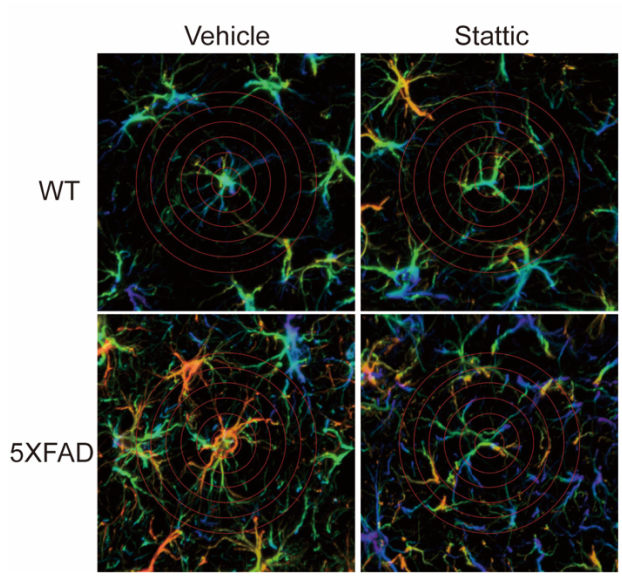
Vehicle
Stattic
WT
5XFAD

(b)

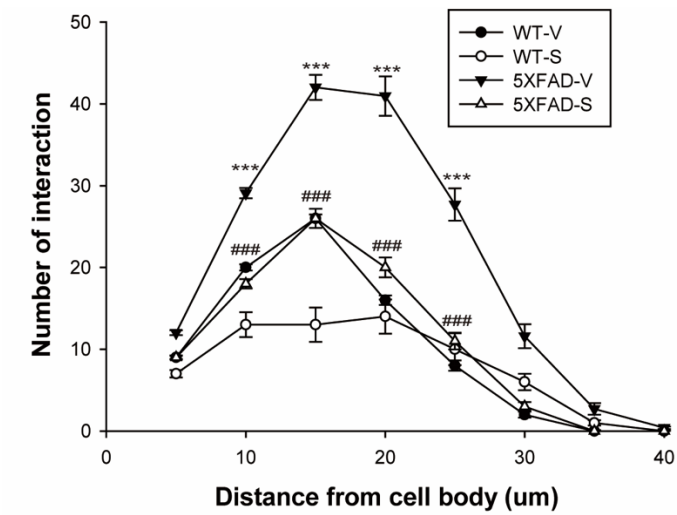
WT-V
WT-S
5XFAD-V
5XFAD-S
Number of interaction
Distance from cell body (um)
0
10
20
30
40
50
***
###

Figure 2-13. Oral administration of Stattic restored the number of processes of astrocytes in the hippocampus of 6-month-old 5XFAD mice

(a) Reconstructed images showing a cross-section along the X-Z axis from a confocal Z-stack; concentric circles are spaced at 10 μm. (b) Quantification of the number of intersections between processes and each circle (WT-V: 5 μm; 9.166 ± 0.257, 10 μm; 16.788 ± 0.378, 15 μm; 21.788 ± 0.492, 20 μm; 16.300 ± 0.580, 25 μm; 7.266 ± 0.632, 30 μm; 1.566 ± 0.367, 35 μm; 0.088 ± 0.064, 40 μm; 0.000 ± 0.000,N=5, WT-S: 5 μm; 7.730 ± 0.461, 10 μm; 14.947 ± 1.523, 15 μm; 19.127 ± 2.091, 20 μm; 15.344 ± 2.097, 25 μm; 7.894 ± 1.950, 30 μm; 3.036 ± 1.006, 35 μm; 0.622 ± 0.319, 40 μm; 0.066 ± 0.044,N=5, 5XFAD-V: 5 μm; 11.904 ± 0.300, 10 μm; 28.992 ± 0.636, 15 μm; 41.904 ± 1.521, 20 μm; 40.238 ± 2.412, 25 μm; 27.468 ± 1.975, 30 μm; 11.206 ± 1.473, 35 μm; 2.531 ± 0.709, 40 μm; 0.357 ± 0.156, N=5, ***p<0.001, 5XFAD-S: 5 μm; 9.814 ± 0.195, 10 μm; 19.981 ± 0.571, 15 μm; 25.444 ± 1.167, 20 μm; 20.833 ± 1.212, 25 μm; 10.981 ± 1.033, 30 μm; 3.388 ± 0.540, 35 μm; 0.351 ± 0.119, 40 μm; 0.018 ± 0.018, N=5, ###p<0.001. The data are displayed as the

mean ± SEM.

(a)

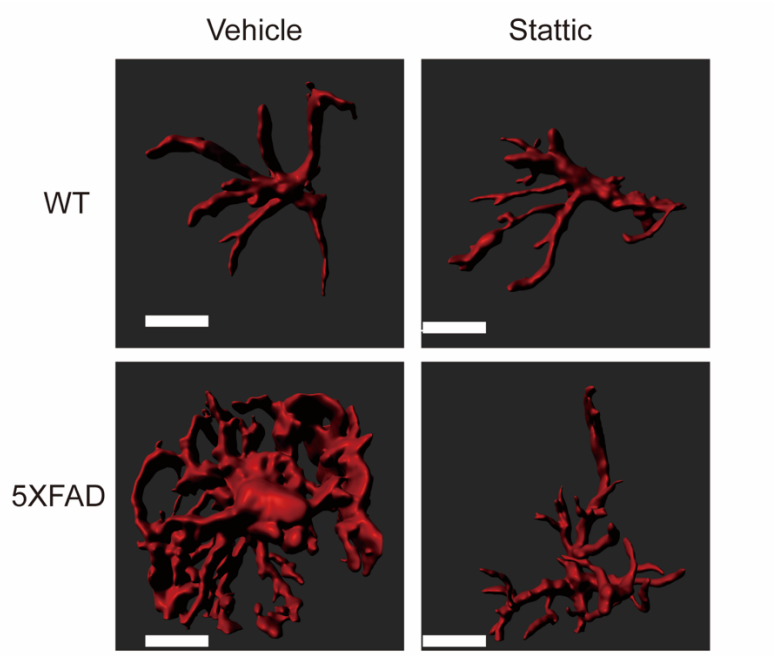
Vehicle
Stattic
WT
5XFAD

(b)

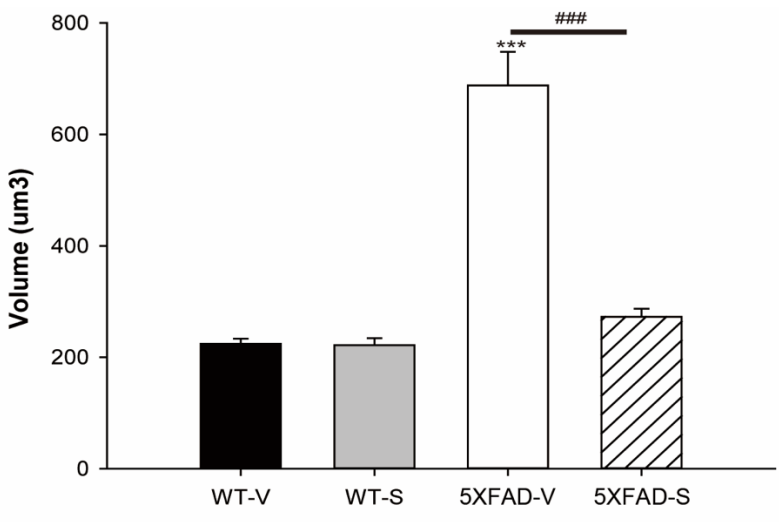
800
600
400
200
0
Volume (um3)
###
***
WT-V
WT-S
5XFAD-V
5XFAD-S

Figure 2-14. Oral administration of Stattic restored the volume of astrocytes in the hippocampus of 6-month-old 5XFAD mice

(a) Reconstructed images of GFAP with IMARIS (scale bar = 5 μm) (b) Quantification of the volume of astrocytes (WT-V: 224.115 ± 9.101, N=5, WT-S: 221.611 ± 12.469, N=5, 5XFAD-V: 687.829 ± 60.310, N=5, ***p<0.01, 5XFAD-S: 272.424 ± 14.415, N=5, ###p<0.001). The data are displayed as the mean ± SEM.

(a)

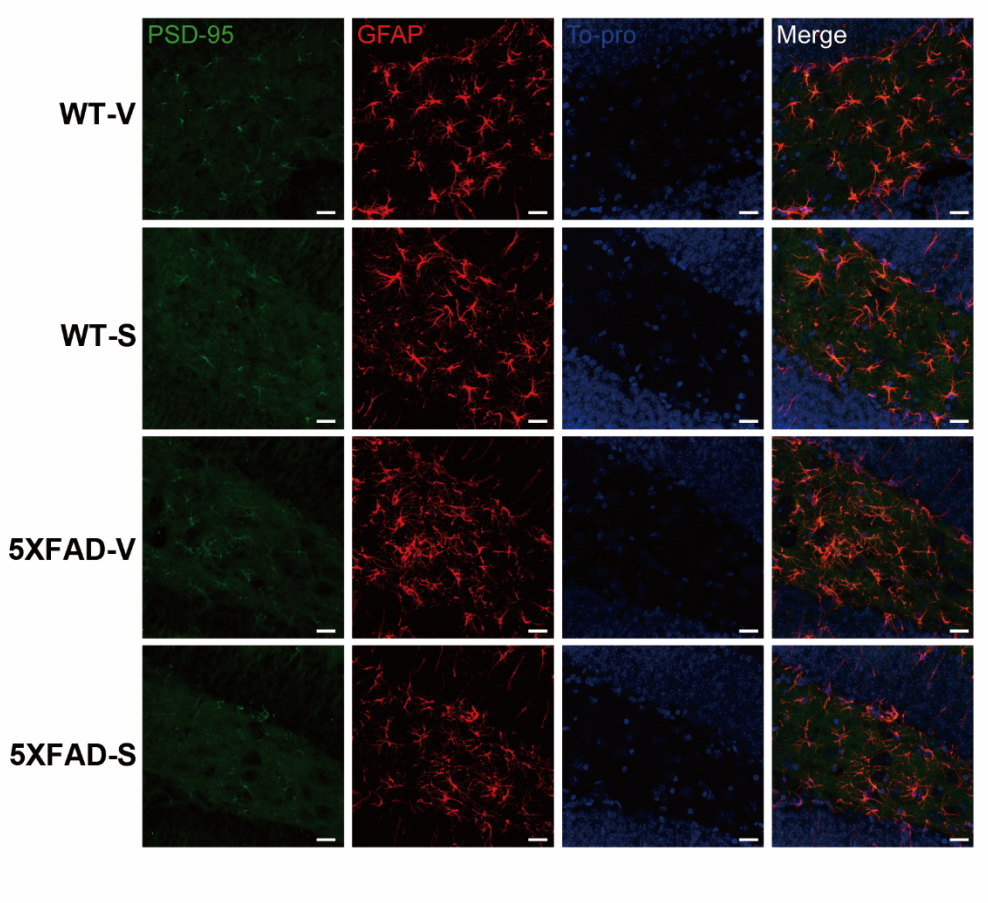

(b)

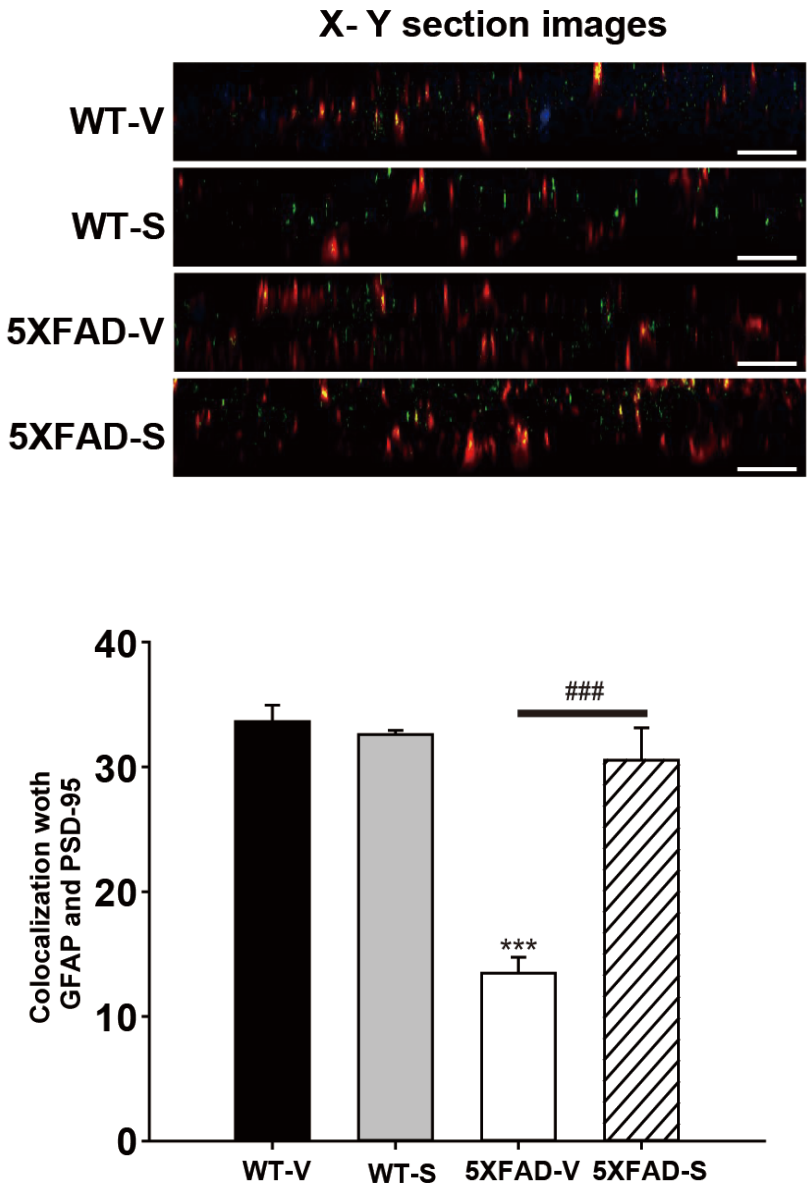
X- Y section images
WT-V
WT-S
5XFAD-V
5XFAD-S
Colocalization woth GFAP and PSD-95
40
30
20
10
0
###
***
WT-V
WT-S
5XFAD-V
5XFAD-S

Figure 2-15. Systemic administration of Stattic restored the decrease in the number of tripartite synapses in 6-month-old 5XFAD mice (A) Immunofluorescence for p-STAT3 and GFAP in the hippocampal DG of both WT and 5XFAD mice that were treated with vehicle or Stattic (scale bar = 10 μm). (F) Reconstructed images showing a cross-section along the X-Z axis from a confocal Z-stack image from both WT and 5XFAD mice that were treated with vehicle or Stattic (scale bar = 10 μm). (G) Quantification of the colocalization of PSD-95 and GFAP in the reconstructed cross-section images in the WT and 5XFAD hippocampal DG of mice given vehicle or stattic. (WT-V: 33.625 ± 1.068, N=12, WT-S: 32.600 ± 0.795, N=12, 5XFAD-V: 13.516 ± 0.721, N=12, ***p<0.001, 5XFAD-S: 30.533 ± 5.488, N=12, ###p<0.001), Data are displayed as the mean ± SEM.

(a)

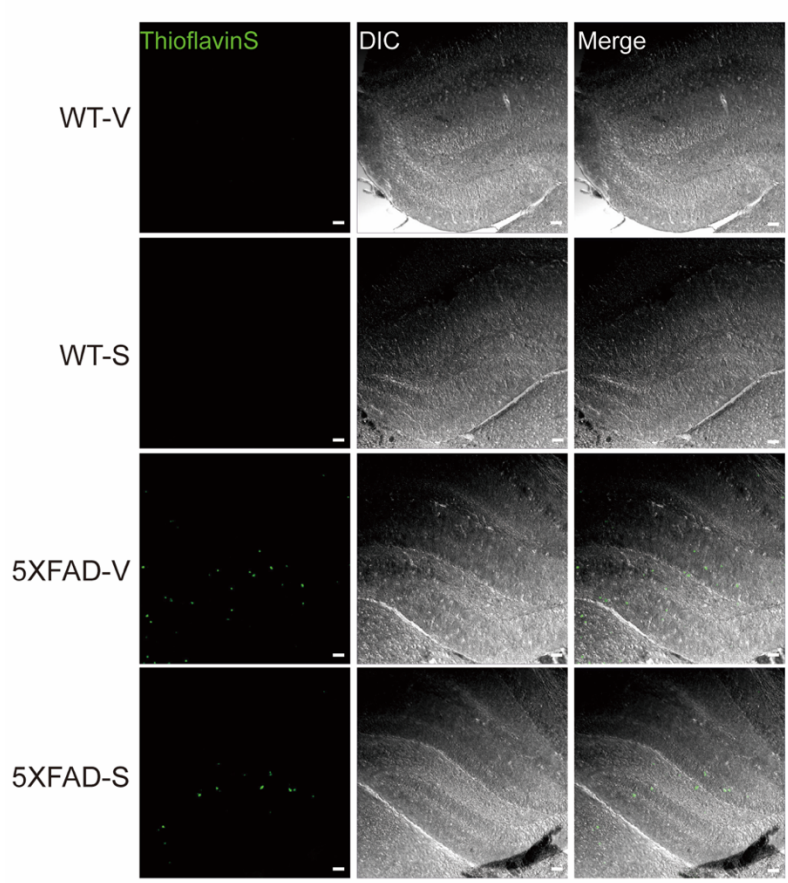
ThioflavinS
DIC
Merge
WT-V
WT-S
5XFAD-V
5XFAD-S

(b)

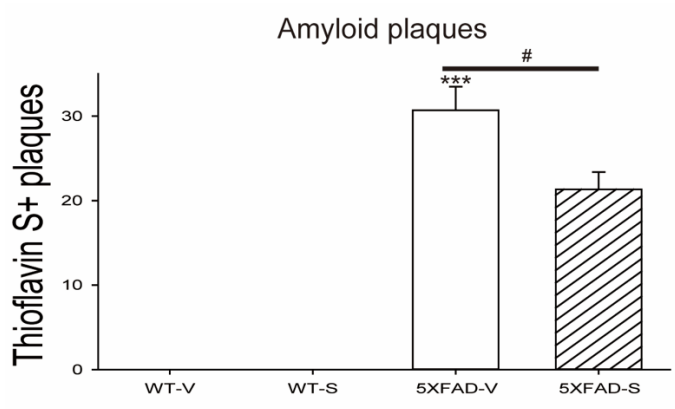
Amyloid plaques
Thioflavin S+ plaques
0
10
20
30
***
#
WT-V
WT-S
5XFAD-V
5XFAD-S

Figure 2-16. Oral administration of Stattic reduced the number of Aβ plaques in the hippocampus of 5XFAD mice

(a) Thioflavin S staining was performed in the hippocampal dentate gyrus (scale bar = 100 μm). (b) Quantification of the number of Aβ plaques (WT-V: N.D., N=10, WT-S: N.D., N=10, 5XFAD-V: 26.800 ± 3.508, N=10, ***p<0.01, 5XFAD-S: 20.700 ± 2.108, N=10, #p<0.05). The data are displayed as the mean ± SEM.

(a)

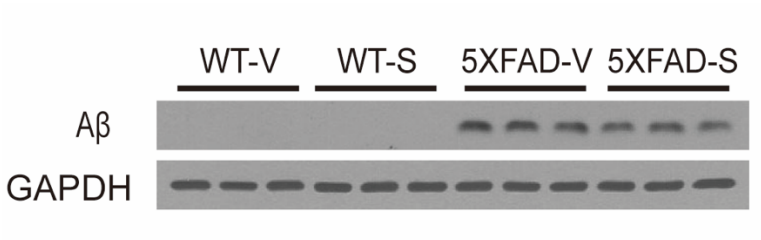
WT-V
WT-S
5XFAD-V
5XFAD-S
Aβ
GAPDH

(b)

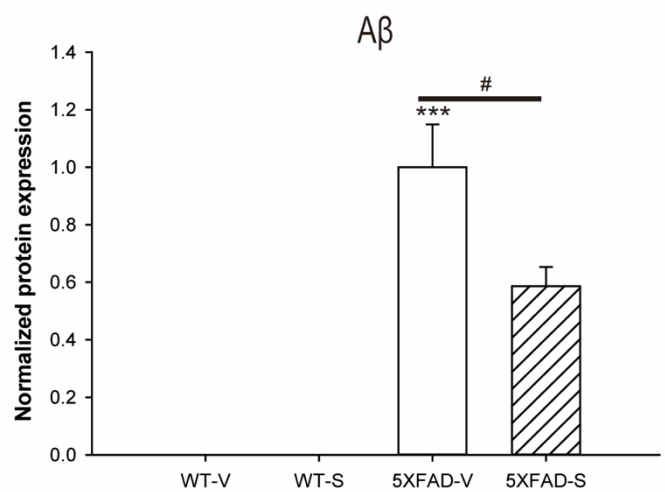
Aβ
Normalized protein expression
1.4
1.2
1.0
0.8
0.6
0.4
0.2
0.0
#
***
WT-V
WT-S
5XFAD-V
5XFAD-S

Figure 2-17. Oral administration of Stattic reduced the protein level of Aβ in the hippocampus of 5XFAD mice

(c) Representative immunoblots showing Aβ. (d) Densitometric analysis of immunoblots of Aβ (WT-V: N.D., N=6, WT-S: N.D., N=6, 5XFAD-V: 1.000 ± 0.149, N=6, ***p<0.01, 5XFAD-S: 0.586 ± 0.066, N=6, #p<0.05). The data are displayed as the mean ± SEM.

(a)

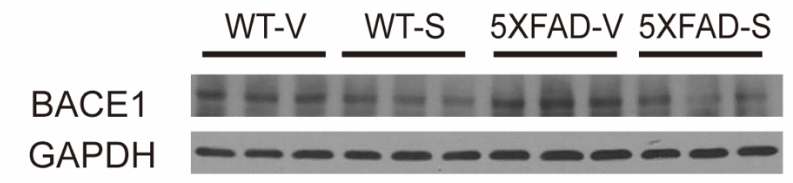
WT-V
WT-S
5XFAD-V
5XFAD-S
BACE1
GAPDH

(b)

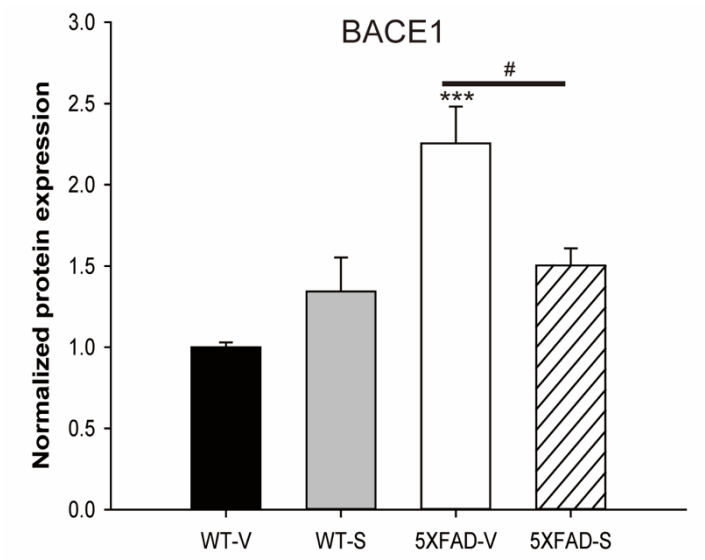
BACE1
Normalized protein expression
3.0
2.5
2.0
1.5
1.0
0.5
0.0
***
#
WT-V
WT-S
5XFAD-V
5XFAD-S

Figure 2-18. Oral administration of Stattic reduced BACE1 expression in the hippocampus of 5XFAD mice

(a) Representative immunoblots showing BACE1 (b) Densitometric analysis of immunoblots of BACE1 (WT-V: 1.000 ± 0.028, N=6, WT-S: 1.342 ± 0.209, N=6, 5XFAD-V: 2.255 ± 0.224, N=6, ***p<0.01, 5XFAD-S: 1.503 ± 0.104, N=6, #p<0.05). The data are displayed as the mean ± SEM.

DISCUSSION

The novel functions of astrocytes in memory formation have been extensively studied in recent decades. Astrocytes increase the number of mature and functional synapses by releasing soluble molecules, such as thrombospondin and cholesterol, to regulate synaptic formation [149]. In addition, astrocytes have been reported to regulate synaptic elimination and spine morphology across brain development [150]. Astrocytes express neurotransmitter receptor G-protein coupled receptors (GPCRs) [151]. However, the binding of neurotransmitters to the receptors does not generate action potential in these cells, but rather increases the intracellular calcium concentration, causing gliotransmitter release in a calcium-dependent manner [152]. The released gliotransmitters can bind to pre- or postsynaptic receptors to regulate neuronal excitability and synaptic transmission. Glutamate released from astrocytes binds to presynaptic NMDAR to promote neurotransmitter release, while ATP released from astrocytes suppresses synaptic transmission. In addition, $_{D}$-serine regulates postsynaptic NMDAR as an endogenous coagonist. Astrocyte-specific knockout animal

models such as GPCR or inositol 1,4,5 – triphosphate receptor type 2 (IP3R2) knockout animals, display a lack of calcium signaling in astrocytes and altered NMDAR-dependent LTP and long-term memory formation [153]. Recently, reactive astrocytes were reported to be significantly increased in a hippocampal dentate zyrus region in a hippocampus-dependent cognitive impairment model [154].

Astrocytes have been classified into A1 type and A2 type according to their genetic expression pattern. A1-type astrocytes have neurotoxic effects whereas A2-type astrocytes have neuroprotective effects. In neurodegenerative disorders such as AD and PD, more type A1-astrocytes than type A2-astrocytes are detected in the brain [73, 75, 155]. The astrocytes morphologically classified as type I, II and III are not fully understood regarding the function of each type of astrocyte in the CNS, as specific genetic and protein markers for each type of astrocyte have not been determined to date. Another problem resides in the *in vitro* morphology of astrocytes. The morphological types of astrocytes are identified with GFAP immunofluorescence staining in an *in vivo* system [156]. However, astrocytes have a process-bearing morphology *in vitro*. Even though single-cell gene

expression analysis techniques have been developed, the morphological categorization of astrocytes *in vitro* remains limited.

Since AD pathologies are the consequence of neuronal death, search for mechanisms and therapeutic approaches have been neurocentric until a recent time [157]. However, the importance of nonneuronal cells, such as astrocytes, is now largely established and opened new research approach that aim at better understanding of the pathology of the disease as well as characterizing new cellular and molecular targets for therapeutics development [158, 159].

Astrocytes are determined to reside in three major states, i.e., the resting, the reactive and the active state. Astrocytes that are involved in memory formation are defined as active astrocytes, which are different from reactive astrocytes, according to several reports [160]. Astrocytes reveal changes in their morphology and transcription according to their status [75]. Astrocytes release various gliotransmitter including glutamate, GABA, $_{D}$-serine, ATP, cytokines and proBDNF [161, 162].

Reactive state of astrocytes was described to be significantly increased at dentate gyrus region in the hippocampus to a

hippocampal-dependent cognitive impairment model [154]. It has been recently reported that the reactive astrocytes abnormally produce GABA by monoamine oxidase-B (MAO-B) and aberrantly release GABA through the bestrophin 1 channel in the dentate gyrus of APP/PS1 mice [163]. Administration with a newly developed reversible MAO-B specific inhibitor, KDS2010, significantly attenuated increased astrocytic GABA release and astrogliosis, enhancing synaptic transmission, and rescued learning and memory impairments in APP/PS1 mice [164].

Traditionally, neurons are thought to be the only cell type that expresses BACE1 and is capable of producing Aβ. Recent studies have demonstrated that astrocytes also express BACE1 and can produce Aβ under stressful conditions [165]. Secreted factors from reactive astrocytes, such as cytokines promote APP and BACE1 protein expression on neurons [165]. Not only neurons but also astrocytes and microglia are known to express APP, BACE1 and γ-secretase subunits, such as PS1, PS2, PEN2 and NCT, in the CNS [166].

Recently, it has been reported that the astrocyte-specific STAT-3 deleted APP/PS1 mice displayed the decreased activation of pro-inflammatory cytokine and lower dystrophic

neurite burden, and were largely protected from cerebral network imbalance. In addition, STAT3 deletion in astrocytes significantly ameliorated the impairment of cognitive function in APP/PS1 mice [167]. These results described above were obtained in APP/PS1 mice of 8 – 11 months when the reduction in neuronal activity was observed compared to WT mice. However, my results showed that reactive state of astrocytes in the hippocampus were significantly increased via STAT3 phosphorylation in the early stage of AD when neuronal loss was not attended. In addition, the activation of the STAT3 pathway in astrocytes promotes the expression of cytoskeletal proteins, such as GFAP and vimentin, and the secretion of cytokines or chemokines, such as TGFβ, TNF-α, IL-1β, INF-γ, IL-6 and CCL2 [168]. Astrocytes and microglia have the potential to clear Aβ in the CNS via phagocytic activity. Secreted factors from astrocytes affect the phagocytic activity of astrocytes and microglia [169]. These studies suggest that the control of astrocyte reactivity is an option for therapeutic strategies for AD.

In recent studies, novel AD therapeutic strategies regulating the JAK / STAT3 axis, one of the pathways leading to reactive state of astrocytes were established. These strategies

improved the impairment of cognitive function and neuronal activity in an AD mouse model [170, 171].

In this study, I focused on the pathological roles of reactive astrocytes in the cognitive function impairments and investigated the pathways involved in activating astrocytes from the resting state to the reactive state in primary cultured astrocytes treated with oAβ and in the hippocampus of 6-month-old 5XFAD mice. Six-month-old 5XFAD mice, which displayed an increase in the protein level of GFAP in the hippocampus and impairments of cognitive function, did not show a significant difference in the neuronal marker or synaptic proteins expression compared with the levels observed in age-matched WT mice. These results indicate that the control of reactive astrocytes could be one of important innovative factors for the rescue of cognitive dysfunction in 6-month-old 5XFAD mice. However, the synaptic function of neurons are not fully explained with neuronal loss or expression of synaptic proteins as PSD-95 and synaptophysin. The neuronal electronic function is analyzed with the flow of ions as amplitude, frequency, LTP and LDT by the electrophysiology studies. It is might cause the cognitive impairment in 6-month-old 5XFAD mice by The neuronal

electronic function. In addition, I found that treatment with oAβ increased the protein level of p-STAT3 and GFAP in primary cultured astrocytes. Stattic attenuated p-STAT3 and GFAP protein levels in primary cultured astrocytes. Furthermore, the systemic administration of Stattic reversed the morphological features of reactive astrocytes and the impairments cognitive function by reducing Aβ production via BACE1 expression in 5XFAD mice. Systemic administration of Stattic could not be astrocyte-specific. However, astrocytes were thought to be more affected by Stattic than other cell types such as neurons and microglia, because GFAP, a well-known astrocyte marker protein was shown to be colocalized with more than approximately 80% of p-STAT3 in 6-month-old 5XFAD mice. Neurons and microglia were colocalized less than 5%. These results indicated that the transition of reactive astrocytes to resting-state cells via inhibiting STAT3 phosphorylation may be a novel therapeutic strategy in AD. The results of Chapter 2 are summarized in Graphical Summary as below.

Taken together, my results suggest that the inhibition of STAT3 phosphorylation rescues the astrocytes of reactive state into the cells of resting state in the hippocampal dentate

gyrus. Furthermore, my results describe a relationship between the regulation of astrocyte activity and cognitive functions. A drug that specifically inhibits STAT3 phosphorylation in astrocytes may be a novel therapeutic strategy before neuronal loss is observed.

CHAPTER 2 GRAPHICAL SUMMARY

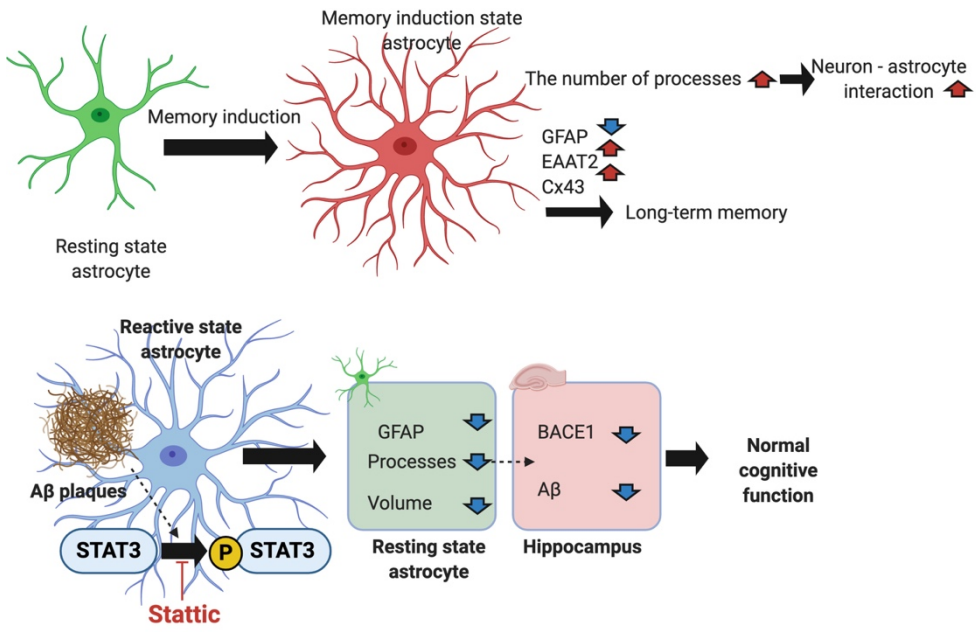

Graphical Summary: Chapter 2

The alteration of molecular and morphological change in the reactive astrocytes after memory induction. The pathological roles of the reactive astrocytes in Alzheimer's disease model.

CONCLUSION

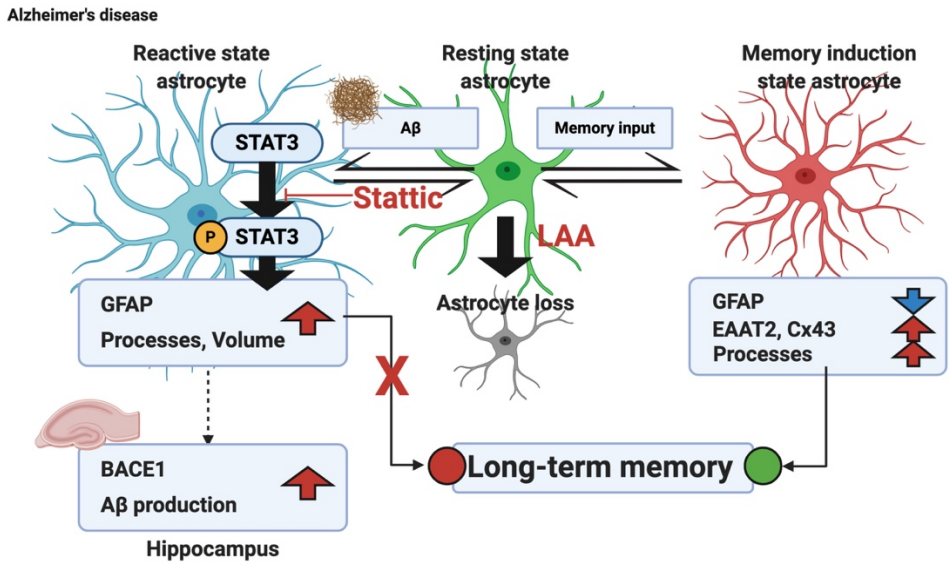

Memory induction by the contextual fear conditioning test in mice activates astrocytes into a memory induction state. The memory induction state of astrocytes has different characteristics than resting and reactive states, such as decreased GFAP expression and increased EAAT2 and Cx43 expression, for molecular changes and promoted the number of processes and the number of interaction between astrocytic processes and neuronal post-synapses. Intriguingly, even in astrocytic loss in the hippocampus, mice showed normal short-term memory but impaired long-term memory. These results indicate that astrocytes are essential for long-term

memory formation; however astrocytes are applied for short-term memory formation. In an AD mouse model, reactive astrocytes are activated by Aβ via STAT3 phosphorylation. Reactive astrocytes showed a decrease in the number of interactions between astrocytic processes and neuronal dendritic spines, even though reactive astrocytes have more processes than memory-induced astrocytes. For long-term memory formation, the number of astrocyte - neuron interactions at the synapse is important. In addition, reactive astrocytes are thought to be involved in the production of Aβ in the hippocampus in AD mouse model.

In conclusion, astrocytes play an essential role in long-term memory by physically interacting with dendritic spines. Reactive astrocytes activated via the STAT3 pathway alter astrocyte – neuron interactions and cause cognitive impairment in an AD mouse model.

REFERENCES

1. Verkhratsky, A., R. Zorec, and V. Parpura, *Stratification of astrocytes in healthy and diseased brain.* Brain Pathol, 2017. **27**(5): p. 629-644.
2. Bushong, E.A., M.E. Martone, and M.H. Ellisman, *Maturation of astrocyte morphology and the establishment of astrocyte domains during postnatal hippocampal development.* Int J Dev Neurosci, 2004. **22**(2): p. 73-86.
3. Zhou, B., Y.X. Zuo, and R.T. Jiang, *Astrocyte morphology: Diversity, plasticity, and role in neurological diseases.* CNS Neurosci Ther, 2019. **25**(6): p. 665-673.
4. Allen, N.J. and C. Eroglu, *Cell Biology of Astrocyte-Synapse Interactions.* Neuron, 2017. **96**(3): p. 697-708.
5. Krencik, R., J.V. van Asperen, and E.M. Ullian, *Human astrocytes are distinct contributors to the complexity of synaptic function.* Brain Res Bull, 2017. **129**: p. 66-73.
6. Schweinhuber, S.K., et al., *Profilin isoforms modulate astrocytic morphology and the motility of astrocytic processes.* PLoS One, 2015. **10**(1): p. e0117244.
7. Choi, M., et al., *Hippocampus-based contextual memory alters the morphological characteristics of astrocytes in the dentate gyrus.* Mol Brain, 2016. **9**(1): p. 72.
8. Chih, C.P. and E.L. Roberts Jr, *Energy substrates for neurons during neural activity: a critical review of the astrocyte-neuron lactate shuttle hypothesis.* J Cereb Blood Flow Metab, 2003. **23**(11): p. 1263-81.
9. Pellerin, L., et al., *Evidence supporting the existence of an activity-dependent astrocyte-neuron lactate shuttle.* Dev Neurosci, 1998. **20**(4-5): p. 291-9.
10. Barker, A.J. and E.M. Ullian, *New roles for astrocytes in developing synaptic circuits.* Commun Integr Biol, 2008. **1**(2): p. 207-11.
11. Kadala, A., et al., *Ion Homeostasis in Rhythmogenesis: The Interplay Between Neurons and Astroglia.* Physiology (Bethesda), 2015. **30**(5): p. 371-88.
12. Olsen, M.L., et al., *New Insights on Astrocyte Ion Channels: Critical for Homeostasis and Neuron-Glia Signaling.* J Neurosci, 2015. **35**(41): p. 13827-35.
13. Tulpule, K., et al., *Uptake of ferrous iron by cultured rat astrocytes.* J Neurosci Res, 2010. **88**(3): p. 563-71.
14. Kirischuk, S., et al., *Astrocyte sodium signaling and the regulation of neurotransmission.* Glia, 2016. **64**(10): p. 1655-66.
15. Miyazaki, H., et al., *Increase of glutamate uptake in astrocytes: a possible mechanism of action of volatile anesthetics.* Anesthesiology, 1997. **86**(6): p. 1359-66; discussion 8A.
16. Amundson, R.H., S.K. Goderie, and H.K. Kimelberg, *Uptake of [3H]serotonin and [3H]glutamate by primary astrocyte cultures. II. Differences in cultures prepared from different brain regions.* Glia, 1992. **6**(1): p. 9-18.
17. Abbott, N.J., L. Ronnback, and E. Hansson, *Astrocyte-endothelial interactions at the blood-brain barrier.* Nat Rev Neurosci, 2006. **7**(1): p. 41-53.
18. Tanaka, M., et al., *Astrocytic Ca2+ signals are required for the functional integrity of tripartite synapses.* Mol Brain, 2013. **6**: p. 6.
19. Honsek, S.D., et al., *Astrocyte calcium signals at Schaffer collateral to CA1 pyramidal cell synapses correlate with the number of activated synapses but not with synaptic strength.* Hippocampus, 2012. **22**(1): p. 29-42.
20. Pannasch, U., et al., *Connexin 30 sets synaptic strength by controlling astroglial synapse invasion.* Nat Neurosci, 2014. **17**(4): p. 549-58.

21. Croft, W., K.L. Dobson, and T.C. Bellamy, *Plasticity of Neuron-Glial Transmission: Equipping Glia for Long-Term Integration of Network Activity.* Neural Plast, 2015. **2015**: p. 765792.
22. Mohn, T.C. and A.O. Koob, *Adult Astrogenesis and the Etiology of Cortical Neurodegeneration.* J Exp Neurosci, 2015. **9**(Suppl 2): p. 25-34.
23. Song, H., C.F. Stevens, and F.H. Gage, *Astroglia induce neurogenesis from adult neural stem cells.* Nature, 2002. **417**(6884): p. 39-44.
24. Bradbury, E.J., et al., *Astrocyte transplants alleviate lesion induced memory deficits independently of cholinergic recovery.* Neuroscience, 1995. **65**(4): p. 955-72.
25. Suzuki, A., et al., *Astrocyte-neuron lactate transport is required for long-term memory formation.* Cell, 2011. **144**(5): p. 810-23.
26. Halassa, M.M., T. Fellin, and P.G. Haydon, *The tripartite synapse: roles for gliotransmission in health and disease.* Trends Mol Med, 2007. **13**(2): p. 54-63.
27. Koizumi, S., *Synchronization of Ca2+ oscillations: involvement of ATP release in astrocytes.* FEBS J, 2010. **277**(2): p. 286-92.
28. Rossi, D., F. Martorana, and L. Brambilla, *Implications of gliotransmission for the pharmacotherapy of CNS disorders.* CNS Drugs, 2011. **25**(8): p. 641-58.
29. Verkhratsky, A., et al., *Glia in the pathogenesis of neurodegenerative diseases.* Biochem Soc Trans, 2014. **42**(5): p. 1291-301.
30. Oya, M., et al., *The G protein-coupled receptor family C group 6 subtype A (GPRC6A) receptor is involved in amino acid-induced glucagon-like peptide-1 secretion from GLUTag cells.* J Biol Chem, 2013. **288**(7): p. 4513-21.
31. Khakh, B.S. and K.D. McCarthy, *Astrocyte calcium signaling: from observations to functions and the challenges therein.* Cold Spring Harb Perspect Biol, 2015. **7**(4): p. a020404.
32. Cornell-Bell, A.H., et al., *Glutamate induces calcium waves in cultured astrocytes: long-range glial signaling.* Science, 1990. **247**(4941): p. 470-3.
33. Rusakov, D.A., et al., *Diversity of astroglial functions alludes to subcellular specialisation.* Trends Neurosci, 2014. **37**(4): p. 228-42.
34. Montana, V., et al., *Vesicular transmitter release from astrocytes.* Glia, 2006. **54**(7): p. 700-15.
35. Martineau, M., *Gliotransmission: focus on exocytotic release of L-glutamate and D-serine from astrocytes.* Biochem Soc Trans, 2013. **41**(6): p. 1557-61.
36. Parpura, V. and R. Zorec, *Gliotransmission: Exocytotic release from astrocytes.* Brain Res Rev, 2010. **63**(1-2): p. 83-92.
37. De Gois, S., et al., *Identification of endophilins 1 and 3 as selective binding partners for VGLUT1 and their co-localization in neocortical glutamatergic synapses: implications for vesicular glutamate transporter trafficking and excitatory vesicle formation.* Cell Mol Neurobiol, 2006. **26**(4-6): p. 679-93.
38. Harada, K., T. Kamiya, and T. Tsuboi, *Gliotransmitter Release from Astrocytes: Functional, Developmental, and Pathological Implications in the Brain.* Front Neurosci, 2015. **9**: p. 499.
39. Duan, S., et al., *P2X7 receptor-mediated release of excitatory amino acids from astrocytes.* J Neurosci, 2003. **23**(4): p. 1320-8.
40. Orellana, J.A. and J. Stehberg, *Hemichannels: new roles in astroglial function.* Front Physiol, 2014. **5**: p. 193.
41. Anderson, C.M. and R.A. Swanson, *Astrocyte glutamate transport: review of properties, regulation, and physiological functions.* Glia, 2000. **32**(1): p. 1-14.
42. Storck, T., et al., *Structure, expression, and functional analysis of a Na(+)-dependent glutamate/aspartate transporter from rat brain.* Proc Natl Acad Sci U S A, 1992. **89**(22): p. 10955-9.

43. Pines, G., et al., *Cloning and expression of a rat brain L-glutamate transporter.* Nature, 1992. **360**(6403): p. 464-7.
44. Rothstein, J.D., et al., *Localization of neuronal and glial glutamate transporters.* Neuron, 1994. **13**(3): p. 713-25.
45. Lehre, K.P. and N.C. Danbolt, *The number of glutamate transporter subtype molecules at glutamatergic synapses: chemical and stereological quantification in young adult rat brain.* J Neurosci, 1998. **18**(21): p. 8751-7.
46. Eulenburg, V. and J. Gomeza, *Neurotransmitter transporters expressed in glial cells as regulators of synapse function.* Brain Res Rev, 2010. **63**(1-2): p. 103-12.
47. Kim, K., et al., *Role of excitatory amino acid transporter-2 (EAAT2) and glutamate in neurodegeneration: opportunities for developing novel therapeutics.* J Cell Physiol, 2011. **226**(10): p. 2484-93.
48. Wolosker, H., *D-serine regulation of NMDA receptor activity.* Sci STKE, 2006. **2006**(356): p. pe41.
49. Neame, S., et al., *The NMDA receptor activation by d-serine and glycine is controlled by an astrocytic Phgdh-dependent serine shuttle.* Proc Natl Acad Sci U S A, 2019. **116**(41): p. 20736-20742.
50. Park, P., et al., *NMDA receptor-dependent long-term potentiation comprises a family of temporally overlapping forms of synaptic plasticity that are induced by different patterns of stimulation.* Philos Trans R Soc Lond B Biol Sci, 2014. **369**(1633): p. 20130131.
51. Baldwin, K.T. and C. Eroglu, *Molecular mechanisms of astrocyte-induced synaptogenesis.* Curr Opin Neurobiol, 2017. **45**: p. 113-120.
52. Christopherson, K.S., et al., *Thrombospondins are astrocyte-secreted proteins that promote CNS synaptogenesis.* Cell, 2005. **120**(3): p. 421-33.
53. Kucukdereli, H., et al., *Control of excitatory CNS synaptogenesis by astrocyte-secreted proteins Hevin and SPARC.* Proc Natl Acad Sci U S A, 2011. **108**(32): p. E440-9.
54. Singh, S.K., et al., *Astrocytes Assemble Thalamocortical Synapses by Bridging NRX1alpha and NL1 via Hevin.* Cell, 2016. **164**(1-2): p. 183-196.
55. Falk, S. and M. Gotz, *Glial control of neurogenesis.* Curr Opin Neurobiol, 2017. **47**: p. 188-195.
56. Akira, S., *Functional roles of STAT family proteins: lessons from knockout mice.* Stem Cells, 1999. **17**(3): p. 138-46.
57. Rebe, C., et al., *STAT3 activation: A key factor in tumor immunoescape.* JAKSTAT, 2013. **2**(1): p. e23010.
58. Thilakasiri, P.S., et al., *Repurposing of drugs as STAT3 inhibitors for cancer therapy.* Semin Cancer Biol, 2019.
59. Ma, J., et al., *A novel sequence in the coiled-coil domain of Stat3 essential for its nuclear translocation.* J Biol Chem, 2003. **278**(31): p. 29252-60.
60. Zhang, T., et al., *The coiled-coil domain of Stat3 is essential for its SH2 domain-mediated receptor binding and subsequent activation induced by epidermal growth factor and interleukin-6.* Mol Cell Biol, 2000. **20**(19): p. 7132-9.
61. Mitchell, T.J. and S. John, *Signal transducer and activator of transcription (STAT) signalling and T-cell lymphomas.* Immunology, 2005. **114**(3): p. 301-12.
62. Haan, S., et al., *Characterization and binding specificity of the monomeric STAT3-SH2 domain.* J Biol Chem, 1999. **274**(3): p. 1342-8.
63. Huang, G., et al., *STAT3 phosphorylation at tyrosine 705 and serine 727 differentially regulates mouse ESC fates.* Stem Cells, 2014. **32**(5): p. 1149-60.
64. Cimica, V., et al., *Dynamics of the STAT3 transcription factor: nuclear import dependent on Ran and importin-beta1.* PLoS One, 2011. **6**(5): p. e20188.

65. Koh, J.S., et al., *Inhibition of STAT3 in gastric cancer: role of pantoprazole as SHP-1 inducer.* Cell Biosci, 2018. **8**: p. 50.
66. Hodge, D.R., E.M. Hurt, and W.L. Farrar, *The role of IL-6 and STAT3 in inflammation and cancer.* Eur J Cancer, 2005. **41**(16): p. 2502-12.
67. Kamran, M.Z., P. Patil, and R.P. Gude, *Role of STAT3 in cancer metastasis and translational advances.* Biomed Res Int, 2013. **2013**: p. 421821.
68. Dutta, P., et al., *Role of STAT3 in lung cancer.* JAKSTAT, 2014. **3**(4): p. e999503.
69. Sosonkina, N., D. Starenki, and J.I. Park, *The Role of STAT3 in Thyroid Cancer.* Cancers (Basel), 2014. **6**(1): p. 526-44.
70. Ma, J.H., L. Qin, and X. Li, *Role of STAT3 signaling pathway in breast cancer.* Cell Commun Signal, 2020. **18**(1): p. 33.
71. Lee, H., A.J. Jeong, and S.K. Ye, *Highlighted STAT3 as a potential drug target for cancer therapy.* BMB Rep, 2019. **52**(7): p. 415-423.
72. Sjoblom-Hallen, A., et al., *Gene expression profiling identifies STAT3 as a novel pathway for immunomodulation by cholera toxin adjuvant.* Mucosal Immunol, 2010. **3**(4): p. 374-86.
73. Liddelow, S.A., et al., *Neurotoxic reactive astrocytes are induced by activated microglia.* Nature, 2017. **541**(7638): p. 481-487.
74. Li, K., et al., *Reactive Astrocytes in Neurodegenerative Diseases.* Aging Dis, 2019. **10**(3): p. 664-675.
75. Liddelow, S.A. and B.A. Barres, *Reactive Astrocytes: Production, Function, and Therapeutic Potential.* Immunity, 2017. **46**(6): p. 957-967.
76. Hsieh, S., et al., *Brain correlates of musical and facial emotion recognition: evidence from the dementias.* Neuropsychologia, 2012. **50**(8): p. 1814-22.
77. Selkoe, D.J., *Cell biology of protein misfolding: The examples of Alzheimer's and Parkinson's diseases.* Nature Cell Biology, 2004. **6**(11): p. 1054-1061.
78. Ling, Y., K. Morgan, and N. Kalsheker, *Amyloid precursor protein (APP) and the biology of proteolytic processing: relevance to Alzheimer's disease.* Int J Biochem Cell Biol, 2003. **35**(11): p. 1505-35.
79. Galvao, F., Jr., et al., *The amyloid precursor protein (APP) processing as a biological link between Alzheimer's disease and cancer.* Ageing Res Rev, 2019. **49**: p. 83-91.
80. Ohyagi, Y., *[Mechanism of senile plaque formation in Alzheimer disease].* Fukuoka Igaku Zasshi, 1999. **90**(4): p. 113-7.
81. Iwatsubo, T., *[Molecular mechanism of Alzheimer disease].* Nihon Naika Gakkai Zasshi, 2002. **91 Suppl**: p. 149-51.
82. Saha, A., et al., *Interaction of Abeta peptide with tubulin causes an inhibition of tubulin polymerization and the apoptotic death of cancer cells.* Chem Commun (Camb), 2015. **51**(12): p. 2249-52.
83. Pop, V., et al., *Abeta aggregation profiles and shifts in APP processing favor amyloidogenesis in canines.* Neurobiol Aging, 2012. **33**(1): p. 108-20.
84. Campion, D., et al., *Early-onset autosomal dominant Alzheimer disease: prevalence, genetic heterogeneity, and mutation spectrum.* Am J Hum Genet, 1999. **65**(3): p. 664-70.
85. Lannfelt, L., et al., *Genetic counseling in a Swedish Alzheimer family with amyloid precursor protein mutation.* Am J Hum Genet, 1995. **56**(1): p. 332-5.
86. Gatz, M., et al., *Role of genes and environments for explaining Alzheimer disease.* Arch Gen Psychiatry, 2006. **63**(2): p. 168-74.
87. Ferreira, S.T. and W.L. Klein, *The Abeta oligomer hypothesis for synapse failure and memory loss in Alzheimer's disease.* Neurobiol Learn Mem, 2011. **96**(4): p. 529-43.
88. Simic, G., et al., *Tau Protein Hyperphosphorylation and Aggregation in Alzheimer's Disease and Other Tauopathies, and Possible Neuroprotective Strategies.*

Biomolecules, 2016. **6**(1): p. 6.
89. Binder, L.I., et al., *Tau, tangles, and Alzheimer's disease.* Biochim Biophys Acta, 2005. **1739**(2-3): p. 216-23.
90. Sala Frigerio, C., et al., *The Major Risk Factors for Alzheimer's Disease: Age, Sex, and Genes Modulate the Microglia Response to Abeta Plaques.* Cell Rep, 2019. **27**(4): p. 1293-1306 e6.
91. R, A.A., *Risk factors for Alzheimer's disease.* Folia Neuropathol, 2019. **57**(2): p. 87-105.
92. Silva, M.V.F., et al., *Alzheimer's disease: risk factors and potentially protective measures.* J Biomed Sci, 2019. **26**(1): p. 33.
93. Kim, J., J.M. Basak, and D.M. Holtzman, *The role of apolipoprotein E in Alzheimer's disease.* Neuron, 2009. **63**(3): p. 287-303.
94. Proctor, C.J. and D.A. Gray, *A unifying hypothesis for familial and sporadic Alzheimer's disease.* Int J Alzheimers Dis, 2012. **2012**: p. 978742.
95. Huang, L.K., S.P. Chao, and C.J. Hu, *Clinical trials of new drugs for Alzheimer disease.* J Biomed Sci, 2020. **27**(1): p. 18.
96. Caselli, R.J., et al., *Alzheimer Disease: Scientific Breakthroughs and Translational Challenges.* Mayo Clin Proc, 2017. **92**(6): p. 978-994.
97. Cummings, J., et al., *Alzheimer's disease drug development pipeline: 2019.* Alzheimers Dement (N Y), 2019. **5**: p. 272-293.
98. Li, J.M., et al., *Effects of triptolide on hippocampal microglial cells and astrocytes in the APP/PS1 double transgenic mouse model of Alzheimer's disease.* Neural Regen Res, 2016. **11**(9): p. 1492-1498.
99. Kim, Y.E., et al., *Inhibitory effect of punicalagin on lipopolysaccharide-induced neuroinflammation, oxidative stress and memory impairment via inhibition of nuclear factor-kappaB.* Neuropharmacology, 2017. **117**: p. 21-32.
100. Aguirre-Rueda, D., et al., *WIN 55,212-2, agonist of cannabinoid receptors, prevents amyloid beta1-42 effects on astrocytes in primary culture.* PLoS One, 2015. **10**(4): p. e0122843.
101. Sohanaki, H., et al., *Pelargonidin improves memory deficit in amyloid beta25-35 rat model of Alzheimer's disease by inhibition of glial activation, cholinesterase, and oxidative stress.* Biomed Pharmacother, 2016. **83**: p. 85-91.
102. Jeong, J.C., et al., *Effects of Bambusae concretio Salicea (Chunchukhwang) on amyloid beta-induced cell toxicity and antioxidative enzymes in cultured rat neuronal astrocytes.* J Ethnopharmacol, 2005. **98**(3): p. 259-66.
103. Wang, G., et al., *The effect of resveratrol on beta amyloid-induced memory impairment involves inhibition of phosphodiesterase-4 related signaling.* Oncotarget, 2016. **7**(14): p. 17380-92.
104. Ibrahim, N.F., et al., *Tocotrienol-Rich Fraction Modulates Amyloid Pathology and Improves Cognitive Function in AbetaPP/PS1 Mice.* J Alzheimers Dis, 2017. **55**(2): p. 597-612.
105. Brann, D.W., et al., *Neurotrophic and neuroprotective actions of estrogen: basic mechanisms and clinical implications.* Steroids, 2007. **72**(5): p. 381-405.
106. Yi, J.H. and A.S. Hazell, *Excitotoxic mechanisms and the role of astrocytic glutamate transporters in traumatic brain injury.* Neurochem Int, 2006. **48**(5): p. 394-403.
107. Sovrea, A.S. and A.B. Bosca, *Astrocytes reassessment - an evolving concept part one: embryology, biology, morphology and reactivity.* J Mol Psychiatry, 2013. **1**: p. 18.
108. Abel, T., et al., *Genetic demonstration of a role for PKA in the late phase of LTP and in hippocampus-based long-term memory.* Cell, 1997. **88**(5): p. 615-26.
109. Gulbransen, B.D. and K.A. Sharkey, *Novel functional roles for enteric glia in the gastrointestinal tract.* Nat Rev Gastroenterol Hepatol, 2012. **9**(11): p. 625-32.

110. Emsley, J.G. and J.D. Macklis, *Astroglial heterogeneity closely reflects the neuronal-defined anatomy of the adult murine CNS.* Neuron Glia Biol, 2006. **2**(3): p. 175-86.
111. Matyash, V. and H. Kettenmann, *Heterogeneity in astrocyte morphology and physiology.* Brain Res Rev, 2010. **63**(1-2): p. 2-10.
112. Yang, F.C. and K.C. Liang, *Interactions of the dorsal hippocampus, medial prefrontal cortex and nucleus accumbens in formation of fear memory: difference in inhibitory avoidance learning and contextual fear conditioning.* Neurobiol Learn Mem, 2014. **112**: p. 186-94.
113. Strekalova, T., et al., *Memory retrieval after contextual fear conditioning induces c-Fos and JunB expression in CA1 hippocampus.* Genes Brain Behav, 2003. **2**(1): p. 3-10.
114. Rudy, J.W. and P. Matus-Amat, *The ventral hippocampus supports a memory representation of context and contextual fear conditioning: implications for a unitary function of the hippocampus.* Behav Neurosci, 2005. **119**(1): p. 154-63.
115. Kimura, R. and M. Ohno, *Impairments in remote memory stabilization precede hippocampal synaptic and cognitive failures in 5XFAD Alzheimer mouse model.* Neurobiol Dis, 2009. **33**(2): p. 229-35.
116. Kimura, R., L. Devi, and M. Ohno, *Partial reduction of BACE1 improves synaptic plasticity, recent and remote memories in Alzheimer's disease transgenic mice.* J Neurochem, 2010. **113**(1): p. 248-61.
117. Sullivan, S.M., et al., *Structural remodeling of gray matter astrocytes in the neonatal pig brain after hypoxia/ischemia.* Glia, 2010. **58**(2): p. 181-94.
118. Yang, E.J., et al., *Phloroglucinol Attenuates the Cognitive Deficits of the 5XFAD Mouse Model of Alzheimer's Disease.* PLoS One, 2015. **10**(8): p. e0135686.
119. Yassa, M.A., et al., *High-resolution structural and functional MRI of hippocampal CA3 and dentate gyrus in patients with amnestic Mild Cognitive Impairment.* Neuroimage, 2010. **51**(3): p. 1242-52.
120. Carlisle, H.J., et al., *Opposing effects of PSD-93 and PSD-95 on long-term potentiation and spike timing-dependent plasticity.* J Physiol, 2008. **586**(Pt 24): p. 5885-900.
121. Holmseth, S., et al., *The concentrations and distributions of three C-terminal variants of the GLT1 (EAAT2; slc1a2) glutamate transporter protein in rat brain tissue suggest differential regulation.* Neuroscience, 2009. **162**(4): p. 1055-71.
122. Miralles, V.J., et al., *Na+ dependent glutamate transporters (EAAT1, EAAT2, and EAAT3) in primary astrocyte cultures: effect of oxidative stress.* Brain Res, 2001. **922**(1): p. 21-9.
123. Brand-Schieber, E., et al., *Connexin43, the major gap junction protein of astrocytes, is down-regulated in inflamed white matter in an animal model of multiple sclerosis.* J Neurosci Res, 2005. **80**(6): p. 798-808.
124. Olney, J.W., O.L. Ho, and V. Rhee, *Cytotoxic effects of acidic and sulphur containing amino acids on the infant mouse central nervous system.* Exp Brain Res, 1971. **14**(1): p. 61-76.
125. Huck, S., F. Grass, and M.E. Hatten, *Gliotoxic effects of alpha-aminoadipic acid on monolayer cultures of dissociated postnatal mouse cerebellum.* Neuroscience, 1984. **12**(3): p. 783-91.
126. McBean, G.J., *Inhibition of the glutamate transporter and glial enzymes in rat striatum by the gliotoxin, alpha aminoadipate.* Br J Pharmacol, 1994. **113**(2): p. 536-40.
127. Eng, L.F., A.C. Yu, and Y.L. Lee, *Astrocytic response to injury.* Prog Brain Res, 1992. **94**: p. 353-65.
128. Saur, L., et al., *Physical exercise increases GFAP expression and induces*

morphological changes in hippocampal astrocytes. Brain Struct Funct, 2014. **219**(1): p. 293-302.
129. Sagi, Y., et al., *Learning in the fast lane: new insights into neuroplasticity.* Neuron, 2012. **73**(6): p. 1195-203.
130. Porter, J.T. and K.D. McCarthy, *Astrocytic neurotransmitter receptors in situ and in vivo.* Prog Neurobiol, 1997. **51**(4): p. 439-55.
131. Porter, J.T. and K.D. McCarthy, *GFAP-positive hippocampal astrocytes in situ respond to glutamatergic neuroligands with increases in [Ca2+]i.* Glia, 1995. **13**(2): p. 101-12.
132. Van den Pol, A.N., *Metabotropic glutamate receptor mGluR1 distribution and ultrastructural localization in hypothalamus.* J Comp Neurol, 1994. **349**(4): p. 615-32.
133. Lima, A., et al., *Astrocyte pathology in the prefrontal cortex impairs the cognitive function of rats.* Mol Psychiatry, 2014. **19**(7): p. 834-41.
134. Pang, P.T. and B. Lu, *Regulation of late-phase LTP and long-term memory in normal and aging hippocampus: role of secreted proteins tPA and BDNF.* Ageing Res Rev, 2004. **3**(4): p. 407-30.
135. Borroni, A.M., et al., *Role of voltage-dependent calcium channel long-term potentiation (LTP) and NMDA LTP in spatial memory.* J Neurosci, 2000. **20**(24): p. 9272-6.
136. Meiri, N., et al., *Memory and long-term potentiation (LTP) dissociated: normal spatial memory despite CA1 LTP elimination with Kv1.4 antisense.* Proc Natl Acad Sci U S A, 1998. **95**(25): p. 15037-42.
137. Montoliu-Gaya, L., et al., *Abeta-oligomer uptake and the resulting inflammatory response in adult human astrocytes are precluded by an anti-Abeta single chain variable fragment in combination with an apoE mimetic peptide.* Mol Cell Neurosci, 2018. **89**: p. 49-59.
138. Franciosi, S., et al., *IL-8 enhancement of amyloid-beta (Abeta 1-42)-induced expression and production of pro-inflammatory cytokines and COX-2 in cultured human microglia.* J Neuroimmunol, 2005. **159**(1-2): p. 66-74.
139. Ben Haim, L., et al., *Elusive roles for reactive astrocytes in neurodegenerative diseases.* Front Cell Neurosci, 2015. **9**: p. 278.
140. Zhou, B., Y.X. Zuo, and R.T. Jiang, *Astrocyte morphology: Diversity, plasticity, and role in neurological diseases.* CNS Neurosci Ther, 2019.
141. Anderson, M.A., et al., *Astrocyte scar formation aids central nervous system axon regeneration.* Nature, 2016. **532**(7598): p. 195-200.
142. Choi, S.S., et al., *Human astrocytes: secretome profiles of cytokines and chemokines.* PLoS One, 2014. **9**(4): p. e92325.
143. Lange, S.C., et al., *Primary Cultures of Astrocytes: Their Value in Understanding Astrocytes in Health and Disease.* Neurochemical Research, 2012. **37**(11): p. 2569-2588.
144. Gilson, V., et al., *Effects of Low Amyloid-beta (Abeta) Concentration on Abeta1-42 Oligomers Binding and GluN2B Membrane Expression.* J Alzheimers Dis, 2015. **47**(2): p. 453-66.
145. Stine, W.B., et al., *Preparing synthetic Abeta in different aggregation states.* Methods Mol Biol, 2011. **670**: p. 13-32.
146. Yang, E.J., et al., *Phloroglucinol ameliorates cognitive impairments by reducing the amyloid beta peptide burden and pro-inflammatory cytokines in the hippocampus of 5XFAD mice.* Free Radic Biol Med, 2018. **126**: p. 221-234.
147. Lin, L., et al., *Novel STAT3 phosphorylation inhibitors exhibit potent growth-suppressive activity in pancreatic and breast cancer cells.* Cancer Res, 2010. **70**(6):

p. 2445-54.
148. Schust, J., et al., *Stattic: a small-molecule inhibitor of STAT3 activation and dimerization.* Chem Biol, 2006. **13**(11): p. 1235-42.
149. Boue-Grabot, E. and Y. Pankratov, *Modulation of Central Synapses by Astrocyte-Released ATP and Postsynaptic P2X Receptors.* Neural Plast, 2017. **2017**: p. 9454275.
150. Chung, W.S., N.J. Allen, and C. Eroglu, *Astrocytes Control Synapse Formation, Function, and Elimination.* Cold Spring Harb Perspect Biol, 2015. **7**(9): p. a020370.
151. Bradley, S.J. and R.A. Challiss, *G protein-coupled receptor signalling in astrocytes in health and disease: a focus on metabotropic glutamate receptors.* Biochem Pharmacol, 2012. **84**(3): p. 249-59.
152. Bonder, D.E. and K.D. McCarthy, *Astrocytic Gq-GPCR-Linked IP3R-Dependent Ca2+ Signaling Does Not Mediate Neurovascular Coupling in Mouse Visual Cortex In Vivo.* Journal of Neuroscience, 2014. **34**(39): p. 13139-13150.
153. Santello, M., N. Toni, and A. Volterra, *Astrocyte function from information processing to cognition and cognitive impairment.* Nat Neurosci, 2019. **22**(2): p. 154-166.
154. Olabarria, M., et al., *Concomitant astroglial atrophy and astrogliosis in a triple transgenic animal model of Alzheimer's disease.* Glia, 2010. **58**(7): p. 831-8.
155. Miller, S.J., *Astrocyte Heterogeneity in the Adult Central Nervous System.* Front Cell Neurosci, 2018. **12**: p. 401.
156. Matsutani, S. and N. Yamamoto, *Neuronal regulation of astrocyte morphology in vitro is mediated by GABAergic signaling.* Glia, 1997. **20**(1): p. 1-9.
157. Vickers, J.C., et al., *The cause of neuronal degeneration in Alzheimer's disease.* Prog Neurobiol, 2000. **60**(2): p. 139-65.
158. Gandy, S., *Alzheimer's disease: new data highlight nonneuronal cell types and the necessity for presymptomatic prevention strategies.* Biol Psychiatry, 2014. **75**(7): p. 553-7.
159. Assefa, B.T., A.K. Gebre, and B.M. Altaye, *Reactive Astrocytes as Drug Target in Alzheimer's Disease.* Biomed Research International, 2018.
160. Adamsky, A., et al., *Astrocytic Activation Generates De Novo Neuronal Potentiation and Memory Enhancement.* Cell, 2018. **174**(1): p. 59-71 e14.
161. Chun, H., et al., *Astrocytic proBDNF and Tonic GABA Distinguish Active versus Reactive Astrocytes in Hippocampus.* Exp Neurobiol, 2018. **27**(3): p. 155-170.
162. Yoon, B.E., et al., *Glial GABA, synthesized by monoamine oxidase B, mediates tonic inhibition.* J Physiol, 2014. **592**(22): p. 4951-68.
163. Jo, S., et al., *GABA from reactive astrocytes impairs memory in mouse models of Alzheimer's disease.* Nat Med, 2014. **20**(8): p. 886-96.
164. Park, J.H., et al., *Newly developed reversible MAO-B inhibitor circumvents the shortcomings of irreversible inhibitors in Alzheimer's disease.* Sci Adv, 2019. **5**(3): p. eaav0316.
165. Frost, G.R. and Y.M. Li, *The role of astrocytes in amyloid production and Alzheimer's disease.* Open Biol, 2017. **7**(12).
166. Grolla, A.A., et al., *Abeta leads to Ca(2)(+) signaling alterations and transcriptional changes in glial cells.* Neurobiol Aging, 2013. **34**(2): p. 511-22.
167. Reichenbach, N., et al., *Inhibition of Stat3-mediated astrogliosis ameliorates pathology in an Alzheimer's disease model.* EMBO Mol Med, 2019. **11**(2).
168. Ben Haim, L., et al., *The JAK/STAT3 Pathway Is a Common Inducer of Astrocyte Reactivity in Alzheimer's and Huntington's Diseases.* Journal of Neuroscience, 2015. **35**(6): p. 2817-2829.
169. Morizawa, Y.M., et al., *Reactive astrocytes function as phagocytes after brain ischemia via ABCA1-mediated pathway (vol 8, 28, 2017).* Nature Communications,

2017. **8**.
170. Ceyzeriat, K., et al., *Modulation of astrocyte reactivity improves functional deficits in mouse models of Alzheimer's disease.* Acta Neuropathol Commun, 2018. **6**(1): p. 104.
171. Wan, J., et al., *Tyk2/STAT3 signaling mediates beta-amyloid-induced neuronal cell death: implications in Alzheimer's disease.* J Neurosci, 2010. **30**(20): p. 6873-81.

국문 초록

중추신경계에서 성상교세포의 다양한 역할들이 보고되어 왔다. 성상교세포는 잠재적으로 활성화 상태와 휴지기 상태의 두 가지의 상태로 변화할 수 있는 능력이 있다. 활성화 성상교세포는 돌기의 두께와 그 수가 증가하고, 세포체 부피의 증가가 특징적으로 나타난다. 또한, 신경교 섬유질 산성단백질 (glial fibrillary acidic protein: GFAP)과 같은 단백질 발현의 증가나 유전자 발현의 변화가 분자적 변화로 나타난다. 하지만, 성상교세포에서 기억을 유도하는 과정 중에 이러한 즉각적인 형태학적, 분자적 변화는 아직 연구가 부족한 상태이다. 알츠하이머병을 포함한 퇴행성신경계질환의 발병 기전에 있어 활성화 상태의 성상교세포의 병리생리학적 역할은 매우 중요한 의미가 있을 것이라 생각된다. 그러나 퇴행성신경계질환이 진행되는 동안 휴지기 상태의 성상교세포가 활성화 상태로 전환되는 구체적인 작용 원리의 이해는 여전히 명백하게 밝혀져 있지 않다. 본 연구에서는 Fvb/n 마우스 뇌내 해마에 존재하는 성상교세포를 공포 상황 조건화 실험 (contextual fear conditioning)을 통해 기억 유도를 하였다. 이후 기억 유도한 성상교세포의 형태학적 분자적 변화를 분석 하였다. 공포 상황 조건화 실험 1시간 후, 타입 2와 타입 3 성상교세포가 활성화와 휴지 상태의 특징이 아닌, 돌기의 수가 증가하고, 신경교 섬유질 산성단백질의 발현이 감소되는 새로운 상태로 관측되었다. 또한, 흥분성 아미노산 운반자 2 (excitatory amino acid transporter 2: EAAT2)의 단백질 발현이 공포 상황 조건화 후

1시간 에서 24시간까지 단백질 발현이 증가하였지만, 흥분성 아미노산 운반자 1은 변화가 없는 것이 확인되었다. 공포 상황 조건화 24시간 후 코넥신 43 (Connexin 43: Cx43) 단백질의 발현의 증가가 확인되었다. 성상교세포 특이적 독성 물질인, 엘-알파-아미노아디페이트 (L-α-aminoadipate: LAA)가 뇌내 해마에 처리된 마우스에서 인지능력의 저하가 확인되었다. 초대 배양 성상교세포에 다량체 아밀로이드 펩티드 (oAβ)를 처치하는 방법과 6개월령 알츠하이머병 동물 모델 5XFAD의 해마 부위에서 어떤 신호전달 경로가 연관되어 있는지 확인하였다. 신경교 섬유질 산성단백질 발현의 증가를 통해서 초대 배양 성상교세포의 다량체 아밀로이드 펩티드 처치는 활성화 성상교세포의 증가의 유도함을 확인하였다. 이러한 초대 배양 성상교세포의 활성화는 신호변환자-전사활성자 3 (signal transducer and activator of transcription: STAT3)의 인산화를 통해 증가하였다. 초대 배양 성상교세포 활성화와 6개월령 알츠하이머동물 모델의 인지능력 저해를 신호변환자-전사활성자 3 인산화 억제제 스테틱(Stattic)의 전신 적용이 완화시킴을 확인하였다. 위 결과를 종합하면, 해마 기반 공포 상황 조건화 실험에 의해 기억 유도된 성상교세포는 새로운 형태를 보이며 이를, 기억 유도 상태가 되었다. 알츠하이머병 뇌 내에서 활성화 상태의 성상교세포로 존재함으로 이러한 기억 유도 상태 성상교세포는 정상적이지 않을 것이다. 알츠하이머병 뇌의 활성화 성상교세포는 신호변환자-전사활성자 3 인산화를 통해서 나타나며, 학습과 기억력의 저하가 신호변환자-전사활성자 3 인산화 억제제를 통해서 완화되었다. 이는 신호변환자-전사활성자 3 인산

화 억제제를 통한 성상교세포의 활성화 조절이 알츠하이머병의 인지능력저하의 새로운 치료 전략으로 제시될 가능성을 보였다.

주요어: 알츠하이머병, 성상교세포, 인지능력, 신호변환자-전사활성자 3, 5XFAD 마우스

학 번:2013-21792